University of Alberta

Prediction of Mechanical Properties of Polymers under Cyclic Loading

by

Tik Man Dick ©

A thesis submitted to the Faculty of Graduate Studies and Research
in partial fulfillment of the requirements for the degree of

Master of Science

Department of Mechanical Engineering

Edmonton, Alberta
Fall 2007

Library and
Archives Canada

Published Heritage
Branch

395 Wellington Street
Ottawa ON K1A 0N4
Canada

Bibliothèque et
Archives Canada

Direction du
Patrimoine de l'édition

395, rue Wellington
Ottawa ON K1A 0N4
Canada

Your file Votre référence
ISBN: 978-0-494-33233-7
Our file Notre référence
ISBN: 978-0-494-33233-7

NOTICE:
The author has granted a non-exclusive license allowing Library and Archives Canada to reproduce, publish, archive, preserve, conserve, communicate to the public by telecommunication or on the Internet, loan, distribute and sell theses worldwide, for commercial or non-commercial purposes, in microform, paper, electronic and/or any other formats.

The author retains copyright ownership and moral rights in this thesis. Neither the thesis nor substantial extracts from it may be printed or otherwise reproduced without the author's permission.

AVIS:
L'auteur a accordé une licence non exclusive permettant à la Bibliothèque et Archives Canada de reproduire, publier, archiver, sauvegarder, conserver, transmettre au public par télécommunication ou par l'Internet, prêter, distribuer et vendre des thèses partout dans le monde, à des fins commerciales ou autres, sur support microforme, papier, électronique et/ou autres formats.

L'auteur conserve la propriété du droit d'auteur et des droits moraux qui protège cette thèse. Ni la thèse ni des extraits substantiels de celle-ci ne doivent être imprimés ou autrement reproduits sans son autorisation.

In compliance with the Canadian Privacy Act some supporting forms may have been removed from this thesis.

While these forms may be included in the document page count, their removal does not represent any loss of content from the thesis.

Conformément à la loi canadienne sur la protection de la vie privée, quelques formulaires secondaires ont été enlevés de cette thèse.

Bien que ces formulaires aient inclus dans la pagination, il n'y aura aucun contenu manquant.

Canada

ABSTRACT

The prediction accuracy of mechanical properties under fatigue loading in engineering plastics is increasingly important. In this study, the resistance to flexural and tensile cyclic loading of brittle and ductile materials was investigated respectively. The experimental results were then compared with theoretical prediction based on two existing residual strength degradation models, and conditions were examined to improve the model's applicability. The residual mechanical properties of the two materials were also evaluated and compared.

A correlation between parameters for a model and loading conditions was proposed. It allows the representation of fatigue life and possibly the residual strength with respect to stress ratio using a minimum number of experimental data. The observation of decreasing total energy absorbed by the specimen with increasing number of fatigue cycles in ductile material provided an insight in developing a fatigue model based on the energy criteria.

ACKNOWLEDGEMENTS

I am particularly indebted to my supervisor, Dr. P.-Y. Ben Jar and Dr. J.-J. R. Cheng for their guidance and financial support throughout this study.

I would like to thank Mr. Bernie Faulkner and Mr. Albert Yuen who offered me excellent technical supports and valuable discussions.

Appreciation is extended to members of the Durable Materials Research Lab: Mr. Chengye Fan, Mr. Yemi Setiadi, Mr. Hyock-Ju Kwon, Mr. Riski Adianto and Mr. Tadayoshi Yamanaka for their friendship and the provision of a pleasant environment.

Special thanks go out to ISIS Canada, NSERC-Discovery, Queen Elizabeth II scholarship, J Gordin Kaplan Graduate Student Award and Mechanical Engineering Department Travel Award for the financial support throughout the study, as well as the material supply (ABS) from Mr. T Shinmura in DENKA Co.

Finally, my gratitude must be given to my husband, Scott H. Dick, and parents, Wai Ming Poon and Yin Ngar Law, for their support throughout the study.

TABLE OF CONTENTS

1. Introduction....................1

1.1 Literature Review....................4

1.2 Objectives and Scope of the Study....................11

2. Fundamental Principles of the Theoretical Models....................14

2.1 Determination of Weibull Parameters....................14

2.2 D'Amore and Caprino's Model (DC model)....................21
2.2.1 Statistical Implementation of the DC model....................24

2.3 Yang and Liu's Model (YL model)....................32
2.3.1 Effect of Overload....................42
2.3.2 Determining Parameters for the YL Model....................44

3. Experimental Details....................47

3.1 Material Information....................47
3.1.1 Glass-Filled Polycarbonate....................47
3.1.2 Poly(acrylonitrile-butadiene-styrene) (ABS)....................49

3.2 Test Methodology....................51
3.2.1 Flexural Monotonic Test (Glass-Filled Polycarbonate)....................53
3.2.2 Flexural Fatigue Test (Glass-Filled Polycarbonate)....................54
3.2.3 Tensile Test for Measuring Residual Strength (ABS)....................56

4. Results and Discussions....................59

4.1 Experimental Results....................59
4.1.1 Flexural Monotonic Test for Glass-Filled Polycarbonate....................59
4.1.2 Flexural Fatigue Test for Glass-Filled Polycarbonate....................62
4.1.3 Tensile Test for Residual Strength of ABS....................67

4.2 Data Analysis....................72
4.2.1 Determining Parameters of Weibull Distribution....................72
4.2.2 Determining Parameters of the DC Model....................75
4.2.3 Determining Parameters of the YL Model....................77

4.3 Prediction Accuracy of the DC Model..........88
4.3.1 Fatigue Life Estimation..........88
4.3.2 Residual Strength Approximation..........90

4.4 Prediction Accuracy of the YL Model..........92
4.4.1 Fatigue Life Estimation..........92
4.4.2 Correlation of Stress Ratio and Model Parameters..........94
4.4.3 Examination of the Invariability of the Parameters in the YL Model..........98
4.4.4 Residual Strength Approximation..........108

4.5 Residual Mechanical Properties of Glass-Filled Polycarbonate and ABS..........109

5. Conclusions and Suggestions for Future Studies..........118

6. Bibliography..........122

LIST OF TABLES

Table 3.1. Four different loading conditions for ABS under tensile cyclic loading 57

Table 4.1. The ultimate strength of 45 glass-filled polycarbonate specimens subjected to flexural monotonic test 61

Table 4.2. Fatigue life of 35 glass-filled polycarbonate specimens with the corresponding stress ratio and maximum applied stress 63

Table 4.3. The residual strength and residual energy of 9 glass-filled polycarbonate specimens after subjected to a pre-set number of cycle n 66

Table 4.4. The measured tensile strengths with respect to the number of pre-cycles at various loading conditions for ABS 68

Table 4.5. The residual energy and maximum elongation at failure with respect to number of pre-cycles at various loading conditions for ABS 70

Table 4.6. Values of α and β determined from flexural fatigue tests of glass-filled polycarbonate at different stress ratios 76

Table 4.7. The determined b, c and K values from literature 78

Table 4.8. Tension-compression fatigue scan data from ref. [37] 81

Table 4.9. Tension-tension fatigue scan data provided by ref. [70] 83

Table 4.10. The 36 possible b, c and K values that yield the minimum sum of fractional difference associated with the theoretical and measured residual strength 87

Table 4.11. The calculated c values with the corresponding loading conditions on glass-filled polycarbonate 102

Table 4.12. The b value evaluated when those irregular c are replaced with the value observed in the trend in Figure 4.22 104

Table 4.13. The b values evaluated when the c follow a completely reverse trend 105

Table 4.14. The values of b^* and c according to equations (4-12) and (4-13) with respect to different loading conditions 106

LIST OF FIGURES

Figure 2.1. A plot of $\ln\{\ln[1/P[\sigma_n(0)]]\}$ against $\ln[\sigma_n(0)]$ for all the measured monotonic ultimate strength (♦), with three chosen points (p1, p2, p3) on the curve 16

Figure 2.2. A plot of $\ln\{\ln[1/P[\sigma_n(0)]]\}$ against $\ln[\sigma_n(0)-y_0]$ for all the measured monotonic ultimate strength (▲), with a linear curve fit 19

Figure 2.3 (a) The distribution function of monotonic ultimate strength and measured data from ref. [35], (b) the distribution function of monotonic ultimate strength and the calculated ultimate strength σ_{cal0} from ref. [35] 28

Figure 2.4. Measured residual strength at two loading conditions with the theoretical prediction from the DC model shown by the curves, from ref. [59]. The bars at each point represent the standard deviation 31

Figure 2.5. A plot of strength against time according to equation (2-42) with $Z>0$, $Z=0$ and $Z<0$, from ref. [27] 32

Figure 2.6. Measured residual strength at two loading conditions with the theoretical prediction from the YL model shown as curves, from ref. [59]. The bars at each point represent the standard deviation 39

Figure 3.1. SEM image clearly shows the presence of glass-fibre in the polycarbonate matrix 49

Figure 3.2. The dimensions of a dum-bell shaped ABS specimen 50

Figure 3.3. Bending moment diagram for glass-filled polycarbonate specimen under (a) 3-point bending test and (b) 4-point bending test 51

Figure 3.4. MTS model 810 material testing system with 4-point bending fixture 53

Figure 3.5. Overall 4-point bending setup and glass-filled polycarbonate specimen dimensions 54

Figure 3.6. Experimental setup of the tensile test and the corresponding ABS specimen configuration 58

Figure 4.1. SEM image of the fracture surface of glass-filled polycarbonate generated by flexural monotonic test 61

Figure 4.2. Typical load-displacement curve of flexural monotonic test of glass-filled polycarbonate 62

Figure 4.3. (a) A plot of maximum cyclic stress against log N for glass-filled polycarbonate specimens tested at R=0.5, 0.4, 0.3 and 0.1 (b) The S-N curve of the measured fatigue life of glass-filled polycarbonate at R=0.5, 0.4, 0.3 and 0.1 64

Figure 4.4. Load-displacement curve for flexural fatigue testing of glass-filled polycarbonate at σ_{max} = 78.3MPa and R = 0.5 ... 65

Figure 4.5. Load-displacement curves of ABS specimens after subjecting to different numbers of fatigue cycles at $R= 0.5$ and $\sigma_{max}=0.8 \cdot \sigma_{t0}$. The curves for 10,000 and 1,000 cycles have offset in both load and displacement, but each curve starts at zero load and zero displacement ... 72

Figure 4.6. The measured monotonic ultimate strength of glass-filled polycarbonate and the probability of survival based on the 2-parameter Weibull distribution ... 73

Figure 4.7. The measured monotonic ultimate strength of glass-filled polycarbonate and the probability of survival based on the 3-parameter Weibull distribution ... 74

Figure 4.8. The distribution of the calculated ultimate strength of glass-filled polycarbonate from fatigue life data using the DC model and the statistical distribution of the monotonic counterpart ... 75

Figure 4.9. Linear curve fit of Q versus $(N^{\beta}-1)$ for determining the constant α and β for flexural fatigue tests of glass-filled polycarbonate carried out at R=0.1, 0.5 ... 77

Figure 4.10. Range and combination of parameters, b, c and K considered for the YL model ... 79

Figure 4.11. The prediction by the YL model (c=39, b=9.5 and K=3E-26), together with the measured residual strength (♦) of glass-filled polycarbonate at R=0.5 and σ_{max}=78.3MPa ... 80

Figure 4.12. Residual strength estimation by the YL model and the measured data of glass-filled polycarbonate at R=0.5 and $\sigma_{max}=0.6\sigma_n(0$ ... 86

Figure 4.13. Non-dimensional maximum applied cyclic stress versus log N for the theoretical and measured flexural fatigue data of glass-filled polycarbonate at R=0.5, 0.4, 0.3 and 0.1 ... 89

Figure 4.14. A plot of Q with respect to log N for all the flexural fatigue data of glass-filled polycarbonate irrespective of stress ratios ... 90

Figure 4.15 Comparison of the DC model prediction and the measured data of glass-filled polycarbonate on residual strength ... 91

Figure 4.16. Theoretical and experimental non-dimensional maximum applied stress against fatigue life of glass-filled polycarbonate for various stress ratio, with b=9.4, c=26, K=5E-20 ... 93

Figure 4.17. Non-dimensional maximum applied cyclic stress versus log N for the YL model prediction and the fatigue life data of glass-filled polycarbonate, with fixed constant c=26 and b=9.4 ... 95

Figure 4.18. Non-dimensional maximum applied cyclic stress versus log N for the YL model prediction and the fatigue life data of glass-filled polycarbonate, with fixed constant c=26 and K=5E-20 ... 95

Figure 4.19. Linear relationship between the YL model parameter b and stress ratio R, with c and K fixed at 26 and 5E-20 respectively 96

Figure 4.20. Exponential relationship between the YL model parameter K and stress ratio R, with c and b fixed at 26 and 9.4 respectively 97

Figure 4.21. A semi-ln plot of K against R, with c and b fixed at 26 and 9.4 respectively 98

Figure 4.22. The general increasing trend of maximum cyclic stress with respect to the value of parameter c based on tests conducted on glass-filled polycarbonate 103

Figure 4.23. Residual strength estimation by the YL model at R=0.5, 0.4, 0.3 and $\sigma_{max}=0.6\sigma_n(0)$, with measured data (♦) of glass-filled polycarbonate at R=0.5 and $\sigma_{max}=0.6\sigma_n(0)$ 108

Figure 4.24. Plot of residual strength against the number of pre-cycle at a loading condition of R=0.5 and $\sigma_{max}=0.6\sigma_n(0)$ for glass-filled polycarbonate 110

Figure 4.25. Plot of residual energy against the number of pre-cycle at a loading condition of R=0.5 and $\sigma_{max}=0.6\sigma_n(0)$ for glass-filled polycarbonate 110

Figure 4.26. A plot of residual tensile strength of ABS against n at $R=0.5$, and $\sigma_{max}=0.8\sigma_n(0)$ 111

Figure 4.27. A plot of residual tensile strength of ABS against n at $R=0.3$, and $\sigma_{max}=0.8\sigma_n(0)$ 112

Figure 4.28. A plot of residual tensile strength of ABS against n at $R=0.1$, and $\sigma_{max}=0.8\sigma_n(0)$ 112

Figure 4.29. A plot of residual tensile strength of ABS against n at $R=0.3$, and $\sigma_{max}=0.6\sigma_n(0)$ 113

Figure 4.30. A plot of tensile residual energy and maximum elongation at failure of ABS against n at $R=0.5$, and $\sigma_{max}=0.8\sigma_n(0)$ 114

Figure 4.31. A plot of tensile residual energy and maximum elongation at failure of ABS against n at $R=0.3$, and $\sigma_{max}=0.8\sigma_n(0)$ 114

Figure 4.32. A plot of tensile residual energy and maximum elongation at failure of ABS against n at $R=0.1$, and $\sigma_{max}=0.8\sigma_n(0)$ 115

Figure 4.33. A plot of tensile residual energy and maximum elongation at failure of ABS against n at $R=0.3$, and $\sigma_{max}=0.6\sigma_n(0)$ 115

LIST OF NOMENCLATURE

A, B	constants
A'	function of applied stress level during cyclic loading
a, a_0, $\bar{b}$, α, β	model constants for the DC model
a'	a value on the abscissa that corresponds to zero in the ordinate
B_0	the probability of a specimen that will fail under a high load r_0
b, c, K	model parameters for the YL model
b_1, K_1	parameters associated with the S-N_1 curve representation
b_{min}, b_{max}	minimum and maximum values of parameter b
b^*	in terms of S, K and N, equation (4-12)
c_{min}, c_{max}	minimum and maximum values of parameter c
ct	half specimen thickness
D	damage parameter
d	constant distance on the ordinate
ΔE	change in Young's modulus after N cycles of loading
E_0	Young's modulus of the virgin material
$E(n)$	Young's modulus after n fatigue pre-cycles
E_f	Young's modulus just before failure
$Er_n(n)$	residual energy after n fatigue cycle
$Er_{tn}(n)$	tensile residual energy after n fatigue cycle
$error_1$, $error_2$, $error_3$	fractional errors associated with the first, second and third central moments
$F_{\sigma_u(0)}$	probability of failure regarding the monotonic ultimate strength
F_N	probability of failure regarding the fatigue lifetime
$f(S, R)$	function of stress range and stress ratio
g_1, g_2	weight factors in calculating the mean square difference
h	number of specimens undergoing flexural monotonic test
i, p, w	positive integers
I	the moment of inertia of the cross section
j	number of specimens undergoing flexural fatigue loading
K_{min}, K_{max}	minimum and maximum values of parameter K
ls	load span
M	bending moment
m_1, m_2, m_3	1st, 2nd and 3rd central moments based on monotonic ultimate strength
N	number of cycles to fatigue failure
N_0	the minimum number of cycles to fatigue failure after surviving r_0
N^*, $\hat{N}$, $\hat{N}'$, N''	arbitrary number of cycles to fatigue failure
$\bar{N}$, N_1	characteristic life for the $S-\bar{N}$ and $S-N_1$ curve representation
N'	random variable in terms of η and N_1
n	number of fatigue cycles
n_0, n_1	arbitrary number of fatigue cycles
$P_s(y)$	probability of survival regarding y

$P\{\sigma_n(0) \leq y\}$	probability of finding a $\sigma_n(0)$ value that is less than or equal to y
P	applied load
P_{max}	maximum applied load
P_{mean}	mean applied load
P_{min}	minimum applied load
p1, p2, p3	denoted as thee points on a curve
$p1', p2', p3'$	the abscissa component of point p1, p2 and p3
Q	left-hand-side term of equation (2-16), $(\frac{\sigma_n(0)}{\sigma_{\max}} - 1) \cdot (\frac{1}{1-R})$
R	stress ratio ($\sigma_{\min} / \sigma_{\max}$)
R_1, R_2	stress ratios corresponds to the 1st and 2nd loading conditions
r	radius of curvature
r_0	the level of high load applied to the specimen
S	stress range ($\sigma_{\max} - \sigma_{\min}$)
Scl_Y	scale factors for the ordinate
s'	function of applied stress level during cyclic loading
ss	support span
T	time when sample fails
Tp	temperature of specimen
t	time
V	variable depending on loading condition at time t
v, L	constants
$x_1, \ldots x_h$	measured ultimate strengths of the corresponding h number of specimens
x_{p1}, x_{p2}, x_{p3} or $\sigma_n(0)_{p1}, \sigma_n(0)_{p2}, \sigma_n(0)_{p3}$	monotonic ultimate strength corresponding to the points p1, p2 and p3
Y_1, Y_2, Y_3	the ordinate components of point p1, p2 and p3
y	parameter of interest for Weibull distribution
y_0	guaranteed value of y
Z	material constant independent of $\sigma_n(t)$ and t
γ	function of stress ratio and fibre angle orientation
δ	shape parameter of Weibull distribution
$\varepsilon_n(n)$	maximum elongation at failure after n fatigue cycle
η	constant in terms of σ_{max}, λ and c
θ	smallest angle between fibre and loading directions
λ	scale parameter or characteristic life of Weibull distribution
μ_1, μ_2, μ_3	1st, 2nd ad 3rd central moments based on equivalent ultimate strength calculated from fatigue test data
σ	stress
σ_{cal0}	calculated ultimate strength from the DC model in equation (2-36)
σ_{eq}	equivalent ultimate strength calculated from the YL model, equation (2-75), using fatigue test data
$\sigma_{experimental}(n)$	experimental residual strength after n fatigue cycles
σ_{max}	maximum applied cyclic stress
σ_{min}	minimum applied cyclic stress

σ_{max1}, σ_{max2}	maximum cyclic stresses corresponds to the 1st and 2nd loading conditions
$\sigma_{max\varsigma\_\tau}$ ($\varsigma, \tau = 1, 2$)	maximum cyclic stresses corresponds to different loading conditions
$\sigma_n(0)$	monotonic ultimate strength of the virgin material
$\sigma_n(n)$	residual strength of the material after *n* cycles of loading
$\sigma_n(t)$	residual strength after time *t*
$\sigma_{tn}(n)$	the ultimate tensile strength after *n* fatigue cycles
σ_{t0}	monotonic ultimate tensile strength of virgin material
$\sigma_{theoretical}(n)$	theoretical residual strength after *n* fatigue cycles
σ_u	monotonic ultimate strength of the virgin material in ref. [50]
φ	parameter which depends on the moisture content, material properties and loading type
ω	loading frequency in Hz

1. INTRODUCTION

The general public usually considers fatigue as a medical condition, which makes a person feel very tired, weary and sleepy. This is typically induced by the lack of quality sleep or experiencing stress or anxiety for a prolonged period of time. However, fatigue means something completely different in the area of material science. It concerns the progressive damage of material when subjected to repeat cyclic loading with the maximum applied cyclic stress less than the ultimate strength of the virgin material. The mode of loading can be axial, torsional, flexural or any combination of the above. Also, some common types of cyclic stresses include fluctuating tensile where the maximum and minimum applied stress are both positive, and completely reversed where maximum applied stress is equal to the negative of minimum applied stress [1]. Fatigue is actually a complicated process as the life of a subject under cyclic loading can be affected by many factors, such as stress amplitude, stress ratio, loading frequency, temperature, humidity etc.

Fatigue damage is basically composed of three major processes in the microscopical level, crack initiation, crack propagation and final failure. For material suffering from repeat plastic deformation, a crack is usually initiated at some weak points or geometric stress raiser such as holes, notches and sharp corners [2] within the material volume. Once a microscopic crack is nucleated, the stress in the localized area would increase, thus causing the crack to grow and propagate further if there is no physical barrier to arrest it. Final failure occurs when the material can no longer withstand the maximum cyclic load, and fracturing of material is imminent. Fatigue damage is slow, but yet cumulative, catastrophic failure can result if the initiation of a crack at the early stage is left undetected or untreated. An example of that is a disaster that happened in 1992 [3]: a 22 years old B747-200 freighter with a history of 45,746 flight hours was ascending to an altitude of 2,000m from the Amsterdam Airport. Suddenly, the right inboard engine and pylon broke off and separated from the wing of the aircraft. While the separated engine was falling down, it interfered with the path of the left engine and caused that to separate from the wing as well. The aircraft was no longer under control as it lost two of its engines, inevitably crashing into an apartment complex and killing fifty civilians and four crew members. Through a detail investigation of the accident, it became clear that fatigue failure of attachment components on the pylon - a couple of 4340 low-alloy steel fuse pins was the cause. Therefore, the area of fatigue loading must be taken into consideration carefully in design.

The history of fatigue was dated back to the 18th century, a comprehensive discussion on the history of fatigue is given by Schutz [4], and some of the significant events are highlighted below. The first article about fatigue was published by Wilhelm Albert in 1837, and the importance of stress concentration effect was recognized in 1842 through investigation of railroad axle failures by William Rankine. Starting from 1860, fatigue testing on various aspects was finally undertaken. The use of optical microscope for studying microcracks became popular in the 1900s [5], and the fatigue failure initiated by microscopic crack was demonstrated. The major contribution by Irwin was the introduction of the stress intensity factor, which forms the basis for fatigue crack growth life prediction [6]. From then on, theories on fatigue crack growth, life prediction, modulus degradation were developed. Even nowadays, the research in the area of fatigue behavior is still of great interest, but the attention has been shifted from traditional metals to biomaterials, nanomaterials, composite materials and polymers, as they can be mass produced, and tailor-made. Due to the environmentally friendly feature of thermoplastics, they are widely used in various applications. Commodity, intermediate, engineering and advanced thermoplastics offer different performance ranging from low to high cost [7]. Particulate fillers (e.g. glass beads and metallic powders) or fibre reinforcements (e.g. glass and carbon fibres) can also be added to polymer resins during the fabrication process, so that some of the desired mechanical properties can be enhanced. Although glass-filled polycarbonate and high impact grade poly(acrylonitrile-butadiene-styrene) (ABS) are both thermoplastics, their fracture behavior is completely different as the former fails in a brittle manner while the later demonstrates ductile failure.

Brittle and ductile failures are common modes of failure in materials. Limited amount of deformation is permitted in brittle materials before final fracture, since the materials lack the ability to absorb a large amount of energy. Therefore, the stress-strain curve of a brittle polymer exhibits a directly proportional relationship until failure occurs, and the final fracture is usually characterized by rapid snapping of the material. On the other hand, ductile failure that takes place at room temperature can either exhibit necking behavior or uniform extension without necking after the yield point [8]. There is a wide range of difference in characteristics and performance between the two classes of materials, so attention must be paid when selecting materials for intended applications.

The attention of the current study is on the fatigue resistance of materials that exhibit brittle or ductile failure, focusing on the prediction accuracy of mechanical properties of the materials after being subjected to cyclic loading.

1.1 Literature Review

There has been over a century worth of theoretical and experimental studies regarding the fatigue behavior of materials, but the shift in material trend from metals to composite materials and engineering plastics was observed in the last few decades. Regardless of the materials under investigation, the area of fatigue study can roughly be classified into three main categories based on degradation mechanisms, manufacturing and processing effect, and failure prediction. Some representative studies from each of the above classifications will be highlighted, with the particular emphasis on the modeling of fatigue life and mechanical properties of materials, as they are the focus of the current study. However, this literature review is not intended to be exhaustive, instead it anticipated to provide a brief overview of some significant fatigue studies in the last few decades.

The driving forces in fatigue damage mechanism can come from mechanical loads, thermal loads, chemical loads, environmental effects, etc. Mechanical loads include tensile, compressive and flexural which are commonly encountered in structural components and load-bearing applications. There are studies concerning fatigue loading in various loading modes of composite materials, and their damage mechanisms such as matrix cracking, fibre-matrix debonding, delamination, etc. have been reported. Three distinct damage mechanisms were related to the foam core of sandwich beams of glass-fibre-reinforced epoxy under flexural fatigue loading. It was observed that the foam skin debonded parallel to the beam axis, then it grew along the interface and finally extended to the core as a shear crack. The unstable growth of the crack marked the final failure of the specimens [9]. The damage in notched pultruded composite rods under rotation and bending fatigue loading [10] was mainly due to fibre-matrix debonding initiated at the notch root. Tensile rupture of fibre resulted if the stress amplitude was high. It was concluded that the stiffness ratio of the damaged specimen to an undamaged specimen can be used to measure the degree of damage. Carbon fibre reinforced polymers were studied under fatigue biaxial bending [11], in which the damage was mainly caused by matrix cracking and delamination during the cyclic loading. The damage mechanism in adhesive-bonded joints is also a popular topic in fatigue studies [12]. For example, crack initially appeared at the adhesive/adhered interface (adhesive failure) for butt joint with plasticizer-modified adhesive, but it appeared in the middle of the adhesive (cohesive failure) layer for butt joint with rubber-modified adhesive. This is because the stress and strain distribution of the adhesive is different in the above two cases. It has been realized that the damage mechanisms in composite materials driven by mechanical loads are matrix cracking, fibre-matrix debonding, and delmaination.

Structures or components are likely to be subjected to thermal cyclic loading if their service environment is under temperature fluctuation constantly. For example, hot and cold water mixes in the T-junction of a piping system causes temperature fluctuation in the inner surface of the pipe, which induces thermal cyclic stress near the pipe surface and can potentially cause crack initiation [13]. Thermal fatigue can also come from the frictional heat variation experienced by disk brakes for automobiles in service [14]. The fatigue response of different materials under thermo-mechanical loading was studied experimentally. It was shown that the reduction in life of specimen under thermo-mechanical load was much more severe than that under iso-thermal low cycle fatigue loading [15]. The coupling of thermal fatigue damage and oxidation damage was investigated, and it was shown that if material subject to thermal cycling in air or oxygen-rich environment, the damage process would be accelerated [16]. The fatigue damage of materials caused by oxidation at different temperatures and/or environments was discussed in the literature [17-19]. The studies suggested that the damage would increase if it is coupled with other degradation mechanisms that were driven by other kinds of loading.

Another popular area in fatigue study of composite materials concerns the manufacturing and processing effect associated with initial defects, machining, curing, stacking sequence, etc. Initial defects are commonly introduced to the materials during the manufacturing and fabrication process, which can be of different size, shape, orientation and location within the volume. Their existence definitely has an impact on the fatigue behavior of the materials, and various studies have been conducted to learn more about their effects. For instance, inclusions and voids are easily introduced to the materials during casting, which are known to be responsible for reducing fatigue life. A study showed that size, shape and number of inclusions and voids on the surface of A359-SiC have the most significant effect in decreasing the fatigue life [20]. The effect of initial defects was investigated for glass-fibre reinforced plastics in helicopter rotor component [21] and springs of freight vehicles [22]. It was found that the cracks are typically initiated from those initial defects and propagate further. The major findings include the allowable initial defect size for the helicopter rotor components which can be calculated using the concept of energy release rate [21]. The constituents of the material and the molding conditions affect greatly the presence of defects in materials, which can significantly reduce their life [22]. Therefore, great attention must be paid during the fabrication process in order to avoid as many defects as possible in the material. For example, the effect of curing conditions, such as applied pressure and temperature, on adhesive joints was found to be important for the load bearing capability of the product [23]. This is due to the residual thermal stresses that arise from pressure increase which in turn increases the curing temperature. Another study was done concerning the effect on adhesive joint based on two different methods of curing, using either oven or induction (electromagnetic heating) [24]. It was reported that the two curing methods produce the adhesive layer with similar strength and critical fracture energy.

Crack growth modeling, life prediction, damage mechanism characterization, and durability enhancement are also popular area of fatigue for study. Actually, fatigue studies can be conducted in various means: finite element analysis, numerical simulation, statistical analysis, theoretical implementation and experimental investigation. The aspect of fatigue life prediction through modeling is especially relevant to the current study and will be reviewed next. Some of the important features regarding the existing fatigue models were pointed out by Degrieck and VanPaepegem [25] who classified the existing fatigue models into three main categories: fatigue life models, progressive damage models, and phenomenological models for predicting residual stiffness and residual strength. Each class of models has its own criteria to determine the final failure for predicting the fatigue life of the materials.

Although the fatigue life modeling does not take into account the damage mechanisms associated with the failure of the materials, it can predict the life based on its failure criteria and information obtained from a S-N curve. The progressive damage model relates more closely to the physical phenomena of the damage process, in which a specific damage is related to the evolution law. Predicting damage growth is usually the objective of this type of model. An alternative progressive damage model is to relate the damage growth to the residual mechanical properties, like residual strength and stiffness. The phenomenological models that are associated with residual stiffness use damage variables to describe the deterioration of the material elastic properties during cyclic loading. The damage growth rate is based on macroscopically observable properties, and is not related to actual damage mechanism. The phenomenological models that predict residual strength describe the deterioration of material strength after a certain number of fatigue cycles. The two theoretical models that have been considered in this study are both strength-based.

Throughout this study, residual strength is defined as the ultimate strength of the material after undergoing a certain number of cyclic loading. Fatigue models associated with residual strength can basically be classified into two categories: sudden death and wearout models. The first kind of models demonstrates that at low-cycle fatigue, the residual strength remains approximately constant throughout the course of the cyclic loading, but it decreases rapidly when approaching final failure. A degradation equation that incorporates the sudden death notion was suggested by Chou and Croman [26], for a given ultimate strength and fatigue life, the residual strength can be predicted based on the strength-life equal rank assumption, firstly proposed by Hahn and Kim [27]. Chou and Croman [28] later derived two expressions which evaluate the mean residual strength of the degradation model and the sudden death model. The prediction was then compared with 6 different sets of experimental data for graphite/epoxy composites subjected to tension-tension fatigue loading. The comparison showed reasonable agreement, especially for the sudden death model that was proven to be most effective in modeling the residual strength of unidirectional composites.

The concept of the residual strength wearout model generally assumes that the residual strength decrease gradually as the number of fatigue cycle increases, it was first proposed and discussed by Halpin, Jerina and Johnson [29]. They suggested that the change in residual strength follows a degradation power law relationship, which was then followed by many researchers. Different residual strength-based models were proposed, which take into account different parameters. For example, Yang and Jones [30] proposed a residual strength relationship with the number of fatigue cycles, which incorporated the statistical distribution of ultimate strength and fatigue life. Daniel and Charewicz's residual strength model [31] for cross-ply graphite/epoxy laminates was based on the normalized change in residual strength in tensile fatigue loading. It was believed that the fatigue damage is only a function of residual strength of the material.

Schaff and Davidson [32] developed a phenomenological strength-base wearout model to predict the residual strength and fatigue life of composite materials under constant amplitude and two stress levels of loading. A residual strength equation was then derived which considered the peak stress, number of loading cycles, constant-amplitude fatigue life and static strength. One of the parameters in the governing equation can act as an indication of the type of degradation trend of residual strength, e.g. linear strength degradation, sudden death degradation and rapid initial loss of material strength. This wear-out model was further developed to consider the randomly-ordered loading spectra [33]. Good agreement was found between theoretical prediction and experimental data.

D'Amore and Caprino [34] proposed a two-parameter residual strength degradation model (DC model), assuming that the residual strength decreases monotonically with the increase in the number of cyclic loading, based on the criterion that at the time of complete failure, residual strength is equal to the maximum cyclic stress applied during the testing. The study showed that the theoretical model provides an effective description of the effect of the stress ratio for composites under flexural fatigue loading. The model also offers a reasonable estimate of the S-N curve. Since there is significant variability in the nature of fatigue data, a statistical model [35], based on the residual strength degradation of the DC model and the 2-parameter Weibull distribution of monotonic ultimate strength, was implemented for the design purpose. The high versatility of the model was demonstrated by its applicability on composites with either thermosetting or thermoplastic matrix, showing that the model has the advantage of using a minimum number of experimental data to characterize the fatigue response of a material by means of residual strength.

The fatigue residual strength degradation model proposed by Yang and Liu [36-37], follows the rate equation in ref. [27] with the change in the time domain. The main assumption for the Yang and Liu's model (YL model) is that the rate of change of the residual strength is inversely proportional to some power of the residual strength itself. Three parameters appear in the governing equation, which can be determined using a set of monotonic and fatigue scan data. The governing equation is expressed in terms of mean monotonic ultimate strength, residual strength, number of pre-cycles, and the scale parameter for the Weibull distribution of the ultimate strength. The model is suggested to be able to predict fatigue life, residual strength, as well as their statistical distribution.

The DC and the YL models are both strength-based models, however, it is more complicated to determined the model constants for the YL model although it offers an extra degree of freedom. The prediction accuracy on fatigue life, residual strength and the applicability of these two models on brittle and ductile materials will be assessed in this study.

1.2 Objectives and Scope of the Study

Structural parts and machine components are likely to be under cyclic loads introduced by vibrations and pressure pulses while in service. The knowledge of fatigue life of those parts is especially important for safety. The mechanical properties of cyclically loaded material, before reaching the point of failure are worth studying. Valuable information regarding the performance of the structure can be obtained if the fatigue life, and the remaining ultimate strength and toughness can be predicted based on experimental data.

Overall, the variation in mechanical properties of cyclically loaded materials fail in brittle and ductile manners is of great interest, and will be explored in further detail using glass-filled polycarbonate and ABS, respectively. Besides, the applicability of two existing residual strength degradation models, the DC and YL models, on those materials will be examined for their prediction accuracy. The pursuit of an energy-based fatigue model is the ultimate objective, which should allow a better estimation of fatigue life for ductile fracture materials under cyclic loading.

A series of flexural monotonic and fatigue tests were performed at various loading conditions on glass-filled polycarbonate. The results were then compared with the theoretical predictions from the DC and YL models for their accuracy in estimating fatigue life, as well as the residual strength. The DC model is under the assumption that the rate of decrease of residual strength is a power law function of the number of cycles, while the YL model assumes that the rate of change of residual strength is inversely proportional to some power of residual strength itself. The effect of stress ratio on fatigue behavior of composite has been well studied [38-44] to establish that by varying the stress ratio, fatigue life changes. The stress ratio effect is accounted for explicitly only in the DC model, therefore a correlation is then proposed to incorporate such a notion into the YL model while the nature of the model parameters is examined in detail. This enables a reasonable representation of the S-N curve associated with a range of stress ratio, but the prediction capability on residual strength still needs to be verified experimentally.

The mechanical properties, such as remaining strength and ability to absorb energy after being subjected to cyclic loading, of a high impact grade ABS was measured under monotonic tensile test after pre-cycled at various stress ratios and maximum applied cyclic stresses. The characteristics of the above mechanical properties with respect to the number of cycles will be examined and compared for different loading conditions. The degradation trend was only observed in the total energy absorption (residual energy) with respect to the number of fatigue cycles, but not on residual strength. Based on this preliminary result, a fatigue residual energy degradation model for ductile materials could be developed and this should offer a better characterization of fatigue behavior of ductile fractured materials. However, the large scatter of measured residual energy has prevented me from obtaining an accurate degradation trend which is needed for the development of such a model.

This thesis provides a comprehensive documentation of the study on the prediction of mechanical properties of brittle and ductile fractured polymers under cyclic loading. Chapter 1 is an introduction and motivation to the topic of fatigue study. Literature review of various subjects related to fatigue, as well as the objective and scope of the study has been given in this chapter. The theoretical derivations, assumptions, and technical details of the DC model and the YL model are provided in Chapter 2, Fundamental Principles of the Theoretical Models. Chapter 3 outlined the experimental details, such as experiential setup and material information concerning the flexural monotonic and fatigue test for glass-filled polycarbonate, and tensile fatigue test for high impact grade ABS. Chapter 4, Results and Discussions contains the experimental results, data analysis for determining the model parameters, and discussion of the results obtained. The conclusions of the study, as well as the recommendations for the future study are suggested in Chapter 5. The last chapter includes the bibliography of all references used in this thesis in the order of appearance.

2. FUNDAMENTAL PRINCIPLES OF THE THEORETICAL MODELS

This chapter is intended to review two existing fatigue models based on residual strength degradation that are essential for this study: D'Amore and Caprino's model (DC model) [34] and Yang and Liu's model (YL model) [36-37]. The subsequent discussion includes assumptions for each of the models', theoretical backgrounds and analytical techniques, concerning mainly the prediction capability on fatigue life and residual strength. The content in refs. [34, 36-37] were followed closely.

2.1 Determination of Weibull Parameters

Weibull distribution is well established in the field of engineering statistics. It is commonly used in describing data related to aging or property decaying of parts. However, focus of the current study is not on the statistical distribution of fatigue life or the statistical distribution of residual strength. Rather, the centre of attention is on the residual mechanical behavior of material that fractures in either a brittle or ductile manner. The DC model and the YL model require knowledge of the scale parameter (to be defined later) of the Weibull distribution. Therefore, only the process of evaluating the Weibull parameters is of interest. Details of the process were outlined in ref. [45], and followed closely here. Waloddi Weibull invented the Weibull distribution in 1937 [46], the expressions for the 3- and 2- parameter Weibull distribution are given in the equations (2-1) and (2-2) respectively:

$$P_s(y) = \exp\left[-\left(\frac{y - y_0}{\lambda - y_0}\right)^{\delta}\right], \qquad y \geq y_0 \qquad (2\text{-}1)$$

$$P_s(y) = \exp\left[-\left(\frac{y}{\lambda}\right)^{\delta}\right], \qquad y \geq 0 \qquad (2\text{-}2)$$

in which $P_s(y)$ = probability of survival

y = parameter of interest

y_0 = guaranteed value of y ($y_0 \geq 0$)

λ = scale parameter or characteristic life ($\lambda \geq y_0$)

δ = shape parameter ($\delta > 0$)

The guaranteed value, scale and shape parameters are all constants to be determined by experiments. The guaranteed value (or location parameter) y_0 represents the boundary on the lower tail of the distribution function, it can shift the function either to the left or right on the abscissa. The 2-parameter Weibull distribution is obtained when y_0 is taken to be zero, which means the probability function starts at the origin. Suppose the parameter of interest y is stress, the probability of survival is 1 when zero stress is applied if there is no failure during specimen production. This also means if the specimens are not under any state of stress, all the specimens are expected to survive. The mathematical formulas of the Weibull distributions suggest that, the probability of survival would decrease if the stress level increases. Also, no specimens are expected to survive if the stress level is infinite. The scale parameter λ can be understood as the level of stress that permits 37% of the specimens to survive. That is, when the value of stress is equal to that of the scale parameter, then the probability of survival is approximately 37%. On the other hand, the shape parameter indicates the rate of strength decay as it approaches the value of the scale parameter. To determine the guaranteed value, shape and scale parameters, a batch of specimens should be tested to determine the probability of survival as a function of stress level. The process for determining the three parameters in equation (2-1) will be discussed as follows, while the parameters for the 2-parameter Weibull distribution can be evaluated in the same way with y_0 taken to be zero.

In order to determine y_0, λ and δ, two plots are needed to rectify the Weibull distribution function. The first one can be used to determine the guaranteed value y_0, while the other one for evaluating the scale and shape parameters. Plot $\ln\left[\ln\left(\frac{1}{P_s[\sigma_n(0)]}\right)\right]$ against $\ln[\sigma_n(0)]$ for all the monotonic test data, where $\sigma_n(0)$ is monotonic ultimate strength for this study. Then a curve is drawn through all the data points (◆).

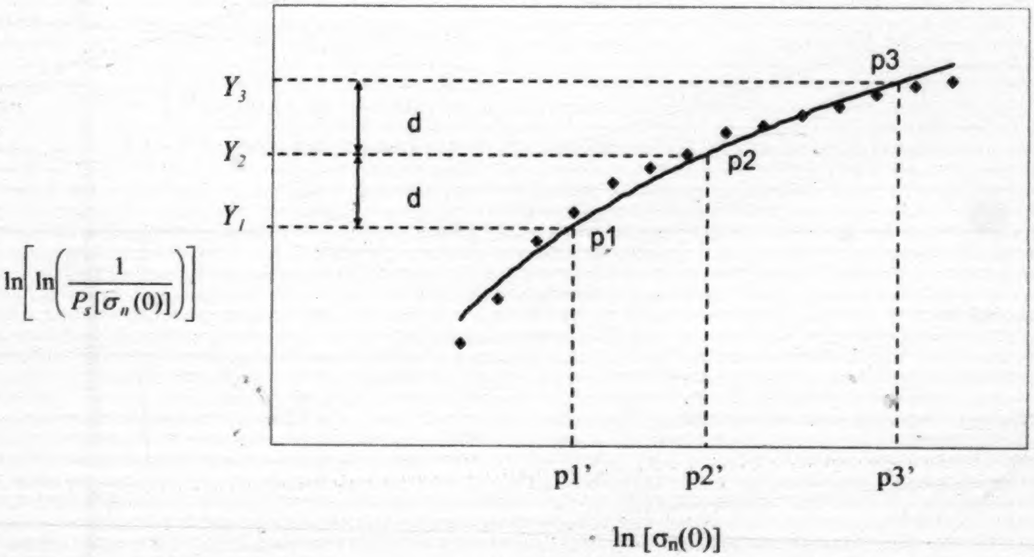
Y_3
Y_2
Y_1
d
d
p1
p2
p3
$\ln\left[\ln\left(\frac{1}{P_s[\sigma_n(0)]}\right)\right]$
p1'
p2'
p3'
$\ln[\sigma_n(0)]$

Figure 2.1. A plot of $\ln\{\ln[1/P[\sigma_n(0)]]\}$ against $\ln[\sigma_n(0)]$ for all the measured monotonic ultimate strength (◆), with three chosen points (p1, p2, p3) on the curve

Then three points (p1, p2 and p3) were located on the curve in Figure 2.1 to be equally spaced with respect to the ordinate. That is, let their corresponding distances from the origin be Y_1, Y_2 and Y_3, respectively. We have:

$$Y_2 - Y_1 = Y_3 - Y_2 = d \tag{2-3}$$

where d is a positive number. If the abscissa values of the points are taken to be p1', p2' and p3' respectively, by applying the natural logarithm to those values, the corresponding monotonic ultimate strengths (x_{p1}, x_{p2}, x_{p3}) are

$$x_{p1} = e^{p1'} \qquad x_{p2} = e^{p2'} \qquad x_{p3} = e^{p3'} \tag{2-4}$$

The ordinate in Figure 2.1 is $\ln\left[\ln\left(\frac{1}{P_s[\sigma_n(0)]}\right)\right]$, therefore the distance on the ordinate from the origin, Y, can be expressed in terms of scale factor Scl_Y as follows,

$$Y = Scl_Y \cdot \ln\left[\ln\left(\frac{1}{P_s[\sigma_n(0)]}\right)\right] \tag{2-5}$$

The scale factor Scl_Y is assumed to be linear and independent of the probability of survival of the virgin material ultimate strength. Thus, substituting equation (2-5) as Y_1, Y_2 and Y_3 into equation (2-3), gives:

$$\begin{aligned} &Scl_Y \cdot \ln\left[\ln\left(\frac{1}{P_s[\sigma_n(0)_{p2}]}\right)\right] - Scl_Y \cdot \ln\left[\ln\left(\frac{1}{P_s[\sigma_n(0)_{p1}]}\right)\right] \\ &\qquad = Scl_Y \cdot \ln\left[\ln\left(\frac{1}{P_s[\sigma_n(0)_{p3}]}\right)\right] - Scl_Y \cdot \ln\left[\ln\left(\frac{1}{P_s[\sigma_n(0)_{p2}]}\right)\right] \end{aligned} \tag{2-6}$$

where $\sigma_n(0)_{p1}$, $\sigma_n(0)_{p2}$ and $\sigma_n(0)_{p3}$ corresponds to the monotonic ultimate strength level of the point p1, p2 and p3, which are denoted as x_{p1}, x_{p2} and x_{p3} respectively in equation (2-

4). If the scale factors are cancelled out in equation (2-6), and replace $\sigma_n(0)_{p1}$, $\sigma_n(0)_{p2}$ and $\sigma_n(0)_{p3}$ with x_{p1}, x_{p2} and x_{p3}, we have:

$$\ln\left[\ln\left(\frac{1}{P_s(x_{p2})}\right)\right]-\ln\left[\ln\left(\frac{1}{P_s(x_{p1})}\right)\right]=\ln\left[\ln\left(\frac{1}{P_s(x_{p3})}\right)\right]-\ln\left[\ln\left(\frac{1}{P_s(x_{p2})}\right)\right] \tag{2-7}$$

Taking the natural logarithm twice on equation (2-1), it becomes:

$$\ln\left[\ln\left(\frac{1}{P_s[\sigma_n(0)]}\right)\right]=\delta\ln[\sigma_n(0)-y_0]-\delta\ln(\lambda-y_0) \tag{2-8}$$

Therefore, for the points p1, p2 and p3, equation (2-8) can be expressed as:

$$\ln\left[\ln\left(\frac{1}{P_s(x_{p1})}\right)\right]=\delta\ln(x_{p1}-y_0)-\delta\ln(\lambda-y_0) \tag{2-9}$$

$$\ln\left[\ln\left(\frac{1}{P_s(x_{p2})}\right)\right]=\delta\ln(x_{p2}-y_0)-\delta\ln(\lambda-y_0) \tag{2-10}$$

$$\ln\left[\ln\left(\frac{1}{P_s(x_{p3})}\right)\right]=\delta\ln(x_{p3}-y_0)-\delta\ln(\lambda-y_0) \tag{2-11}$$

Substituting equations (2-9) - (2-11) into equation (2-7), yields,

$$\begin{aligned}&\delta\ln(x_{p2}-y_0)-\delta\ln(\lambda-y_0)-\delta\ln(x_{p1}-y_0)+\delta\ln(\lambda-y_0)\\&=\delta\ln(x_{p3}-y_0)-\delta\ln(\lambda-y_0)-\delta\ln(x_{p2}-y_0)+\delta\ln(\lambda-y_0)\end{aligned} \tag{2-12}$$

Simplify equation (2-12) yields:

$$\ln(x_{p2}-y_0)-\ln(x_{p1}-y_0)=\ln(x_{p3}-y_0)-\ln(x_{p2}-y_0) \tag{2-13}$$

By taking the natural logarithm of equation (2-13) and through rearrangement, it generates the equation for calculating the guaranteed value y_0. The guaranteed value y_0 can be expressed as,

$$y_0 = x_{p2} - \frac{(x_{p3} - x_{p2})(x_{p2} - x_{p1})}{(x_{p3} - x_{p2}) - (x_{p2} - x_{p1})} \qquad (2\text{-}14)$$

With the known value of y_0, a plot of $\ln\left[\ln\left(\frac{1}{P_s[\sigma_n(0)]}\right)\right]$ against $\ln[\sigma_n(0) - y_0]$ can now be obtained for the measured monotonic ultimate strengths, in which a linear curve fit is also presented, as shown in Figure 2.2.

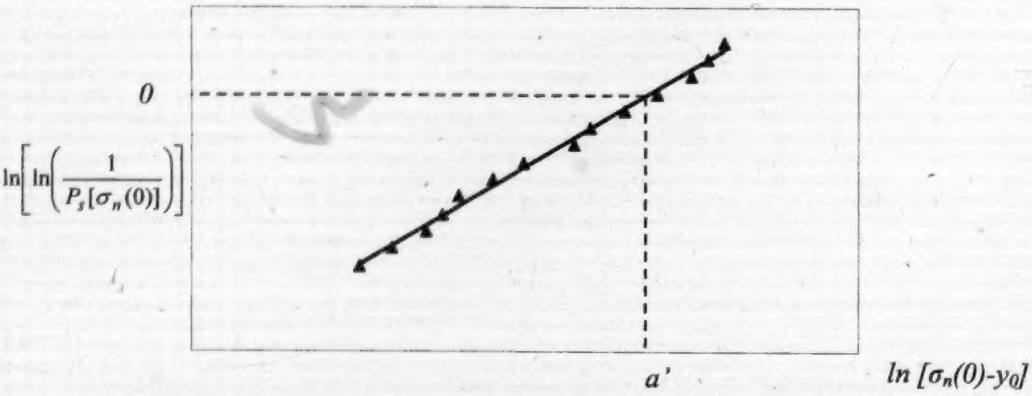

Figure 2.2. A plot of $\ln\{\ln[1/P[\sigma_n(0)]]\}$ against $\ln[\sigma_n(0)-y_0]$ for all the measured monotonic ultimate strength (▲), with a linear curve fit

Note that, if the data do not exhibit a linear trend, then it cannot be described by the Weibull distribution function. However, if the data can indeed be described effectively by the Weibull distribution, then the remaining parameters (λ and δ) can be evaluated as follows. If a point on the straight line in Figure 2.2 which corresponds to the value of zero for the ordinate component, that is,

$$\ln\left[\ln\left(\frac{1}{P[\sigma_n(0)]}\right)\right] = 0 \qquad (2\text{-}15)$$

Solving for $P[\sigma_n(0)]$ in equation (2-15) gives the reliability of,

$$P[\sigma_n(0)] = \frac{1}{e} = \frac{1}{2.718} = 0.368 \approx 37\% \tag{2-16}$$

We should keep in mind that the scale parameter λ is the level of applied monotonic stress that allows 37% of the specimens to survive the test. Thus, if a point on the line in Figure 2.2 which has a value of zero for the ordinate component and its value for the abscissa component is denoted as a', then,

$$\ln(\lambda - y_0) = a' \tag{2-17}$$

Thus, the scale parameter λ can be evaluated by equation (2-17):

$$\lambda = e^{a'} + y_0 \tag{2-18}$$

Lastly, the shape parameter δ is just the slope of the fitted straight line in Figure 2.2, since $\ln\left[\ln\left(\frac{1}{P[\sigma_n(0)]}\right)\right] = \delta \cdot \ln[\frac{\sigma_n(0) - y_0}{\lambda - y_0}]$.

The shape and scale parameters for the 2-parameter Weibull distribution can be determined through the same procedure as discussed above, with the guaranteed value y_0 taken to be zero. It is recognized that the 2-parameter Weibull distribution are more commonly used due to its simplicity and effectiveness. However, the 3-parameter Weibull distribution should be considered if the plot of $\ln\left[\ln\left(\frac{1}{P[\sigma_n(0)]}\right)\right]$ against $\ln[\sigma_n(0)]$ follows a curve instead of a straight line. Moreover, the guaranteed value in the 3-parameter Weibull distribution is non-zero. Therefore, a justification is needed for the probability function not starting at the origin. For example, specimen failure could happen during production or fabrication which is before the actual testing. In this case, the probability of survival $P_s(y)$ could be of some value smaller than of 1 when zero stress is applied [47].

2.2 D'Amore and Caprino's Model (DC model)

A power-law damage rate equation based on the stiffness failure criterion was proposed by Wang et al. [48] to study the rate of fatigue damage evolution and accumulation:

$$\frac{dD}{dn} = A \cdot n^{-B} \tag{2-19}$$

In equation (2-19), D is the damage parameter which describes the change in stiffness of the material as a function of n, where n is the number of fatigue cycles that the specimen undergoes. The constants A and B can be determined experimentally. The damage parameter D can also be used to describe other degradation phenomena, such as the ultimate strength and total energy absorbed by the material.

D'Amore et al. [34] presented a residual strength degradation model which accounts for the effect of stress ratio, while predicting the fatigue life of composite materials. The material strength is assumed to undergo a continuous decay during the cyclic loading, and the rate of decrease in material ultimate strength is assumed to follow a power-law relationship with respect to the number of fatigue cycles, in the following formulation that is similar to equation (2-19).

$$\frac{d\sigma_n(n)}{dn} = -a \cdot n^{-\bar{b}} \tag{2-20}$$

in which $\sigma_n(n)$ is the residual strength of the material after n cycles of loading, and constants a and $\bar{b}$ are positive. In order to incorporate the stress level into the model, the assumption was made to relate at least one of the constants to the stress level. In this case, constant $\bar{b}$ is assumed to depend on materials and loading type, while constant a increases linearly with stress range as follows,

$$a = a_0 \cdot S \tag{2-21}$$

where a_0 is a material constant that depends on the loading type, and the stress range S is defined as the difference between maximum and minimum applied stresses during the cyclic loading, i.e.

$$S = \sigma_{\max} - \sigma_{\min} \tag{2-22}$$

Substituting equation (2-21) into equation (2-20) yields:

$$\frac{d\sigma_n(n)}{dn} = -a_0 \cdot S \cdot n^{-\bar{b}} \tag{2-23}$$

Integrating equation (2-23) with respect to n, and replacing S with $\sigma_{max}(1-R)$, where R is the stress ratio $\frac{\sigma_{\min}}{\sigma_{\max}}$, we have

$$\sigma_n(n) = -a_0 \cdot \sigma_{\max} \cdot (1-R) \cdot \frac{n^{1-\bar{b}}}{1-\bar{b}} + const. \tag{2-24}$$

The integration constant that appears in equation (2-24) can be evaluated using the boundary condition that the number of fatigue cycles should be 1 if the residual strength is the same as the ultimate strength of the virgin material, $\sigma_n(0)$. That is, when $n=1$, $\sigma_n(n)=\sigma_n(0)$.

Using this condition, the integration constant was found to be:

$$const. = \sigma_n(0) + a_0 \cdot \sigma_{\max} \cdot (1-R) \cdot (\frac{1}{1-\bar{b}}) \tag{2-25}$$

Substituting equation (2-25) into equation (2-24) yields:

$$\sigma_n(0) - \sigma_n(n) = \alpha \cdot \sigma_{\max} \cdot (1-R) \cdot (n^{\beta} - 1) \tag{2-26}$$

$$\text{with } \alpha = \frac{a_0}{1-\bar{b}} \text{ and } \beta = 1 - \bar{b} \tag{2-27}$$

Based on equation (2-26), the residual strength of the material after being subjected to a number of fatigue cycles can be determined, as long as the constant α and β are known. It is important to note that failure is expected to occur when the residual strength possessed by the material is reduced to the maximum applied stress during cyclic loading. Following this notion that when $\sigma_n(n)=\sigma_{max}$, $n=N$, one can solve for N as

$$N = [1 + \frac{1}{\alpha \cdot (1-R)} \cdot (\frac{\sigma_n(0)}{\sigma_{\max}} - 1)]^{\frac{1}{\beta}} \tag{2-28}$$

Although equation (2-28) was originally derived based on a given S, it was extended to applications that have σ_{max} and R as two independent variables. Equation (2-28) can be rearranged to have the following form:

$$(\frac{\sigma_n(0)}{\sigma_{\max}} - 1) \cdot (\frac{1}{1-R}) = \alpha \cdot (N^{\beta} - 1) \tag{2-29}$$

based on which the two constants α and β can be determined by linear fitting the left-hand side, denoted as Q, against $(N^{\beta} - 1)$ at an assumed β value. The β value is adjusted until the linear fitting of Q versus $(N^{\beta} - 1)$ passes through the origin, of which the slope is the value for α. According to equation (2-29), all fatigue data irrespective of their R values should collapse into a single master curve when Q is plotted against N. If it is indeed so, the DC model can sufficiently account for the effect of cyclic loading on the strength degradation of the material.

Fatigue sensitivity of materials was studied by Caprino et al. [49] using the DC model, by examining how rapidly the strength decreases with the increase of the number of cyclic loading. According to equations (2-20) and (2-21), the rate of decrease in material strength by the cyclic loading is a combined effect of stress range S and the number of cyclic loading n. Equation (2-21) suggests that a_0 represents the material sensitivity to stress range S. Equation (2-23) suggests that the higher the a_0, the more rapid the decrease is in material strength for low cycle fatigue, and thus increase the fatigue sensitivity. The exponent $\bar{b}$ in equation (2-23) is a measure of the effect of n on the rate of decrease of material strength. If $\bar{b}$ increases for high cycle fatigue, the rate of decrease in material strength would decrease, thus lowering the fatigue sensitivity. Overall, the fatigue sensitivity is dominated by a_0 at low cycles, and $\bar{b}$ at high cycles. Equation (2-23) provides a reasonable explanation for different fatigue responses of a material at low-cycle and high-cycle fatigue loading [49].

The DC model was verified experimentally under flexural 4-point bending for various kinds of composite materials, including thermosetting and thermoplastic resins, and a variety of reinforcement. The advantage of this model is that only a small number of experimental data is needed to characterize the fatigue response of a material, and the procedure for determining α and β is relatively simple.

2.2.1 Statistical Implementation of the DC Model

The DC model [35] provides a statistical means to determine the S-N curve for a given probability of failure. The assumptions for the analysis are: (1) the constants α and β in equation (2-26) are not statistical variables, (2) scatter in fatigue data is uniquely due to variability of material strength under monotonic loading, and (3) the scatter in ultimate strength of material can be sufficiently represented by the 2-parameter Weibull distribution.

The analytical process for the statistical analysis in the DC model generally follows the approach taken in ref. [36]. The probability of failure of the monotonic ultimate strength $F_{\sigma n(0)}(y)$ at a stress level y, or the probability $P\{\sigma_n(0) \le y\}$ of finding a $\sigma_n(0)$ value that is less than or equal to y is given as follows:

$$F_{\sigma_n(0)}(y) = P\{\sigma_n(0) \le y\} = 1 - \exp\left[-\left(\frac{y}{\lambda} \right)^{\delta} \right] \tag{2-30}$$

where δ and λ are the shape and scale parameters of 2-parameter Weibull distribution, respectively. It has been established that since $\sigma_n(0)$ is a statistical variable and all other terms except N in equation (2-28) are constants at a given loading condition, N is also a statistical variable. Thus, if $\sigma_n(0)$ follows a 2-parameter Weibull distribution, so does N. Utilizing the expression of N in equation (2-28), the probability of finding a value of N less than or equal to the fatigue life N^* is:

$$F_N(N^*) = P\{N \le N^*\} = P\left\{ \left[1 + \frac{1}{\alpha(1-R)} \cdot \left(\frac{\sigma_n(0)}{\sigma_{\max}} - 1 \right) \right]^{\frac{1}{\beta}} \le N^* \right\} \tag{2-31}$$

Rearranging equation (2-31) yields:

$$F_N(N^*) = P\{\sigma_n(0) \le \sigma_{\max} \cdot [1 + \alpha(N^{*\beta} - 1) \cdot (1 - R)]\} \tag{2-32}$$

Now the probability of failure $F_N(N^*)$ is expressed as the probability of finding a $\sigma_n(0)$ value that is less than or equal to the term $\sigma_{\max} \cdot [1+\alpha(N^{*\beta}-1)\cdot(1-R)]$. By applying equation (2-30) to equation (2-32), the statistical distribution of the fatigue life is:

$$F_N(N^*) = 1 - \exp\left[-\left(\frac{\sigma_{\max}^{\delta}[1+\alpha(N^{*\beta}-1)\cdot(1-R)]^{\delta}}{\lambda^{\delta}}\right)\right] \tag{2-33}$$

When $N^*=1$, equation (2-33) can be reduced to:

$$F_N(1) = 1 - \exp\left[-\left(\frac{\sigma_{\max}}{\lambda}\right)^{\delta}\right] \tag{2-34}$$

which is similar to the distribution of monotonic ultimate strength, as in equation (2-30). Therefore, if a specimen is subject to 1 cycle of fatigue loading, the probability of failure is the same as that under monotonic loading. Thus, the statistical distribution of monotonic ultimate strength is the same as that of fatigue life after 1 cycle. By rearranging equation (2-33), the fatigue life can be calculated directly for a fixed probability of failure at a given R value as in equation (2-35).

$$N^* = \sqrt[\beta]{1+\frac{1}{\alpha\cdot(1-R)}\cdot\left\{\frac{\lambda}{\sigma_{\max}}\cdot\left|\ln[1-F_N(N^*)]\right|^{\frac{1}{\delta}}-1\right\}} \tag{2-35}$$

Based on the assumption of the statistical implementation of the DC model, the scatter in monotonic ultimate strength represented by the 2-parameter Weibull distribution can also represent the statistical distribution of the fatigue test data. In order to assess this hypothesis, solving for $\sigma_n(0)$ in equation (2-28) gives:

$$\sigma_n(0) = \sigma_{cal0} = \sigma_{\max}[1+\alpha(1-R)(N^{\beta}-1)] \tag{2-36}$$

σ_{cal0} is the calculated ultimate strength and it can be evaluated based on the fatigue test data, provided that α and β are determined. It was suggested that the statistical distribution of the monotonic strength can provide a reasonable estimate for the statistical distribution of the calculated ultimate strength from the fatigue test data, since the scatter in the fatigue data is uniquely due to the variability in the monotonic test data. This was indeed illustrated in ref. [35] and shown in Figure 2.3. Figure 2.3(a), the measured monotonic strength and the associated statistical distribution are plotted. Then, the same statistical distribution was plotted in Figure 2.3(b) together with the calculated ultimate strength for each fatigue test data. A good agreement was observed for both cases. The above analysis in ref. [35] does show the validity of the DC model and its statistical approach.

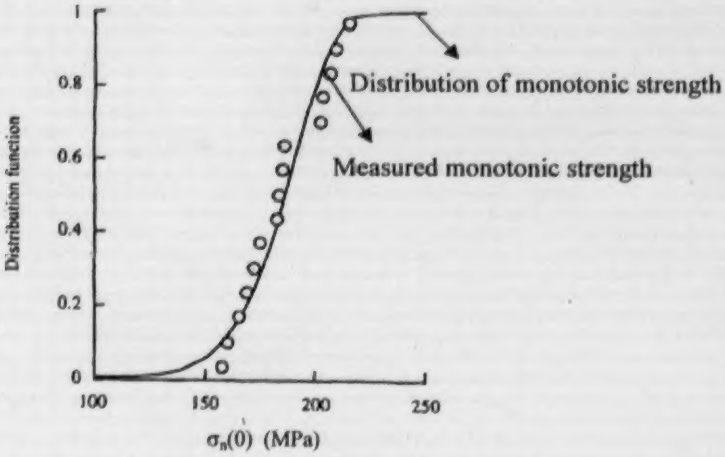

(a)

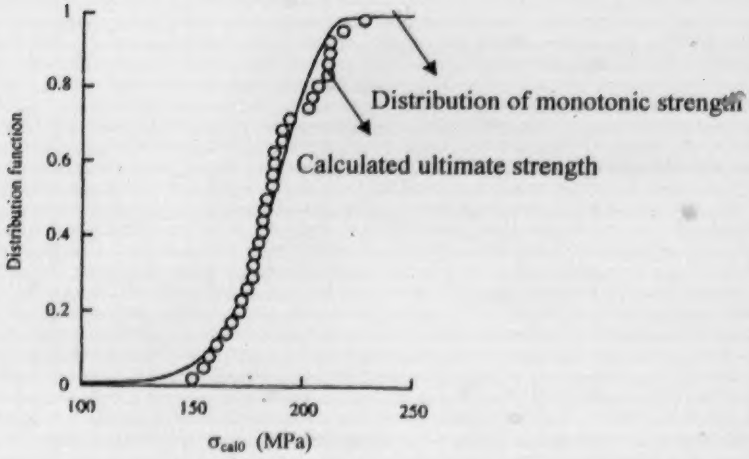

(b)

Figure 2.3 (a) The distribution function of monotonic ultimate strength and measured data from ref. [35] (b) The distribution function of monotonic ultimate strength and the calculated ultimate strength σ_{cal0} from ref. [35]

Based on the rate of residual strength degradation described in equation (2-20), Epaarachchi and Clausen [50] developed a fatigue model which takes into account the effect of stress ratio, loading frequency, and fibre orientation. In the DC model, the constant *a* in equation (2-20) was replaced with a function that is composed of stress ratio *R*, temperature of the specimen *Tp*, ultimate strength of the virgin material σ_u, maximum cyclic stress σ_{max}, and a parameter φ which depends on the moisture content, material properties and loading type. However, the effect of temperature and moisture was not considered. Therefore, the rate of degradation with respect to time *t*, as in equation (2-20), if $f(\varphi, Tp)$ is equal to a constant *A*,

$$\frac{d\sigma}{dt} = -Af(R, \sigma_{\max}, \sigma_u)t^{-M} \tag{2-37}$$

Under a fixed loading frequency, time can be expressed in terms of number of fatigue cycles. Through integration of equation (2-37) from *t=0* to *t=T*, where *T* is the time when sample fails, and by replacing *T* by *N*, where *N* is the number of cycles to failure, we have:

$$\sigma_u - \sigma_{\max} = \alpha f(R, \sigma_{\max}, \sigma_u)\frac{1}{\omega^\beta}(N^\beta - 1) \tag{2-38}$$

where ω is the loading frequency in Hz that relates to the number of fatigue cycles *N* and time *t* as: $\omega = N/t$, and α and β are material constants similar to those in the DC model. Based on the deterministic equation developed by Sendeckyi [51], and Hertzberg and Manson [52], the following relationship was proposed for the function *f*:

$$f(R, \sigma_{\max}, \sigma_u) = \sigma_u^{1-\gamma}\sigma_{\max}^{\gamma}(1-R)^{\gamma} \tag{2-39}$$

It was determined experimentally that based on the rate of fatigue damage propagation in composites, the value for the constant γ should be between 0.6 and 7.6. Epaarachchi and Clausen [50] proposed the following relationship to account for the effect of fibre orientation,

$$\gamma = 1.6 - \phi\sin\theta \tag{2-40}$$

where θ is the smallest angle between fibre direction and loading direction if no fibre is orientated at 0°. The other parameter in equation (2-40), ϕ, is postulated as a function of stress ratio R in the following formulation:

$\phi = \mathrm{R}$ for $-\infty < R < 1$ (tension-tension and reverse loading)

$\phi = \dfrac{1}{R}$ for $1 < R < \infty$ (compression-compression)

For the case of tension-tension cyclic loading, both maximum and minimum applied stresses are positive, therefore R should be between 0 and 1. As for reversed loading, σ_{max} is positive while σ_{min} is negative, and so the stress ratio should be in the negative range. In compression-compression cyclic loading, a negative σ_{min} divided by a negative σ_{max} to yield a positive stress ratio, therefore the stress ratio is somewhere between 1 and infinity.

Substituting equation (2-40) into equation (2-39), then into equation (2-38) gives:

$$\left(\frac{\sigma_u}{\sigma_{\max}}-1\right)\left(\frac{\sigma_u}{\sigma_{\max}}\right)^{0.6-\phi|\sin\theta|}\left(\frac{1}{(1-\phi)^{1.6-\phi|\sin\theta|}}\omega^{\beta}\right)=\alpha\left(N^{\beta}-1\right) \tag{2-41}$$

This particular model was verified using uniaxial and flexural fatigue data from various sources [35, 51, 53-57]. Equation (2-41) is relatively complex, compared with the governing equation of the DC model, as it takes into account fibre orientation and loading frequency. In my study, however, since the glass fibre in the matrix is randomly dispersed, the Epaarachchi and Clausen's model may not be especially useful.

It has been shown that the DC model is capable of predicting fatigue life under 4-point bending using flexural fatigue data [34-35, 49]. D'Amore et al. [58] suggested that the DC model can also predict the tensile fatigue life based on the preliminary flexural fatigue data from 4-point bending tests at a single loading condition, provided that the same failure mode governs the life of the material under tensile and flexural loading. Later, Caprino [59] recognized that the DC model can only give a conservative estimate of the residual strength for carbon-fibre-reinforced laminates when subjected to tension-tension fatigue loading, as shown in Figure 2.4 below. In the figure, residual strengths were measured using monotonic tests on samples after 31,400 pre-cycles at σ_{max}=50ksi and R=0, represented by symbol ■, and on samples after 364,000 pre-cycles at σ_{max}=42ksi and R=0, represented by symbol ▲. The figure shows a large discrepancy between the measured data and the theoretical prediction based on the DC model, represented by the curves.

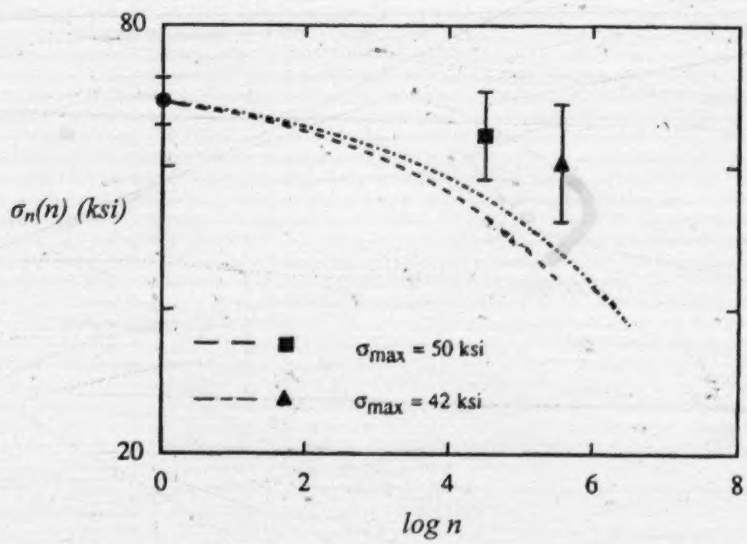

Figure 2.4. Measured residual strength at two loading conditions with the theoretical prediction from the DC model shown by the curves, from ref. [59]. The bars at each point represent the standard deviation

2.3 Yang and Liu's Model (YL model)

Hahn and Kim [27] proposed a non-linear relationship between the rate of change of residual strength with respect to time and the residual strength σ_n:

$$\frac{d\sigma_n(t)}{dt} = -V \cdot \sigma_n(t)^{-Z} \tag{2-42}$$

in which V depends on loading condition at time t, whereas the exponent Z is a material constant independent of $\sigma_n(t)$ and t. The above equation can show different characteristics depending on the sign of the exponent Z, as illustrated in Figure 2.5.

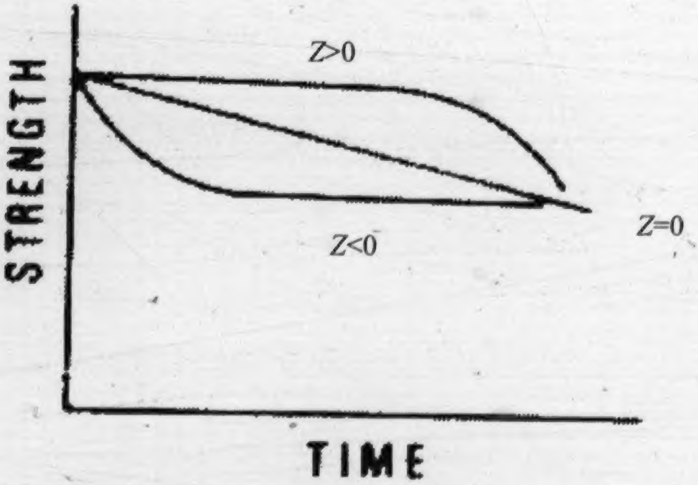

Figure 2.5. A plot of strength against time according to equation (2-42) with $Z>0$, $Z=0$ and $Z<0$, from ref. [27]

In most cases, the exponent Z is greater than zero. That is, the residual strength remains at a constant level for a period of time, then degrades rapidly. Since the residual strength was also observed to decrease monotonically with respect to the number of fatigue cycles n [60], Yang and Liu proposed a residual strength degradation model in the n domain, assuming that the rate of change of residual strength $\sigma_n(n)$ is inversely proportional to the residual strength itself to a power of $c-1$. The YL model was first proposed for zero-tension fatigue [36], and later generalized for the case of tension-compression fatigue [37]. Since the former is a special case of the later with the minimum applied stress σ_{min} equal to zero, only the case of tension-compression fatigue in ref. [37] is discussed here.

The rate equation for the YL model is as follows:

$$\frac{d\sigma_n(n)}{dn} = -\frac{f(S,\omega,R)}{c \cdot \sigma_n^{c-1}(n)} \tag{2-43}$$

where c is a constant, and $f(S,\omega,R)$ a function of stress range, loading frequency in Hz and stress ratio R. For constant ω, function f depends on stress range S and stress ratio R. Therefore, equation (2-43) can be simplified to become:

$$\frac{d\sigma_n(n)}{dn} = -\frac{f(S,R)}{c \cdot \sigma_n^{c-1}(n)} \tag{2-44}$$

Integrating equation (2-44) with respect to n, from n_0 to n_1 cycles, results in:

$$\sigma_n^c(n_1) = \sigma_n^c(n_0) - f(S,R) \cdot (n_1 - n_0) \tag{2-45}$$

If the cyclic loading starts at cycle 0 and finishes at cycle n, then by substituting $n_0=0$ and $n_1=n$, equation (2-45) can be further reduced to:

$$\sigma_n^c(n) = \sigma_n^c(0) - f(S,R) \cdot n \tag{2-46}$$

The above equation expresses residual strength in terms of ultimate strength of the virgin material $\sigma_n(0)$, number of fatigue cycles n, stress range S, stress ratio R and a constant c.

In order to determine the function $f(S,R)$, we must understand the statistical distribution of the ultimate strength, which is assumed to follow the 2-parameter Weibull distribution [27, 36, 61, 62-66]. The probability of failure $F_{\sigma n(0)}(y)$ at stress level y, or $P[\sigma_n(0) \le y]$, is given by:

$$F_{\sigma n(0)}(y) = P[\sigma_n(0) \le y] = 1 - \exp\left[-\left(\frac{y}{\lambda}\right)^{\delta}\right] \tag{2-47}$$

The shape parameter and scale parameter (or characteristic life) of the Weibull distribution are denoted as δ and λ, respectively, in equation (2-47). Fatigue failure is expected to occur when residual strength of the material is reduced to the maximum applied cyclic stress, thus n is equal to the number of cycles to failure N. By applying the boundary condition to equation (2-46), i.e. $\sigma_n(n) = \sigma_{\max}$ when $n = N$, an expression for N is obtained:

$$N = \frac{\sigma_n^c(0) - \sigma_{\max}^c}{f(S,R)} \tag{2-48}$$

It has been well established that $\sigma_n(0)$ is a statistical variable, therefore the number of cycles to failure N is also a statistical variable. If the scatter in $\sigma_n(0)$ can be represented by a 2-parameter Weibull distribution in equation (2-47), then the statistical distribution of N should also follow such a distribution. By substituting equation (2-48) into $P\{N \le \hat{N}\}$ and through rearrangement, we have the probability of finding an N that is less than or equal to $\hat{N}$:

$$F_N(\hat{N}) = P[N \le \hat{N}] = P[\frac{\sigma_n^c(0) - \sigma_{\max}^c}{f(S,R)} \le \hat{N}] = P[\sigma_n(0) \le \{\hat{N} \cdot f(S,R) + \sigma_{\max}^c\}^{\frac{1}{c}}] \tag{2-49}$$

By applying a similar expression of the 2-parameter Weibull distribution, equation (2-47), in term of fatigue life to equation (2-49), we have,

$$F_N(\hat{N}) = p[N \le \hat{N}] = 1 - \exp\left\{ - \left[\frac{\hat{N} + \frac{\sigma_{\max}^c}{f(S,R)}}{\frac{\lambda^c}{f(S,R)}} \right]^{\frac{\delta}{c}} \right\} \tag{2-50}$$

Based on the format of equation (2-50), the statistical distribution of the number of cycles to fatigue failure follows a 3-parameter Weibull distribution, where $\frac{\delta}{c}$, $\frac{\sigma_{\max}^c}{f(S,R)}$ and $\frac{\lambda^c}{f(S,R)}$ are shape parameter, guaranteed value, and the difference between scale parameter and guaranteed value (generally known as the scale parameter of the 3-parameter Weibull distribution), respectively.

Two scenarios are considered in the following discussion: low stress amplitude fatigue and high stress amplitude fatigue. In the low stress amplitude fatigue, the number of cycles to fatigue failure is high since the damage introduced by each cycle is small. Assuming that the maximum applied cyclic stress σ_{max} is much less than λ, i.e. $\sigma_{\max} << \lambda$, the term $\frac{\frac{\sigma_{\max}^c}{f(S,R)}}{\frac{\lambda^c}{f(S,R)}}$ in equation (2-50) becomes negligible. Therefore, $F_N(\hat{N})$ in equation (2-50) can be approximated by the 2-parameter Weibull distribution with the shape parameter and scale parameter (or characteristic life) being $\frac{\delta}{c}$ and $\frac{\lambda^c}{f(S,R)}$, respectively. That is,

$$F_N(\hat{N}) = 1 - \exp\left\{ - \left[\frac{\hat{N}}{\frac{\lambda^c}{f(S,R)}} \right]^{\frac{\delta}{c}} \right\} \tag{2-51}$$

We should now evaluate the expression for function $f(S,R)$ in equation (2-46). Traditionally, the $S-\overline{N}$ curve of constant-amplitude fatigue data can be approximated by associating the characteristic life $\overline{N}$ with the stress range S, through the following equation [36-37]:

$$KS^b\overline{N} = 1 \tag{2-52}$$

where K and b are functions of either the stress ratio or minimum applied cyclic stress, as demonstrated experimentally by Ryder and Walker [61] with a plot of stress range against fatigue life for different minimum cyclic stresses. It is worth noting that Yang and Liu [36] pointed out that the establishment of equation (2-52) requires the generation of extensive amount of statistical data, which can be extremely complicated and should not be attempted. Instead, equation (2-52) only serves as a tool in the development of the YL model.

Rearranging (2-52) gives an expression for the characteristic life $\overline{N}$:

$$\overline{N} = \frac{1}{KS^b} \tag{2-53}$$

If the scale parameter or characteristic life in equation (2-51) is equated with the characteristic life $\overline{N}$ in equation (2-53), then,

$$\frac{\lambda^c}{f(S,R)} = \frac{1}{KS^b} \tag{2-54}$$

By rearranging equation (2-54), $f(S,R) = \lambda^c KS^b$ (2-55)

Substituting equation (2-55) into equation (2-46), the governing equation for the YL model is expressed as:

$$\sigma_n^c(n) = \sigma_n^c(0) - \lambda^c K S^b n \tag{2-56}$$

An expression for the fatigue life can be obtained by substituting equation (2-55) into equation (2-48), as shown in the following equation:

$$N = \frac{\sigma_n^c(0) - \sigma_{\max}^c}{\lambda^c K S^b} \tag{2-57}$$

In high-cycle fatigue, equation (2-56) can be used for the calculation of residual strength after a certain number of pre-cycles, and equation (2-57) for determining the fatigue life at a given stress range.

For the case of low-cycle fatigue, the applied stress amplitude is relatively high, thus the term $\dfrac{\frac{\sigma_{\max}^c}{f(S,R)}}{\frac{\lambda^c}{f(S,R)}}$ in equation (2-50) may not be negligible. In order to evaluate the function $f(S,R)$ for the low-cycle fatigue, two new variables are introduced so that equation (2-50) can be transformed to the format of a 2-parameter Weibull distribution. That is, the statistical distribution of fatigue life would follow the 2-parameter Weibull distribution. The approach is given as follows.

Let η and N_1 be defined as:

$$\eta = \left(\frac{\sigma_{\max}}{\lambda}\right)^c \quad \text{and} \quad N_1 = \frac{\lambda^c}{f(S,R)} \tag{2-58}$$

Formulating a new random variable N' in terms of N, η and N_1, with the product of η and N_1 equal to $\dfrac{\sigma_{\max}^c}{f(S,R)}$. That is,

$$N' = N + \eta \cdot N_1 = N + \frac{\sigma_{\max}^c}{f(S,R)} \tag{2-59}$$

We can obtain the statistical distribution of the fatigue life N' from equation (2-50), the probability of finding a N' that is less than or equal to $\hat{N}'$ is as follows,

$$F_{N'}(\hat{N}') = P[N' \le \hat{N}'] = 1 - \exp\left\{ -\left(\frac{\hat{N}'}{N_1} \right)^{\frac{\delta}{c}} \right\} \tag{2-60}$$

Once again, equation (2-60) is in a form of the 2-paramter Weibull distribution, with the shape parameter $\frac{\delta}{c}$ and characteristic life N_1. The S-N$_1$ curve can be approximated as follows, which is similar to equation (2-52):

$$K_1 S^{b_1} N_1 = 1 \tag{2-61}$$

Substituting the definition of characteristic life N_1 in (2-58) into equation (2-61) yields the following expression:

$$f(S,R) = \lambda^c K_1 S^{b_1} \tag{2-62}$$

Replacing *f(S,R)* in equation (2-46) by the function in equation (2-62) gives the governing equation for the case of low-cycle fatigue, which is similar to the case for high cycle fatigue, i.e. equation (2-56).

$$\sigma_n^c(n) = \sigma_n^c(0) - \lambda^c K_1 S^{b_1} n \tag{2-63}$$

Since the constants *b*, *b$_1$*, *K* and *K$_1$* are arbitrary and can be determined based on the experimental data, the governing equation for the YL model is actually similar between low- cycle fatigue, equation (2-63), and the high-cycle fatigue, equation (2-56). For both cases, the governing equation for the YL model can simply be taken to be the expression of equation (2-56). Caprino [59] actually showed that the YL model can provide a fairly good estimate of the residual strength, as shown by the plot of the theoretical prediction and the measured data in Figure 2.6. In the figure, residual strengths were measured using monotonic tests on samples after 31,400 pre-cycles at σ_{max}=50 ksi and R=0, represented by symbol ■, and on those after 364,000 pre-cycles at σ_{max}=42ksi and R=0, represented by symbol ▲. The two curves are the theoretical prediction from the YL model.

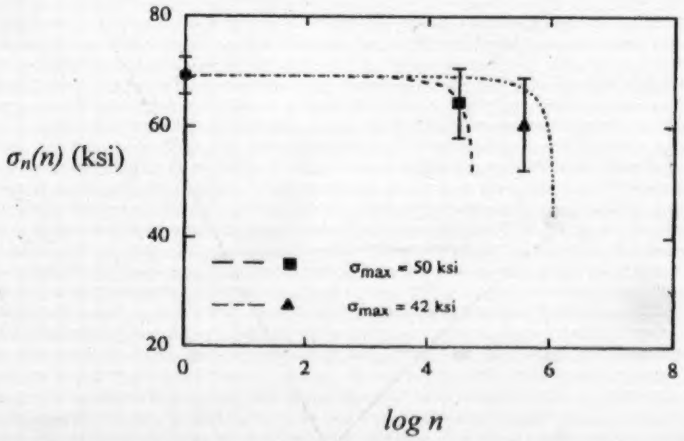

Figure 2.6. Measured residual strength at two loading conditions with the theoretical prediction from the YL model shown as curves, from ref. [59]. The bars at each point represent the standard deviation.

Now we should look at the statistical distribution of fatigue life N for any value of σ_{max}. By substituting equation (2-55) into equation (2-50), we have:

$$F_N(\hat{N}) = 1 - \exp\left\{ - \left[\frac{\hat{N} + \dfrac{\sigma_{\max}^c}{\lambda^c K S^b}}{\dfrac{1}{K S^b}} \right]^{\frac{\delta}{c}} \right\} \tag{2-64}$$

Based on the format of equation (2-64), the fatigue life distribution follows a 3-parameter Weibull distribution. It is possible that some of the specimens will fail within the first cycle of the fatigue loading, if their ultimate strengths of the virgin material are less than σ_{max}. Therefore, the statistical distribution of N should be rewritten as:

$$
\begin{aligned}
F_N(\hat{N}) &= 0 && \text{if } \hat{N} < 1 \\
&= 1 - \exp\left\{ -\left[\frac{\hat{N} + \dfrac{\sigma_{\max}^c}{\lambda^c K S^b}}{\dfrac{1^c}{K S^b}} \right]^{\frac{\delta}{c}} \right\} && \text{if } \hat{N} \geq 1
\end{aligned}
\qquad (2\text{-}65)
$$

The probability of failure in one cycle $F_N(1)$ is the same as the probability of ultimate strength of the specimen that is less than the maximum applied stress for the cyclic loading.

The same statistical analysis can also be applied to evaluate the distribution for residual strength, $\sigma_n(n)$, after n cycles. Following the same idea as in the development of the statistical distribution of N, $\sigma_n(n)$ follows the 2-parameter Weibull distribution. If n is a statistical variable, so is $\sigma_n(n)$. This is indicated in equation (2-56) as all the other terms are fixed at a given loading condition. Now, the probability of failure of the specimens after n cycles at stress level y, or the probability of finding an $\sigma_n(n)$ value less than or equal to y, can be obtained by equation (2-47) through the transformation of the governing equation (2-56):

$$
\begin{aligned}
F_{\sigma_n(n)}(y) &= P\{\sigma_n(n) \leq y\} = P[\sigma_n^c(0) - \lambda^c K S^b n \leq y^c] \\
&= P[\sigma_n(0) \leq (y^c + \lambda^c K S^b n)^{\frac{1}{c}}] \\
&= 1 - \exp\left\{ -\left(\frac{y^c + \lambda^c K S^b n}{\lambda^c} \right)^{\frac{\delta}{c}} \right\}
\end{aligned}
\qquad (2\text{-}66)
$$

Based on the format of equation (2-66), the probability of failure of residual strength after n cycles follows a 3-parameter Weibull distribution. It is possible that some of the specimens will fail before reaching n cycles. Therefore, the probability of a specimen that cannot survive n stress cycles is:

$$F_{\sigma_n(n)}(y) = 0 \qquad \text{if } y < 0$$

$$= 1 - \exp\left\{ - \left[\left(\frac{y^c + \lambda^c K S^b n}{\lambda^c} \right) \right]^{\frac{\delta}{c}} \right\} \qquad \text{if } y \geq 0 \tag{2-67}$$

Applicability of the YL model was generalized by Jen et al. [67] to include the notion of Young's modulus degradation, for developing a residual strength-stiffness reduction model. It was assumed that the degradation ratio of Young's modulus $\frac{\Delta E}{E_0}$ is proportional to a power function of N.

$$\frac{\Delta E}{E_0} = A' N^{s'} \tag{2-68}$$

ΔE is the change in Young's modulus after N cycles of loading, and E_0 the Young's modulus of the virgin material. The constants A' and s' are functions of the applied stress level during the fatigue loading. Based on the YL model [36] and the residual strength degradation model developed by Tanimoto et al. [68], it was summarized that the residual strength after n pre-cycles can be represented in terms of initial Young's modulus E_0, Young's modulus after n pre-cycles $E(n)$, and Young's modulus immediately prior to failure E_f as follows:

$$\sigma_n^v(n) = \sigma_n^v(0) + \left[\sigma_{\max}^v - \sigma_n^v(0)\right] \cdot \left(\frac{E_0 - E(n)}{E_0 - E_f} \right)^{\frac{L}{s'}} \tag{2-69}$$

Once constants v, L and s are determined using experimental data, the residual strength can be evaluated by measuring the Young's modulus at various stages during the fatigue loading. This approach is effective because the measurement of Young's modulus is non-destructive.

Other than the applicability in tension-tension fatigue and tension-compression fatigue, the YL model can also be extended to assess the fatigue properties of materials under shear loading [69], as excellent agreement was found between the measured and theoretical estimate of fatigue life and residual strength. The YL model was found to be an effective fatigue residual strength degradation model that allows me to characterize the fatigue behavior of many different kinds of composite materials using a minimum amount of test data.

2.3.1 Effect of Overload

The prediction accuracy of the YL model on the effect of overload during fatigue loading was studied by various researchers [70-72]. It was verified that a specimen can survive a minimum number of cycles after surviving an initial overload. The theoretical derivation of such a model is outlined in ref. [70], and briefly described hereafter.

Let r_0 be the level of overload applied to the specimen before undergoing fatigue loading. If a specimen survives an initial overload of r_0, it is reasonable to think that its ultimate strength is greater than or equal to r_0. It is of interest to estimate the minimum number of cycles that the specimen can sustain after surviving the initial overload. Define N_0 to be the minimum number of cycles to fatigue failure after surviving r_0. By substituting N with N_0, and $\sigma_n(0)$ with r_0 in equation (2-57), we have

$$N_0 = \frac{r_0^c - \sigma_{\max}^c}{\lambda^c K S^b} \tag{2-70}$$

Therefore, a specimen surviving an initial overload r_0 is guaranteed to last for a minimum of N_0 number of cycles at σ_{max} and S. If all other terms in equation (2-70) remain the same, then it is obvious that as the overload r_0 increases, N_0 would increase as well. The associated treatment for the probability of failure under overload is outlined in detail in ref. [36, 70], only the results are presented here.

The probability of a specimen that will fail under a overload r_0 is denoted as B_0, in equation (2-71),

$$B_0 = P[\sigma_n(0) \le r_0] = 1 - \exp\left[-\left(\frac{r_0}{\lambda}\right)^{\delta}\right] \tag{2-71}$$

where λ and δ are the scale and shape parameters of the 2-parameter Weibull distribution of the monotonic ultimate strength. The probability of failure of fatigue life for the specimen having survived r_0 is given as,

$$\begin{aligned} F_N(N^*) &= 0 && \text{for } N^* < N_0 \\ &= 1 - \exp\left\{\left(\frac{r_0}{\lambda}\right)^{\delta} - \left[KS^b N^* + \left(\frac{\sigma_{\max}}{\lambda}\right)^{c}\right]^{\frac{\delta}{c}}\right\} && \text{for } N^* \ge N_0 \end{aligned} \tag{2-72}$$

While the probability of failure of residual strength after survived r_0 or the probability of finding an $\sigma_n(n)$ value that is less than or equal to stress level y after surviving a overload of r_0 is given in equation (2-73),

$$F_{\sigma_n(n)}(y) = 1 - \exp\left\{\left(\frac{r_0}{\lambda}\right)^{\delta} - \left[\frac{y^c + \lambda^c KS^b n}{\lambda^c}\right]^{\frac{\delta}{c}}\right\} \qquad \text{for } y \ge \sigma_{\max} \tag{2-73}$$

2.3.2 Determining Parameters for the YL Model

In order to predict the residual strength and fatigue life of a material using the YL model, values of the parameters b, c and K must be determined. It is worth noting that the scale parameter of Weibull distribution λ can be determined from the flexural monotonic test data, thus λ is a constant throughout the analysis for determining the model parameters. There are three model parameters, b, c, and K appearing in the governing equation (2-56), which can be evaluated from a set of monotonic test data and a set of fatigue scan data. The procedure for determining these constants was outlined in detail in refs. [36-37], and is modified in this study. A brief description of the original and modified procedure is given below.

Suppose that h specimens are subjected to monotonic tests with the corresponding measured ultimate strengths designated as $x_1, x_2, \ldots x_h$. Three central moments of the measured data can be formulated as

$$m_1 = \frac{1}{h}\sum_{i=1}^{h} x_i \qquad m_2 = \frac{1}{h}\sum_{i=1}^{h}(x_i - m_1)^2 \qquad m_3 = \frac{1}{h}\sum_{i=1}^{h}(x_i - m_1)^3 \tag{2-74}$$

m_1, m_2 and m_3 in equation (2-74) are referred to as the first, second and third central moments, respectively.

Then, three central moments for the equivalent ultimate strength computed based on the fatigue data are calculated and compared against m_1, m_2 and m_3, to solve for b, c and K. Through rearrangement of equation (2-56), the expression for the equivalent ultimate strength, σ_{eq}:

$$\sigma_{eq} = \sigma_n(0) = [\sigma_n^c(n) + \lambda^c K S^b n]^{\frac{1}{c}} \tag{2-75}$$

It is assumed that when final failure occurs in a specimen, the residual strength and the number of pre-cycles on the specimen are equal to the maximum applied stress during fatigue and the fatigue life, respectively. Under these conditions, σ_{eq} can be estimated for a set of j specimens subjected to cyclic loading until final fracture. Alternatively, if the residual strengths of specimens were measured after fatigue pre-cycles, equation (2-75) can be used directly to calculate the equivalent ultimate strength. The first central moment μ_1, second central moment μ_2, and third central moment μ_3 based on the equivalent ultimate strength are:

$$\mu_1 = \frac{1}{j}\sum_{i=1}^{j}\sigma_{eqi} \qquad \mu_2 = \frac{1}{j}\sum_{i=1}^{j}(\sigma_{eqi} - \mu_1)^2 \qquad \mu_3 = \frac{1}{j}\sum_{i=1}^{j}(\sigma_{eqi} - \mu_1)^3 \tag{2-76}$$

If there are an infinite number of specimens in each set of data, the central moments calculated from the monotonic test data should theoretically match that from the fatigue test data, i.e. $m_1=\mu_1$, $m_2=\mu_2$ and $m_3=\mu_3$. In reality, the number of samples is finite and it is possible that fluctuation exists among the data. Therefore, the three parameters b, c and K have to be determined by minimizing the difference between the 2 sets of central moments, as defined in the following in terms of the mean square difference:

$$\textit{Mean square difference} = (m_1 - \mu_1)^2 + g_1(\sqrt{m_2} - \sqrt{\mu_2})^2 + g_2(\sqrt[3]{m_3} - \sqrt[3]{\mu_3})^2 \tag{2-77}$$

where g_1 and g_2 are assigned positive weighing factors for indicating the relative importance of matching the first, second and third central moments calculated from the monotonic and fatigue tests data, respectively. Since there is no clear information on how to select g_1 and g_2, and different selections can yield entirely different results, equation (2-77) was not adopted in this study. Instead, selection of b, c and K values was based on the minimum discrepancy among the central moments obtained from monotonic and fatigue test data, respectively. That is, fractional errors associated with the first, second and third central moments ($error_1$, $error_2$, $error_3$) were computed for each of the b, c, and K combinations as follows:

$$error_1 = \left|\frac{m_1 - \mu_1}{m_1}\right| \qquad error_2 = \left|\frac{m_2 - \mu_2}{m_2}\right| \qquad error_3 = \left|\frac{m_3 - \mu_3}{m_3}\right| \tag{2-78}$$

The three model parameters selected should have the b, c and K values that yield the smallest total absolute error from the following equation:

$$Total\ absolute\ error = error_1 + error_2 + error_3 \tag{2-79}$$

This assessment was used to offer a direct quantitative comparison of different sets of b, c, and K values in matching the three central moments derived from the monotonic and the fatigue test data.

3. EXPERIMENTAL DETAILS

The purpose of experiments conducted in this study was to collect necessary information for investigating and verifying the D'Amore and Caprino's Model (DC model), and the Yang and Liu's Model (YL model), as discussed in Chapter 2.

3.1. Material Information

3.1.1 Glass-Filled Polycarbonate

Polycarbonate is a thermoplastic polymer that is nowadays commercially available in different grades and qualities for various usages. Its high impact toughness, temperature resistance and optical properties made it an ideal candidate for industrial and household applications, e.g. impact shields, scientific and analytical instrument components, housings and covers, electrical components etc. Different addictives, coatings or treatments might be added to the polymer during the fabrication process, in order to enhance the desired properties and thus boost the performance. For example, bullet-resistant polycarbonate made with bisphenol A is laminated to provide a strong media to protect against breakage and entry of foreign material. Static-dissipative polycarbonate is coated with a transparent layer of metal/plastic that can reduce the amount of static electricity on the surface, while providing high tensile and impact strength.

The material used in this study was glass-filled polycarbonate sheet of 0.5" in nominal thickness, supplied by McMaster-Carr in USA. The 20% glass constituent is expected to increase the overall tensile strength. A scanning electron microscope (SEM, JEOL JSM-6301F) was used to examine the fracture surface of the material and determine the form of the glass constituent. Each specimen of interest was cut to appropriate size, mounted on a sample holder and coated with a thin layer of chromium just before the examination. Figure 3.1 is an SEM image showing the dispersion of glass-fibre strand in the matrix. The presence of glass-fibre in the polycarbonate matrix greatly contributed to the brittle nature of the material. This characteristic is particularly important for the study, since the two theoretical models considered use strength-based failure criteria that require a one-to-one stress-strain relation. According to the supplier, the tensile and impact strength of the glass-filled polycarbonate are 110.3MPa and 106.77J/m respectively. For unfilled polycarbonate, a lower tensile strength of 68.9MPa and higher impact strength of 854.06J/m are claimed by the supplier. The increase of tensile strength is due to the reinforcement provided by glass fibre, but at the same time the fibre also introduces sites for defect that decrease the ability to resist impact loading. In general, the glass-filled polycarbonate has higher tensile strength and lower coefficient of thermal expansion than the pure polycarbonate. The material can be molded, welded, cut, and drilled relatively easily.

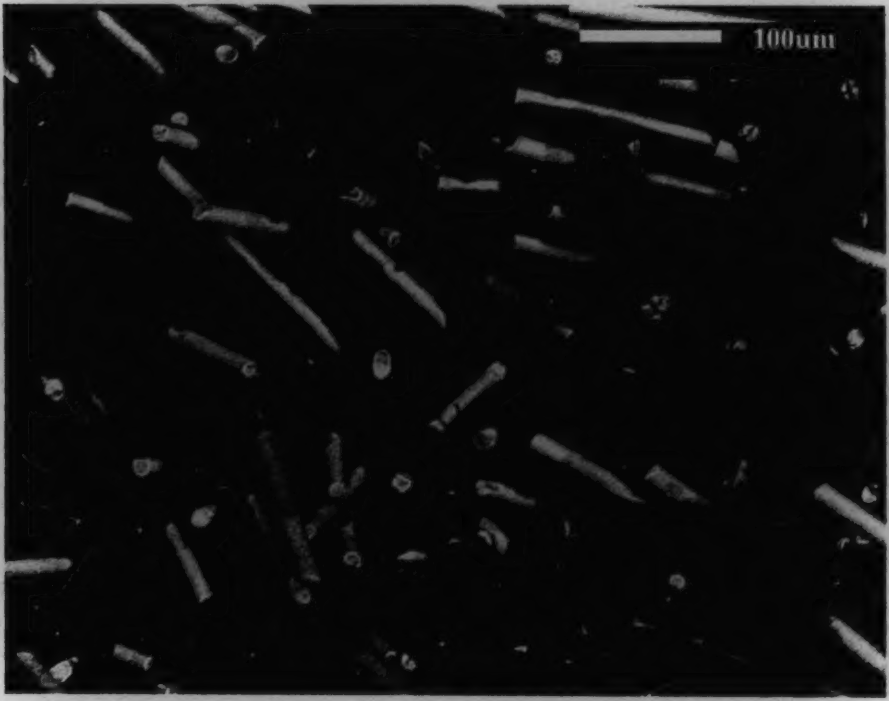

Figure 3.1. SEM image clearly shows the presence of glass-fibre in the polycarbonate matrix

The glass-filled polycarbonate sheet was cut into rectangular strip specimens of approximately 80mm long, 14mm wide, and 6mm thick. A table saw was used for specimen cutting. In order to obtain a smooth surface finish, a high quality blade only for cutting plastics was used.

3.1.2 Poly(acrylonitrile-butadiene-styrene) (ABS)

ABS is an engineering thermoplastic commercially available since 1940's. It is composed of three types of monomers: acrylonitrile, butadiene and styrene. Each monomer contributes a unique set of desirable properties to the polymer. For example, acrylonitrile provides superior chemical resistant, butadiene offers toughness and impact strength, and styrene provides rigidity for easy processing [73]. ABS is available in different grades by varying the additives and/or the monomers ratio, and through alloying with other polymers to enhance the desired properties. For example, transparency in ABS can be achieved by reducing the size of the dispersed phase [74], and increase in heat deflection temperature can be accomplished by using α-methyl styrene instead of styrene as the monomer [74]. This material can also be blended with various kinds of polymers and fibers to widen its range of applications. The good balance between toughness, strength, surface finishes and price made ABS the ideal candidate in casings for household appliances, interior automotive components, computer housings etc. In the current study, a high impact grade (GR-2000) ABS supplied by DENKA Co., was used to assess the change of ultimate strength and energy absorption capability after cyclic loading. The ABS specimens were injection-molded to ensure consistency in shape, dimension and quality. ASTM standard tests show that the tensile and Izod impact strength of this grade of ABS are 47MPa and 225J/m, respectively, as specified by the supplier. The shape and dimensions of one of the ABS specimens are shown in Figure 3.2.

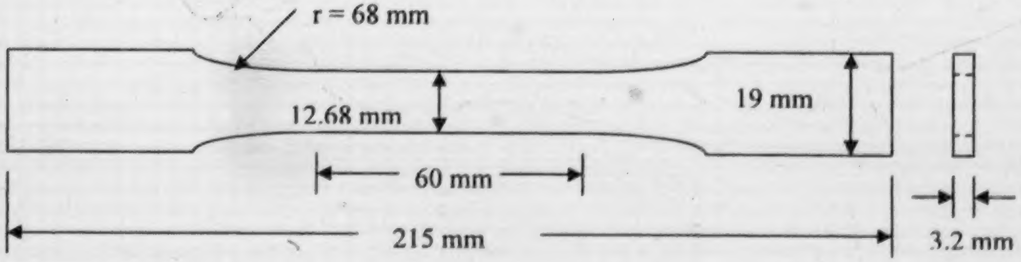

Figure 3.2. The dimensions of a dum-bell shaped ABS specimen

3.2 Test Methodology

Different type of mechanical tests can be performed on materials to evaluate their properties. Common tests include tensile test, compressive test and flexural test (3-point bending and 4-point bending). They are all relatively easy and inexpensive to perform. However, if a large number of specimens are needed, then the shape of each specimen must be simple enough to allow easy machining. In this study, flexural test was chosen to evaluate the fatigue behavior of glass-filled polycarbonate since the number of tests required was substantial and only a simple rectangular-shaped specimen is specified for such test. The main difference between 3-point and 4-point bending tests is the location of maximum bending moment applied to the specimen, as illustrated in Figure 3.3.

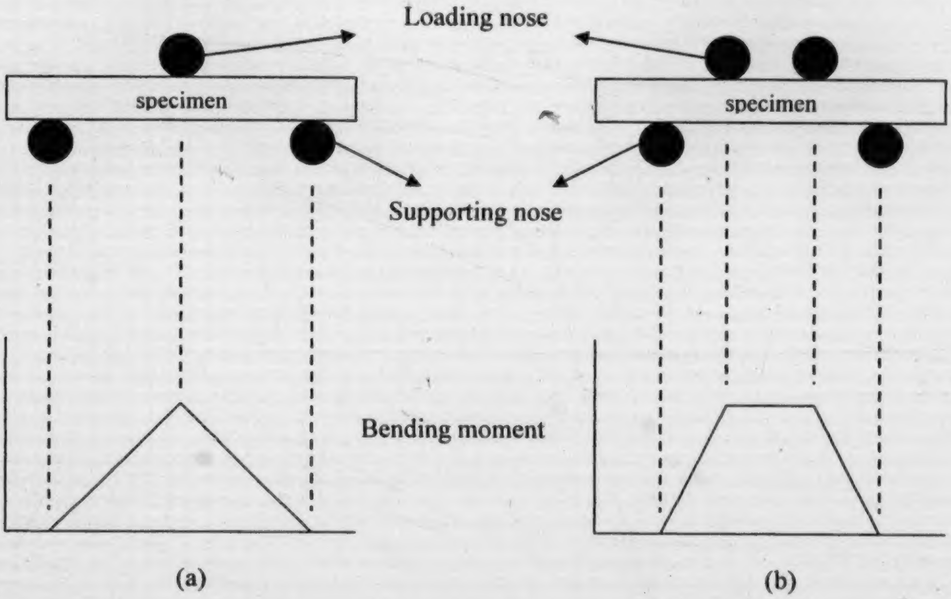

Figure 3.3. Bending moment diagram for glass-filled polycarbonate specimen under (a) 3-point bending test and (b) 4-point bending test

For 3-point bending, Figure 3.3(a), a specimen is placed on the supporting noses, while the load is applied by a single loading nose at the center. In this case, the bending moment increases from one of the supporting nose to reach maximum at the loading nose, and decreases linearly until reaching the other supporting nose. On the other hand, 2 identical loading noses were used for 4-point bending, thus the section between those loading noses are under constant maximum bending moment. As a result, the area under maximum bending moment is considerably larger in 4-point bending, which is more likely to subject sections containing defects or inclusions to maximum bending moment. This is expected to generate more consistent results. Therefore, 4-point bending flexural test was adopted.

Ideally, a relative ductile material such as ABS should also undergo the 4-point bending flexural test for a direct comparison with glass-filled polycarbonate on fatigue response under the same loading mode. However, fracture behavior of a ductile material is difficult to generate in flexural tests due to its ability to absorb a large amount of energy before final failure. Sometimes, the specimen would not even fracture in the bending mode until large deflection was generated, due to its ductility. The tensile loading, on the other hand, allows a greater amount of inclusions to be dispersed in the gauge section for fracture initiation. Based on the above consideration, tensile tests were conducted on ABS specimens, to have a better chance to generate fracture in this relatively ductile material.

All tests were carried out at room temperature and atmospheric pressure. Flexural monotonic and flexural fatigue tests were conducted on a hydraulic MTS material testing system Model 810, as shown in Figure 3.4, with 4-point bending fixture attached to the hydraulic wedge grips.

3.2.1 Flexural Monotonic Test (Glass-Filled Polycarbonate)

The load and the support spans of the 4-point bending fixture are 25.4mm and 66mm, respectively. The overall test setup with respect to the specimen position is given in Figure 3.5. Alignment of the loading and supporting noses was checked each time before the test using a jig that has the cutouts for the proper placement of the four loading points. Stroke controlled setting along with a low cross-head speed of 5mm/min was prescribed for these monotonic tests, in order to avoid instability of the specimen during the experiments. Load, stroke and time were recorded through the data acquisition system at a sampling rate of 25 Hz.

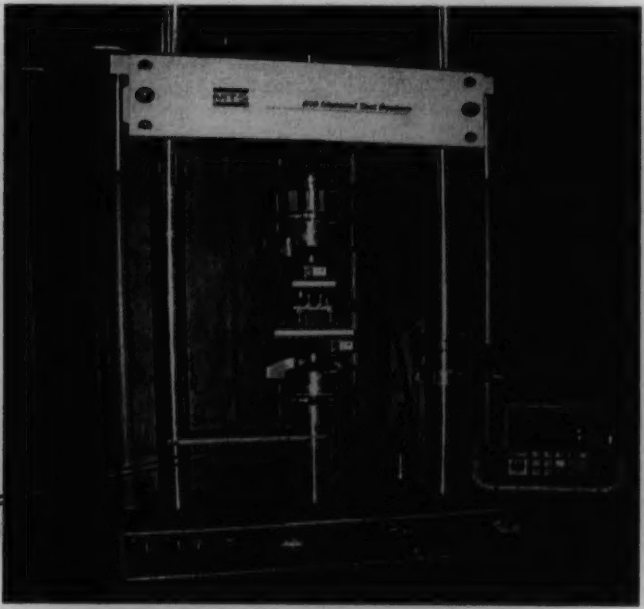

Figure 3.4. MTS model 810 material testing system with 4-point bending fixture

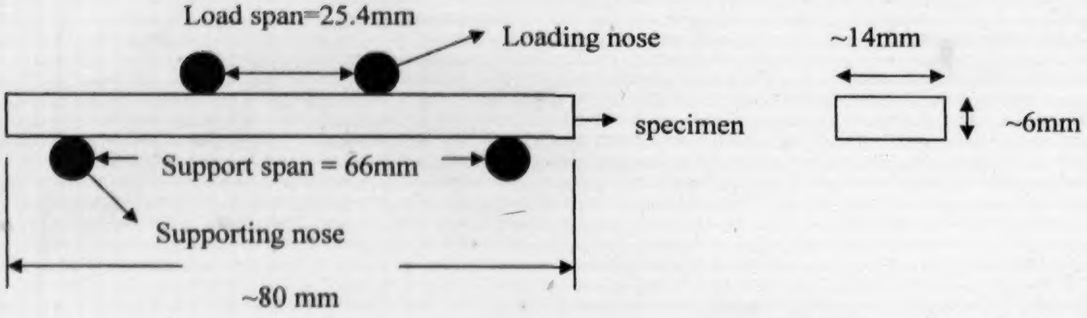

Figure 3.5. Overall 4-point bending setup and glass-filled polycarbonate specimen dimensions

3.2.2 Flexural Fatigue Test (Glass-Filled Polycarbonate)

Flexural fatigue tests were carried out on the same MTS material testing system with 4-point bending fixture, adopting basically the same setup configuration as in the monotonic test. Dally and Broutman [75] showed that temperature of the glass-reinforced plastics increases with the increases of the loading frequency, but the temperature rise is insignificant at a frequency of 1 Hz. Therefore, a testing frequency of 0.3 Hz was adopted in this study, in order to prevent significant heating of the material, thus avoiding the change of its original property. Various stress ratios, *R* defined as the ratio of minimum stress to maximum stress (0.1, 0.3, 0.4 and 0.5), were implemented in the load-controlled cyclic tests to study the effect of stress ratio. The maximum stress level was set to be between 0.4 - 0.85 of the material flexural monotonic strength. For a given stress ratio and stress level, the maximum, minimum and mean applied loads were determined according to the dimensions of each specimen.

The moment generated between the load span of 4-point bending (Figure 3.5) was determined using the following equation:

$$M = \frac{P}{2} * (\frac{ss - ls}{2}) \tag{3-1}$$

where M is moment, P applied load, ss support span (66mm) and ls load span (25.4mm). Stress (σ) was determined based on the simple beam theory:

$$\sigma = \frac{M * ct}{I} \tag{3-2}$$

where ct is the half specimen thickness and I the moment of inertia of the cross section. Note that thickness and width of each specimen were measured before testing, since the dimensions might vary slightly among specimens due to machining. The corresponding fatigue load applied to the specimens was set to ensure that the desired stress level was generated for each specimen. For the fatigue experiments, the applied load was initially ramped up to the mean load (P_{mean}) within 20 seconds, and then varied in a sinusoidal waveform of constant amplitude, between the maximum load (P_{max}) and the minimum load (P_{min}). Some fatigue tests were conducted until the specimens fractured completely, while the others were stopped after a pre-set number of cycles and then monotonic loading was applied to determine the remaining flexural ultimate strength (residual strength). Note that for a valid flexural test, the point of fracture must be between the loading noses where the maximum moment is experienced. For the measurement of residual strengths, only 9 specimens were used to vary the number of fatigue cycles at one loading condition, due to the limited number of specimens. The fatigue loading applied for measuring the residual strength has the stress ratio R set at 0.5 and the maximum stress at 60% of the flexural ultimate strength. The flexural monotonic tests were conducted immediately after the pre-set number of cyclic loading, so that unnecessary shifting of the specimen on the supporting noses could be avoided. The residual energy is determined using the area under the load-displacement curve from the monotonic test.

One of the main difficulties encountered during experiments was the movement of specimens on the 4-point bending fixture. This was especially severe when specimens were subjected to loading of large stress amplitude, i.e. small *R* value. Rotation of the hydraulic piston for which the 4-point bending fixture was attached to was deemed to be one of the contributing factors in the specimens shifting. The hydraulic piston rotated slightly, but this was enough to cause mis-alignment of the loading and supporting noses, thus resulting in the imbalanced loading of the specimen. Another possible reason for the specimen movement was the uneven thickness of the specimen due to machining. The problem of specimen movement was eventually resolved by constraining the rotation of the hydraulic piston using a metal structure indicated in Figure 3.4. This constraining mechanism is important for ensuring the reliability of the measured data.

3.2.3 Tensile Test for Measuring Residual Strength (ABS)

MTS model 810 material testing system was also used for measuring the residual strength of the ABS specimens. The specimen configuration with respect to the hydraulic wedge grips of the testing system is given in Figure 3.6. Approximately 100 specimens were utilized, subjected to tension-tension cyclic loading for any pre-set number of cycles before the residual ultimate strength was measured. Four different conditions were prescribed for the experiments, as tabulated in Table 3.1, so that the effect of stress ratio and maximum cyclic stress level can be compared effectively.

Table 3.1. Four different loading conditions for ABS under tensile cyclic loading

R	σ_{max}
0.1	$0.8\sigma_n(0)$
0.3	$0.8\sigma_n(0)$
0.5	$0.8\sigma_n(0)$
0.3	$0.6\sigma_n(0)$

The tests were conducted at a loading frequency of 0.3 Hz, which is the same as the flexural test. The fatigue load was applied in such a way that it ramped up to the mean load, then adapting a sinusoidal waveform with constant amplitude. The monotonic test was engaged immediately after the cyclic loading, until the specimen was pulled to fracture, thus the residual ultimate strength of the specimen can be measured. The data acquisition rate for the fatigue and monotonic tensile test are 100Hz and 25Hz respectively. Note that for the test to be valid, the point of fracture must be within the gauge section of the specimen. The tensile residual energy was determined in the same way as the flexural residual energy, by integrating the area under the load-displacement curve from the monotonic test.

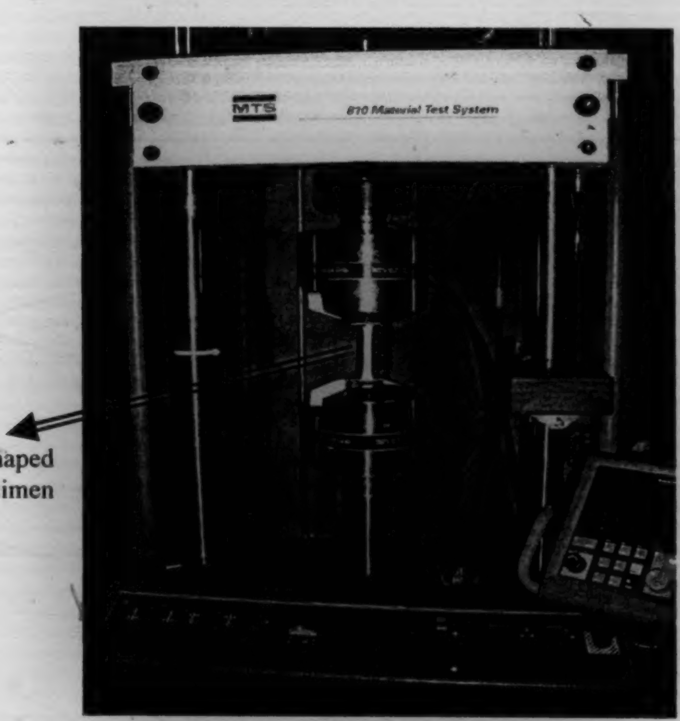
MTS
810 Material Test System

Dum-bell shaped
ABS specimen

Figure 3.6. Experimental setup of the tensile test and the corresponding ABS specimen configuration

4. RESULTS AND DISCUSSIONS

In this chapter, the experimental results of flexural monotonic and fatigue tests for glass-filled polycarbonate, as well as the tensile test results for ABS will be presented. The data analysis for the determination of various model parameters and Weibull parameters would then follow. Prediction accuracy of the D'Amore and Caprino's model (DC model) and Yang and Liu's model (YL model), as well as the characteristics of residual mechanical properties of materials fractured in a brittle and ductile manner will be explored and discussed in great details.

4.1 Experimental Results

4.1.1 Flexural Monotonic Test for Glass-Filled Polycarbonate

Based on the Student's t-distribution, when the sample size is big enough, say 30, the sample mean value is within 4% of the population mean. In my case of 45 specimens, the possible difference between the sample mean strength and that for the population is within 3%. Therefore, the sample mean strength can represent the mean strength of the glass-filled polycarbonate. Forty-five rectangular-shaped specimens, cut from the same glass-filled polycarbonate plate, were tested under the same condition for their flexural ultimate strength. Due to machining, manufacturing defects and inherent flaws in the material, strength variation among specimens can be high. Values of the measured flexural ultimate strength for the specimens are tabulated in Table 4.1, which range from

109MPa to 153MPa, with mean flexural ultimate strength of 129MPa. Failure is generally characterized by a smooth mirror-like region representing slow crack propagation, surrounded by a coarser area indicating fast crack growth [8]. Through visual inspection of the specimens, it can be observed that there were two distinct regions appearing on the fracture surface: a darker region at one corner that is believed to be the crack initiation site with slow crack growth, and a surrounding brighter section representing fast crack growth. A typical scanning electron microscopic image of the fracture surface is given in Figure 4.1 which shows that the darker region for slow crack growth has a high density of fiber in parallel to the fracture surface, but the majority of fibre in the area for faster crack propagation is orientated in a random fashion. It is speculated that these phenomena can be resulted from two possibilities: (i) the fibres were pressed and rotated to be parallel to the fracture surface during the cyclic loading, or (ii) the region in which the fibers had a preferred orientation was favored for crack initiation. More investigation is needed by examining the SEM images at different stages during cyclic loading and of the virgin material, which may help determining the cause.

A typical load-displacement curve from the monotonic tests is presented in Figure 4.2, which shows that the load increase remained linear up to 0.8kN, followed by a non-linear increase of the load. The load drops to zero immediately after attaining the highest load level, suggesting that fast crack growth was involved at this stage of fracture process. The observation suggests that the glass-filled polycarbonate used in the study is a relatively brittle material, due to the presence of glass-fibre.

Table 4.1. The ultimate strength of 45 glass-filled polycarbonate specimens subjected to flexural monotonic test

Failure Order	*Ultimate strength (MPa)*	*Failure Order*	*Ultimate strength (MPa)*	*Failure Order*	*Ultimate strength (MPa)*
1	**109.123**	16	**126.799**	31	**130.92**
2	**120.145**	17	**126.814**	32	**131.259**
3	**121.063**	18	**127.236**	33	**131.759**
4	**123.564**	19	**127.836**	34	**132.164**
5	**123.894**	20	**127.839**	35	**132.219**
6	**124.873**	21	**128.122**	36	**132.346**
7	**124.964**	22	**128.248**	37	**132.886**
8	**125.218**	23	**128.67**	38	**133.391**
9	**125.306**	24	**128.803**	39	**133.528**
10	**125.332**	25	**129.079**	40	**133.837**
11	**125.52**	26	**129.417**	41	**134.984**
12	**125.861**	27	**129.877**	42	**136.251**
13	**126.065**	28	**130.163**	43	**136.26**
14	**126.157**	29	**130.307**	44	**136.965**
15	**126.458**	30	**130.742**	45	**153.352**

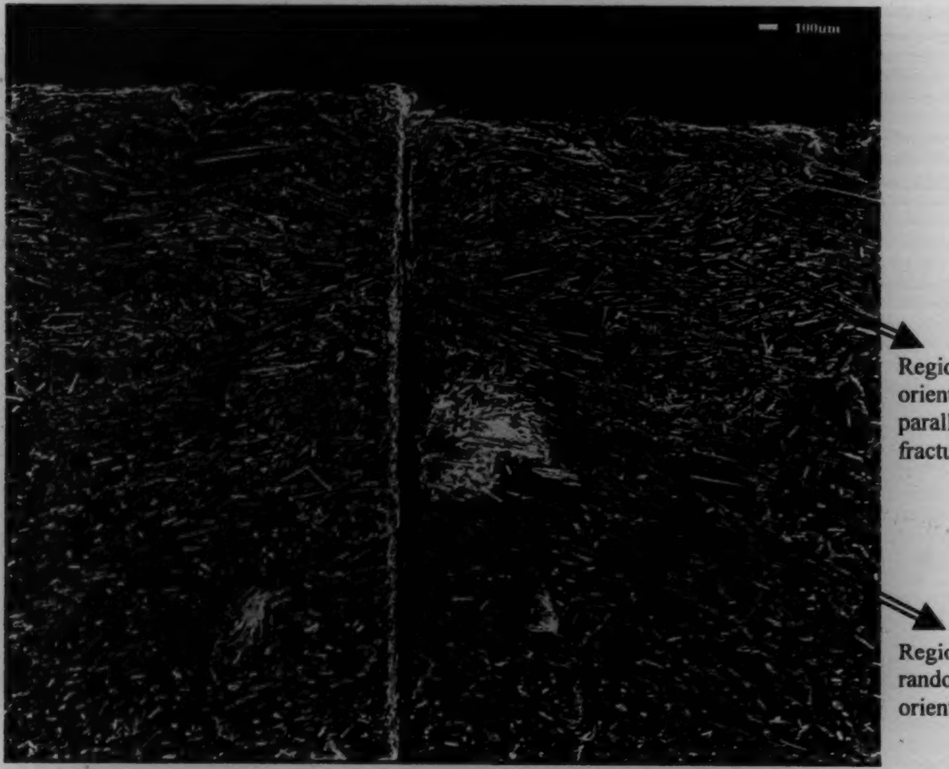

Region with fibre orientated in parallel to the fracture surface

Region of random fibre orientation

Figure 4.1. SEM image of the fracture surface of glass-filled polycarbonate generated by flexural monotonic test

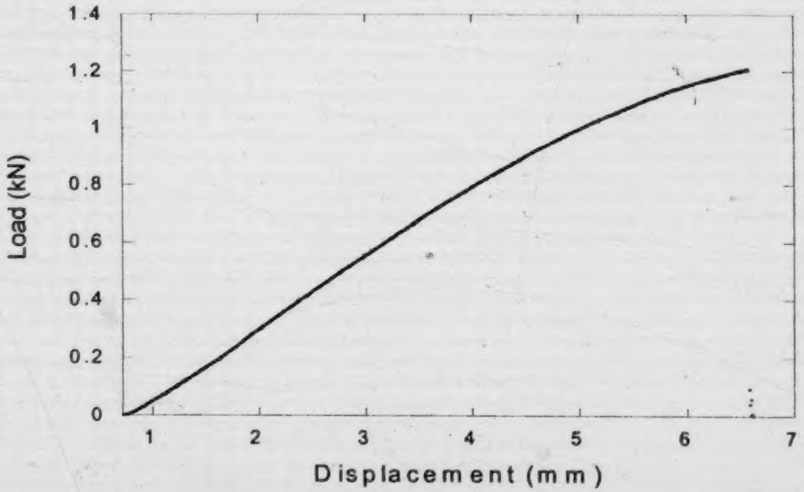

Figure 4.2. Typical load-displacement curve of flexural monotonic test of glass-filled polycarbonate

4.1.2 Flexural Fatigue Test for Glass-Filled Polycarbonate

Two kinds of flexural fatigue tests were conducted on glass-filled polycarbonate: (i) constant amplitude cyclic loading till fracture to measure the fatigue life, (ii) monotonic loading to pre-cycled specimens to measure the residual strengths.

Totally, 35 specimens were used in the first kind of test at assorted combination of stress ratios and maximum cyclic stresses. The measured fatigue life for each specimen, along with the corresponding stress ratio R and maximum applied cyclic stress σ_{max} are given in Table 4.2.

Table 4.2. Fatigue life of 35 glass-filled polycarbonate specimens with the corresponding stress ratio and maximum applied cyclic stress

R=0.5		*R*=0.4		*R*=0.3		*R*=0.1	
σ_{max} (MPa)	*N* (cycle)	σ_{max} (MPa)	*N* (cycle)	σ_{max} (MPa)	*N* (cycle)	σ_{max} (MPa)	*N* (cycle)
65.23	81,186	65.23	21,624	78.28	2,454	71.75	2,138
71.75	35,635	71.75	16,503	78.28	3,636	78.28	1,531
78.28	20,257	78.28	5,534	84.80	2,670	84.80	1,004
84.80	12,544	84.80	4,120	91.32	1,069	91.32	537
91.32	6,476	91.32	2,935	97.84	625	91.32	396
97.84	2,982	97.84	1,216	104.37	223	97.84	275
97.84	3,993	97.84	1,605	104.37	300	97.84	222
104.37	1,998	104.37	507	110.89	253	104.37	125
110.89	530	110.89	363	-	-	110.89	74

The above table shows that fatigue life *N* generally follows a decreasing trend with the increase of the maximum cyclic stress, regardless of the stress ratios used. This is because higher cyclic stresses caused more damage to the specimen during the cyclic loading. For example, the fatigue life decreased from 81,186 cycles to 20,257 cycles when the maximum cyclic stress increase from 65.23MPa to 78.28MPa at *R* equal to 0.5. The same is observed at the other three stress ratios, in order to show this trend clearly, σ_{max} is plotted against *N* in Figure 4.3(a) for each stress ratio.

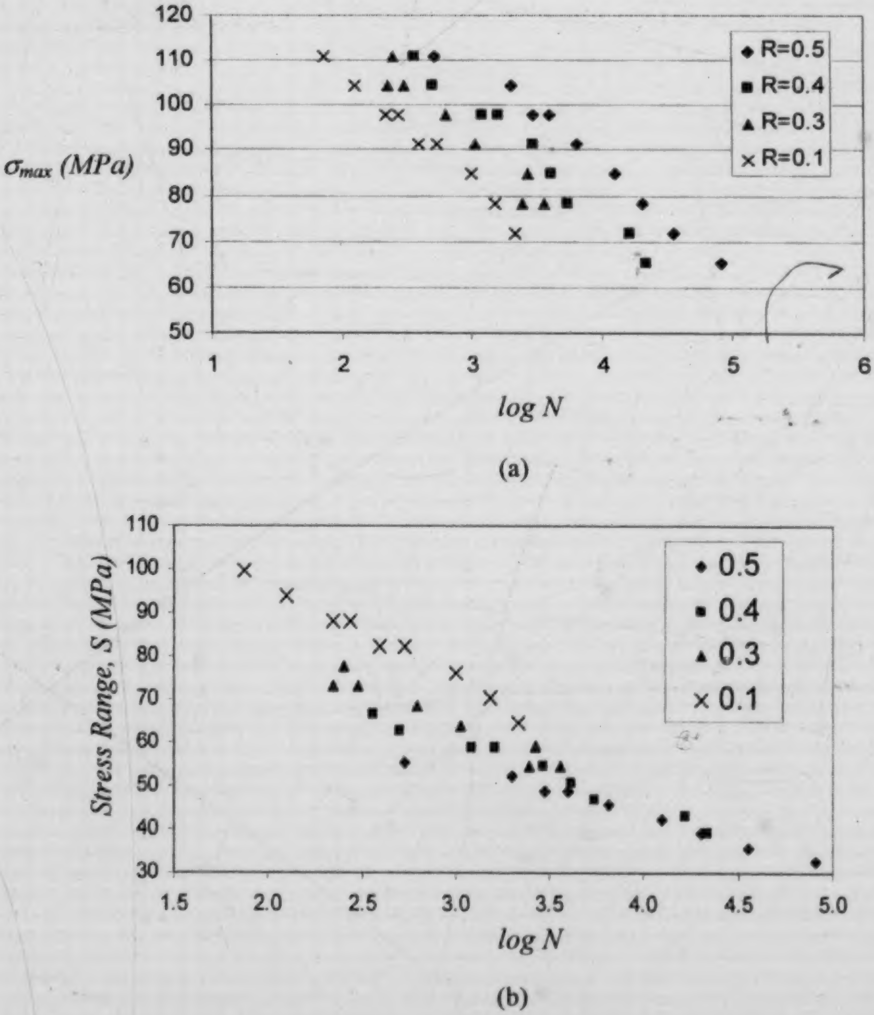

Figure 4.3. (a) A plot of maximum cyclic stress against log *N* for glass-filled polycarbonate specimens tested at *R*=0.5, 0.4, 0.3 and 0.1 (b) The S-N curve of the measured fatigue life of glass-filled polycarbonate at *R*=0.5, 0.4, 0.3 and 0.1

A smaller stress ratio implies a larger stress amplitude during the fatigue loading, causing the specimen to have greater difference in deflection between the maximum and minimum applied stresses. This increases damage to the specimens per cycle, thus shortening their fatigue life. The S-N curves in Figure 4.3(b) for various stress ratios show that the increase in stress range causes decrease of the number of cycles to failure in the cyclic loading. The figure suggests that with the same stress range, the *N* values are relatively consistent for different *R* values. However, some discrepancy does exist at low cycles, such as *N* less than 1,000 cycles.

Fracture surface of the fatigue tested specimen was very similar to that generated by the monotonic test, except the area size of the dark region is larger than that of the monotonically loaded specimen. A typical load-displacement curve at 100 and 10,000 cycles for one of the specimens under flexural fatigue loading is shown in Figure 4.4. For this particular specimen, final failure occurred at 20,257cycles. It was noted from the graph that the load-displacement response at the two cycles are very similar. However, the stroke of the loading noses increases with the increase of the number of cycles, which implies that the region on the specimen between the loading noses was also subject to increase in deflection. This was possibly due to the nucleation of microscopic cracks which weakened the specimen, and resulted in a larger vertical displacement when load was applied.

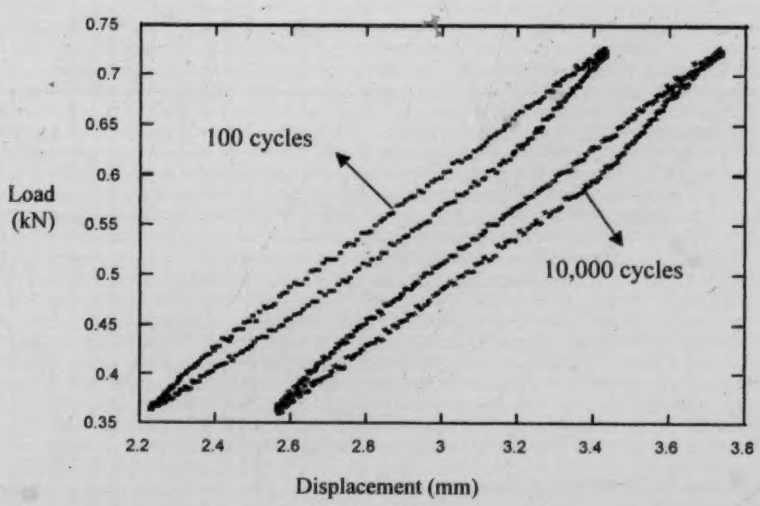

Figure 4.4. Load-displacement curve for flexural fatigue testing of glass-filled polycarbonate at $\sigma_{max} = 78.3$MPa and $R = 0.5$

Another set of fatigue data was generated, but this time each specimen was firstly subjected to a pre-set number of cycles and then fractured under monotonic loading to determine the residual flexural strength. The loading conditions for a total of 9 specimens were all the same, with stress ratio R of 0.5 and the maximum applied cyclic stress at 60% of the flexural ultimate strength of the virgin material. Table 4.3 shows the number of pre-cycles n and the corresponding residual strength $\sigma_n(n)$ and residual energy $Er_n(n)$ for each of the specimens under examination. It was expected that the residual strength of the specimen decreases as the number of fatigue cycles increase. This is because cyclic loading caused damage to the specimen in a progressive manner, which facilitated crack growth, thus reducing its ultimate strength. According to Table 4.3, the residual strength maintained at a fairly constant level for the first 7,000cycles, and then decreased gradually to 98.07MPa. A similar degradation trend was also observed in the residual energy.

Table 4.3. The residual strength and residual energy of 9 glass-filled polycarbonate specimens after subjected to a pre-set number of cycle *n*

R=0.5		
n (cycle)	$\sigma_n(n)$ (MPa)	$Er_n(n)$ (kN-mm)
500	128.13	2.819
1,000	128.25	2.931
2,000	127.80	2.815
4,500	125.03	2.692
7,000	127.47	2.598
9,000	116.70	2.175
11,000	116.65	2.190
14,000	108.90	1.763
16,000	98.07	1.370

4.1.3 Tensile Test for Residual Strength of ABS

Since the high impact grade ABS was made by injection molding, the quality of each specimen should be very consistent. A tensile strength of 47MPa according to the ASTM standard, specified by the manufacturer, was verified by subjecting 2 specimens to monotonic tensile test. The measured tensile strengths were 46.89MPa and 46.97MPa. Therefore, the mean ultimate tensile strength, σ_{t0}, of these high impact grade ABS specimens can be simply assigned to be 47MPa. A total of 106 specimens were tested at 4 different loading conditions, so that the effect of stress ratio and maximum cyclic stress level on ultimate tensile strength after the cyclic loading can be investigated. Table 4.4 documented the loading conditions, as well as the measured residual tensile strength for all specimens subjected to monotonic tensile test.

Table 4.4. The measured tensile strengths with respect to the number of pre-cycles at various loading conditions for ABS

R=0.5; σ_{max}=0.8σ_{t0}		R=0.3; σ_{max}=0.8σ_{t0}		R=0.1; σ_{max}=0.8σ_{t0}		R=0.3; σ_{max}=0.6σ_{t0}	
n (cycle)	$\sigma_{tn}(n)$ (MPa)	n (cycle)	$\sigma_{tn}(n)$ (MPa)	n (cycle)	$\sigma_{tn}(n)$ (MPa)	n (cycle)	$\sigma_{tn}(n)$ (MPa)
500	47.94	100	47.85	50	47.96	1,000	48.04
1,000	48.25	100	47.67	50	48.13	1,000	48.19
2,000	47.72	100	47.85	100	48.13	1,000	48.19
2,500	48.12	200	48.27	100	48.12	1,000	48.13
3,000	47.62	300	47.96	100	48.01	2,000	48.37
3,500	47.39	300	47.69	100	48.19	2,000	48.55
3,500	48.75	400	48.54	150	48.74	2,000	48.75
3,500	47.70	500	48.08	200	48.24	3,000	48.14
3,500	47.25	600	48.19	250	48.09	3,000	48.26
4,000	46.94	600	48.68	250	48.42	3,000	48.33
4,500	47.64	700	47.70	250	48.31	4,000	48.37
6,000	47.01	800	47.95	300	48.24	5,000	48.23
6,000	46.89	900	48.59	400	48.36	5,000	48.23
6,000	46.52	900	48.69	500	48.26	7,000	48.43
7,500	47.40	1,000	47.75	600	48.25	7,000	48.16
8,000	47.17	1,000	48.89	700	48.37	8,000	48.51
10,000	47.29	1,000	48.98	700	48.28	9,000	48.43
11,000	47.02	1,000	48.92	700	48.11	9,000	48.49
11,500	47.40	1,100	48.60	800	48.40	10,000	48.30
13,000	47.05	1,200	48.21	850	48.13	11,500	48.83
13,000	47.10	1,300	48.42	850	48.45	13,000	48.47
15,000	47.21	1,300	48.79	900	48.50	15,000	48.63
16,000	46.66	1,400	48.29	1,000	48.40	15,000	48.76
-	-	1,500	47.34	1,100	47.89	17,000	48.49
-	-	1,600	48.43	1,200	47.60	17,000	48.42
-	-	1,700	47.21	-	-	20,110	48.83
-	-	1,900	47.67	-	-	23,000	48.54
-	-	2,000	47.24	-	-	-	-
-	-	2,150	48.49	-	-	-	-
-	-	2,300	47.03	-	-	-	-

The measured residual strengths did not drop noticeably with the number of pre-cycles for each of the loading conditions. Note that the tensile strength of the virgin material is 47MPa, which is generally smaller than the tensile residual strength values listed in Table 4.4. The fact that the ultimate tensile strength is lower in virgin material than those pre-cycled specimens was unexpected, and had not been reported in the past. It is speculated that this phenomenon is due to some residual stress introduced during the material fabrication process, which was relieved by the fatigue loading for a small number of cycles, resulting in the increase of ductility of the material, thus causing fluctuation of the test results. The overall ductility in the virgin material was shown to decrease eventually by the cyclic loading. According to Table 4.4, the residual strengths maintained at a fairly constant level with respect to the number of fatigue cycles, while the residual energy $Er_{tn}(n)$ and maximum elongation at failure $\Delta(n)$ showed a much more rapid drop during the early fatigue cycles, as indicated in Table 4.5. The number of fatigue cycles selected for each test depends on the degradation trend observed in the residual energy and the maximum elongation at failure, i.e. I chose the maximum number of cycles at which $Er_{tn}(n)$ and $\Delta(n)$ approached zero. Since no obvious degradation of the material strength was detected and the residual energy data is scattered significantly, the result could not be used to determine the constants in the DC model and YL model. Therefore, feasibility of using the DC model and YL model for the prediction of fatigue properties of ABS could not be evaluated.

Table 4.5. The residual energy and maximum elongation at failure with respect to number of pre-cycles at various loading conditions for ABS

$R=0.5;\ \sigma_{max}=0.8\sigma_{t0}$			$R=0.3;\ \sigma_{max}=0.8\sigma_{t0}$			$R=0.1;\ \sigma_{max}=0.8\sigma_{t0}$			$R=0.3;\ \sigma_{max}=0.6\sigma_{t0}$		
n (cycle)	$Er_{in}(n)$ (kN-mm)	$\Delta(n)$ (mm)	n (cycle)	$Er_{in}(n)$ (kN-mm)	$\Delta(n)$ (mm)	n (cycle)	$Er_{in}(n)$ (kN-mm)	$\Delta(n)$ (mm)	n (cycle)	$Er_{in}(n)$ (kN-mm)	$\Delta(n)$ (mm)
500	75.76	50.34	100	61.93	40.70	50	69.51	45.49	1,000	35.79	23.14
1,000	75.41	49.41	100	69.87	46.32	50	80.20	52.31	1,000	45.81	29.59
2,000	57.32	38.01	100	61.93	40.70	100	59.16	38.44	1,000	53.97	34.92
2,500	41.57	27.14	200	75.79	49.42	100	71.45	46.61	1,000	55.41	35.86
3,000	48.15	31.84	300	52.38	34.34	100	57.71	37.52	2,000	41.65	26.82
3,500	33.81	22.29	300	74.38	49.57	100	81.09	53.01	2,000	66.82	42.95
3,500	45.27	29.22	400	66.09	42.97	150	74.64	47.94	2,000	54.82	34.89
3,500	32.86	21.65	500	52.28	34.23	200	70.53	46.23	3,000	19.98	13.06
3,500	58.54	38.78	600	66.26	43.54	250	41.05	26.54	3,000	37.97	24.37
4,000	44.03	21.78	600	49.44	31.73	250	67.86	44.04	3,000	47.31	30.31
4,500	53.44	35.01	700	46.25	30.63	250	37.77	24.15	4,000	51.69	33.16
6,000	34.14	22.57	800	42.34	27.77	300	42.62	27.47	5,000	45.63	29.30
6,000	32.42	21.78	900	32.35	20.84	400	35.62	22.91	5,000	43.28	27.97
6,000	39.86	26.80	900	31.30	20.04	500	28.54	18.45	7,000	56.38	36.27
7,500	34.53	22.63	1000	10.41	7.34	600	18.82	12.31	7,000	38.88	25.00
8,000	29.01	19.31	1000	42.00	26.80	700	3.35	2.90	8,000	33.53	21.32
10,000	26.76	18.00	1000	8.24	5.81	700	18.36	12.04	9,000	42.60	27.06
11,000	20.04	14.04	1000	30.65	19.47	700	14.47	9.66	9,000	31.98	20.60
11,500	14.30	10.44	1100	37.29	23.70	800	14.95	9.92	10,000	18.05	11.86
13,000	6.72	6.24	1200	28.02	18.26	850	4.69	3.70	11,500	15.37	9.96
13,000	14.61	10.76	1300	9.64	6.78	850	14.57	9.68	13,000	25.85	16.63
15,000	13.26	10.04	1300	26.24	16.86	900	5.26	4.12	15,000	7.20	5.17
16,000	13.97	11.21	1400	18.72	12.40	1,000	3.67	3.22	15,000	18.25	11.73
-	-	-	1500	6.75	5.17	1,100	3.68	3.25	17,000	14.32	9.51
-	-	-	1600	8.58	6.14	1,200	2.89	2.85	17,000	20.94	13.59
-	-	-	1700	4.77	4.02	-	-	-	20,110	16.08	10.29
-	-	-	1900	2.83	2.96	-	-	-	23,000	5.89	4.57
-	-	-	2000	3.17	3.01	-	-	-	-	-	-
-	-	-	2150	5.82	4.55	-	-	-	-	-	-
-	-	-	2300	2.85	3.02	-	-	-	-	-	-

The evolution of the load-displacement response of ABS specimens after subjected to 1000, 10000 and 16000 cycles at R=0.5 and σ_{max}=0.8σ_{t0} is presented in Figure 4.5. The three curves have an offset in both displacement and load for clarity, but they all start from zero load and zero displacement. It is shown that the toughness of the specimens decrease with the increase of the number of fatigue cycles, possibly due to damage accumulated in the material. Note that the specimen did not fracture immediately after reaching the yield point. Instead, the load decreased slowly with respect to the displacement until final failure. Characteristic of this load-displacement curve illustrates ductile fracture behavior [8], with extensive elongation and plastic deformation when subjected to monotonic tensile loading. The fractured specimen showed substantial elongation, necking and whitening (crazing) within the gauge section. It should be noted that specimens will eventually fracture with insignificant amount of elongation if they were cyclically-loaded to a sufficiently large number of cycles. It is speculated that the cyclic loading will finally generate cracks or micro-voids in the specimen, which tends to weaken the material and lower its tensile strength.

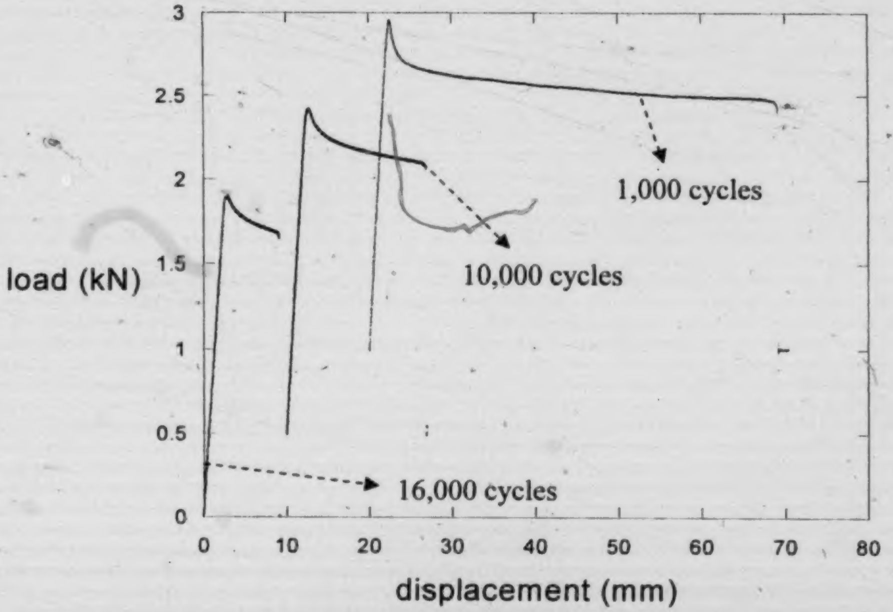

Figure 4.5. Load-displacement curves of ABS specimens after subjecting to different numbers of fatigue cycles at *R= 0.5* and $\sigma_{max}=0.8\cdot\sigma_{t0}$. The curves for 10,000 and 1,000 cycles have offset in both load and displacement, but each curve starts at zero load and zero displacement

4.2 Data Analysis

4.2.1 Determining Parameters of Weibull Distribution

The parameters for the Weibull distribution can be determined from the flexural monotonic test results of glass-filled polycarbonate listed in Table 4.1. Based on the procedure discussed in Chapter 2, the shape and scale parameters of the 2-parameter Weibull distribution are 33.4 and 130.5MPa; while the guarantee value, shape and scale parameters for the 3-parameter Weibull distribution were determined to be 120MPa, 2.3 and 130.4MPa, respectively. The expression for 2- and 3-parameter Weibull distribution can be formulated as in equation (4-1) and (4-2) respectively. The measured flexural ultimate strength and its statistical distribution based on the 2- and 3-parameter Weibull distribution is given in Figures 4.6 and 4.7.

$$P_s[\sigma_n(0)] = \exp\left[-\left(\frac{\sigma_n(0)}{130.5}\right)^{33.4}\right] \tag{4-1}$$

$$P_s[\sigma_n(0)] = \exp\left[-\left(\frac{\sigma_n(0)-120}{130.4-120}\right)^{2.3}\right] \tag{4-2}$$

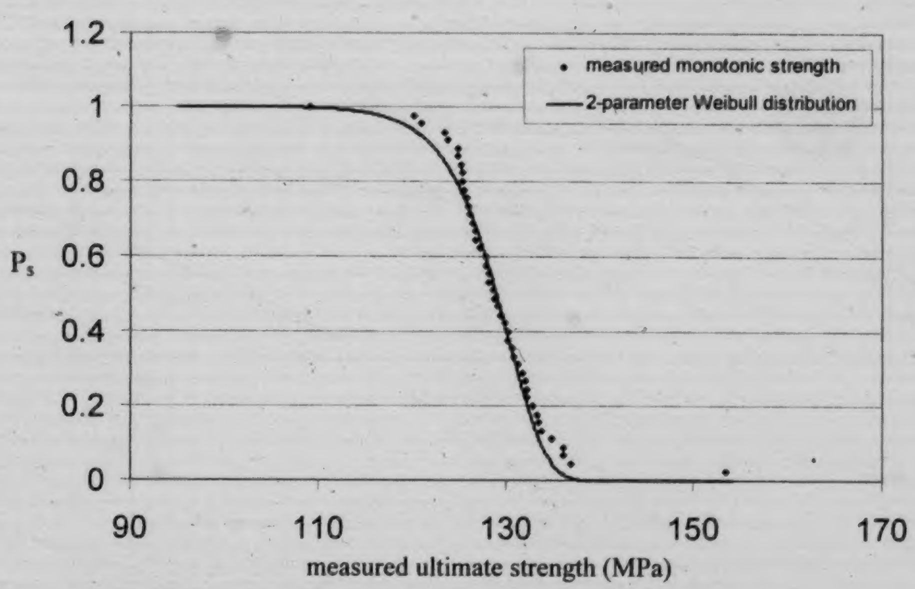

Figure 4.6. The measured monotonic ultimate strength of glass-filled polycarbonate and the probability of survival based on the 2-parameter Weibull distribution

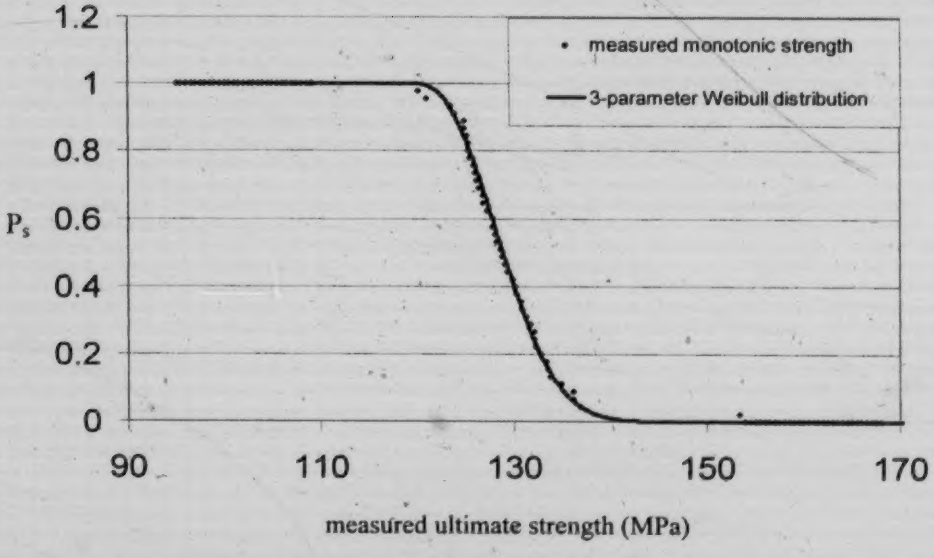

Figure 4.7. The measured monotonic ultimate strength of glass-filled polycarbonate and the probability of survival based on the 3-parameter Weibull distribution

It was observed that the 2-parameter Weibull distribution represents the statistical distribution of the measured ultimate strength reasonably well, except at the upper and lower tail portions. On the other hand, the 3-parameter Weibull distribution followed the trend of the measured ultimate strength much closer at both end portions.

In the statistical implementation of the DC model, one of the assumptions is that the scatter in fatigue life is solely due to the scatter in the ultimate strength from the monotonic tests, which can be well represented by the 2-parameter Weibull distribution. Therefore, the calculated ultimate strength from the measured fatigue life in Table 4.2 can be represented by the statistical distribution given in equation (4-1), and the result is presented in Figure 4.8. Slight deviation is observed between the monotonic statistical distribution and the calculated ultimate strength distribution, which might be due to the variation in quality of the specimens.

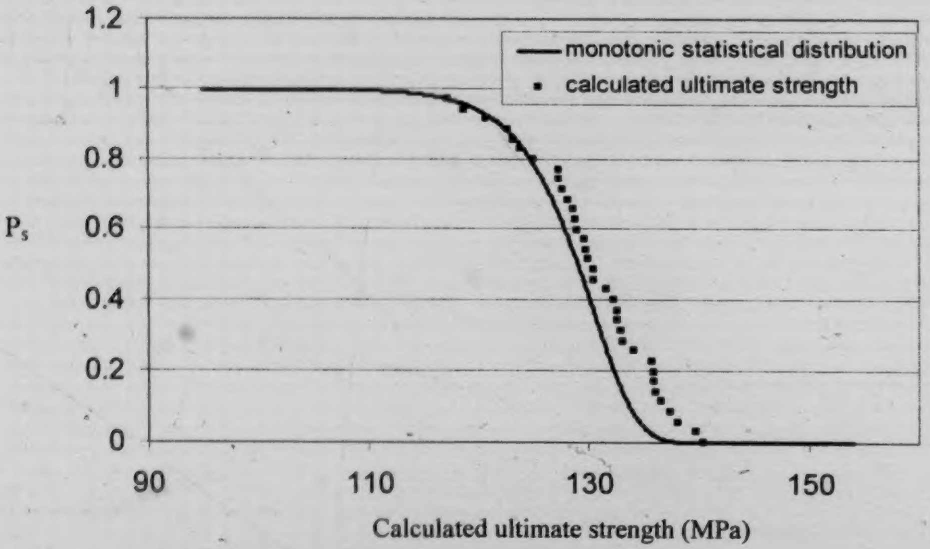

Figure 4.8. The distribution of the calculated ultimate strength of glass-filled polycarbonate from fatigue life data using the DC model and the statistical distribution of the monotonic counterpart

4.2.2 Determining Parameters of the DC Model

In this study, the DC model was only used to assess the flexural fatigue behavior of glass-filled polycarbonate. The model could not be applied to ABS due to the lack of degradation trend in the residual strength with respect to the number of fatigue cycles. The flexural monotonic and fatigue test data in Tables 4.1 and 4.2 were used to evaluate those parameters. For this particular model, the value of the mean ultimate strength $\sigma_n(0)$ in the governing equation (2-26) is equal to the scale parameter of the Weibull distribution, which is the flexural ultimate strength that allows 37% of the specimens to survive. This offers a conservative estimate of fatigue life, and residual strength.

In ref. [34], only data of the stress ratio R=0.7 were used in the plot of Q versus $(N^{\beta}-1)$ to determine α and β. On the other hand, data from more than one stress ratio were involved when evaluating constants α and β [35, 49]. As α and β were assumed to be material constants, they should be fixed for a given material. Each data set corresponded to a stress ratio and their combination was investigated to see whether they all yielded the same values for α and β. The procedure for determining α and β by plotting Q versus $(N^{\beta}-1)$, as discussed in Chapter 2, were followed. The α and β values so determined with respect to stress ratio(s) are summarized in Table 4.6.

Table 4.6. Values of α and β determined from flexural fatigue tests of glass-filled polycarbonate at different stress ratios

R	α	β
0.5	0.045	0.34
0.4	0.046	0.36
0.3	0.045	0.38
0.1	0.054	0.37
0.5, 0.4	0.059	0.32
0.5, 0.3	0.088	0.28
0.5, 0.1	0.11	0.26
0.4, 0.3	0.057	0.33
0.4, 0.1	0.076	0.31
0.3, 0.1	0.055	0.35
0.5, 0.4, 0.3, 0.1	0.1	0.28

The model constants for each set of data of constant R are fairly consistent in the order of magnitude, except the α value for R=0.5, 0.1 and R=0.5, 0.4, 0.3, 0.1. Of all the cases considered in Table 4.6, all the data fall into a straight line when Q is plotted against $N^{\beta}-1$ with the corresponding β values. Therefore, the α and β values determined from the fatigue data associated with different stress ratio were found to be reliable. Nevertheless, the DC model capability in the prediction of residual strength and fatigue life with different α and β values in Table 4.6 would be investigated in the later section. For the purpose of illustration, the α and β values determined from the condition (R=0.5, 0.1) were used in this study. Thus, following the procedure to determine α and β discussed in Chapter 2, α was found to be 0.103 and β, 0.265. The associated plot of Q verses $N^{\beta}-1$ is given in Figure 4.9.

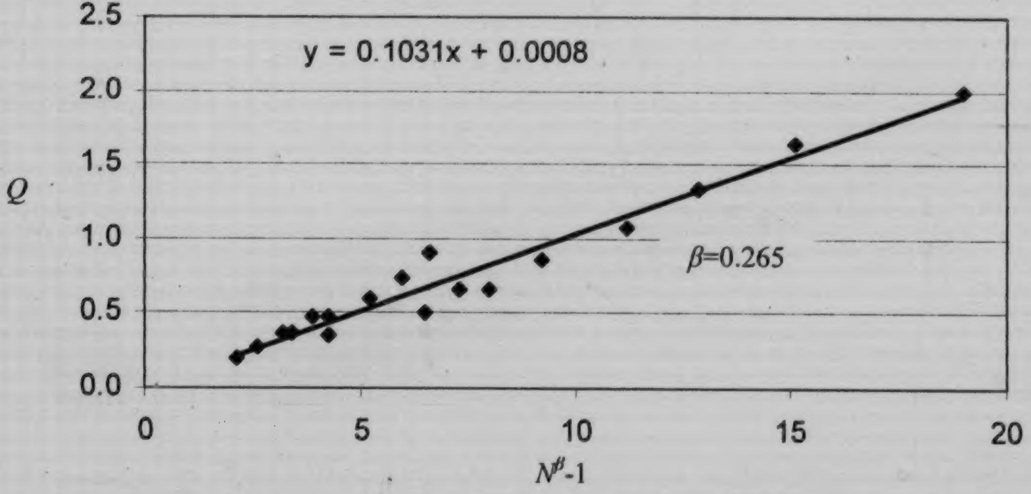

Figure 4.9. Linear curve fit of Q versus $(N^{\beta}-1)$ for determining the constant α and β for flexural fatigue tests of glass-filled polycarbonate carried out at R=0.1, 0.5

4.2.3 Determining Parameters of the YL Model

In this study, the YL model was only used to assess the flexural fatigue behavior of glass-filled polycarbonate, not of ABS due to the lack of degradation trend in its residual strength with respect to the number of fatigue cycles. Its governing equation, as given in equation (2-56), is,

$$\sigma_n^c(n) = \sigma_n^c(0) - \lambda^c K S^b n \qquad (2\text{-}56)$$

Based on the 45 data points in Table 4.1, the average flexural ultimate strength is 129MPa which was used as $\sigma_n(0)$. The model parameters b, c and K were to be determined by the flexural monotonic and fatigue scan data, as shown in Tables 4.1 and 4.2. Based on the previous studies using the YL model [36-37, 70, 72], the b, c and K values determined for different loading modes are tabulated in Table 4.7.

Table 4.7. The determined b, c and K values from literature

	b	c	K
Tension-compression fatigue [37]	12.267	12	$5.56\text{x}10^{-27}$
Tension-tension fatigue [37]	17.34	12.13	$4.99\text{x}10^{-35}$
Tension-tension fatigue [70]	14.98	12.2	$7.49\text{x}10^{-32}$
Tension-tension fatigue [36]	17.78	10.818	$1.8285\text{x}10^{-36}$
Tension-tension fatigue [72]	10.49	18.497	$1.3\text{x}10^{-22}$

Based on the above table, a wider range of possible b, c, and K values were selected to search for the b, c and K values that enable equation (2-56) to fit the experimental data of glass-filled polycarbonate. The selected range and combination of b, c, and K values are given in Figure 4.10.

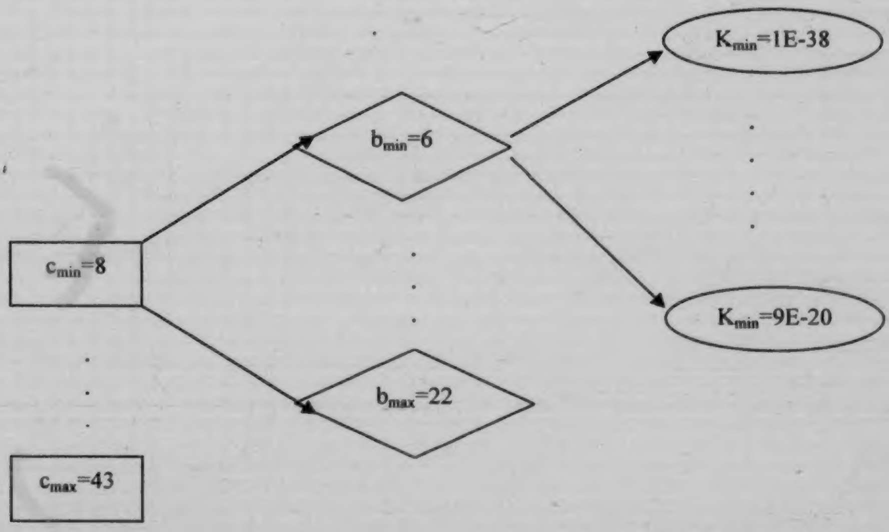

Figure 4.10. Range and combination of parameters, *b*, *c* and *K* considered for the YL model

The constants *b* and *c* ranged from 6 to 22 and 8 to 43, with an increment of 0.1 and 1 respectively. *K* is selected according to the format of *p*E-*w*, where *p* and *w* are positive integers with the increment of *p* and *w* being 1. That is, *p* ranged from 1 to 9, and *w* from 20 to 38, hence parameter *K* was from 1E-38 to 9E-20. With various combinations of *b*, *c*, and *K*, the equivalent ultimate strengths and thus the three central moments μ_1, μ_2 and μ_3 could be evaluated. These values were then compared with the three central moments m_1, m_2 and m_3 calculated from the monotonic test data. The best set of *b*, *c*, and *K* values that yielded the smallest total error of 0.2423 are 9.5, 39 and 3E-26, respectively ($error_1$=0.2356, $error_2$=0.00361 and $error_3$=0.00303). Although the three parameters were determined, it was still necessary to verify its validity in estimating residual strength. With the three model parameters, the residual strength for a loading condition e.g. R=0.5, $\sigma_{max}=0.6\sigma_n(0)$, was estimated based on the YL model and was then compared with the experimental data, as shown in Figure 4.11.

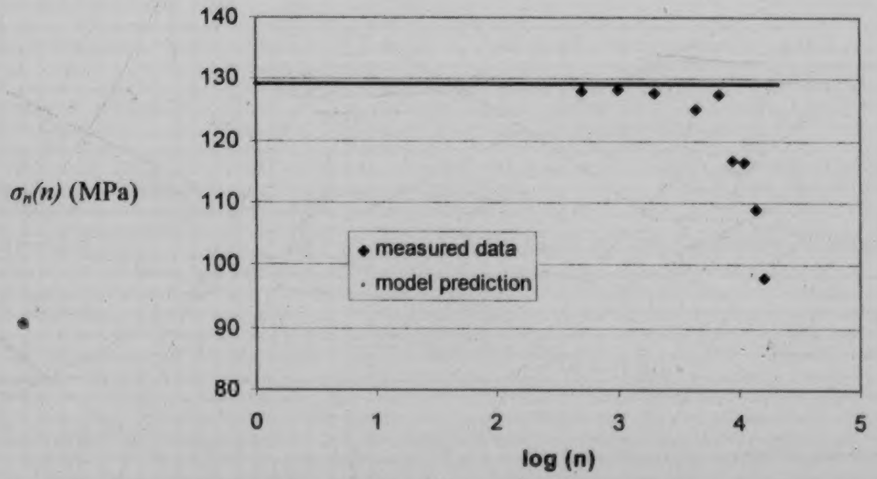

Figure 4.11. The prediction by the YL model (c=39, b=9.5 and K=3E-26), together with the measured residual strength (◆) of glass-filled polycarbonate at R=0.5 and σ_{max}=78.3MPa

From the above plot, it is clear that the YL model does not correctly estimate the measured data. The dropping trend at near 10^4 cycles in the data cannot be described by the prediction using these parameters.

Yang et. al utilized the experimental data of tension-compression and tension-tension fatigue tests [37, 70] to determine the model parameters (b, c and K) and examined the statistical distribution of fatigue life and residual strength according to those parameters determined. The modified method for determining b, c and K, discussed in Chapter 2 was followed, using the same experimental data to evaluate the b, c and K values and investigate the prediction accuracy of fatigue life and residual strength. In the following analysis, the two sets of b, c and K values (one determined by Yang et. al, and the other by me) were compared and examined to check the agreement between the theoretical prediction and experimental results.

The monotonic ultimate tensile strengths of 25 specimens [37] were reported to be 503.3, 477.8, 477.8, 495, 511.6, 519.9, 466.1, 444, 455.1, 496.4, 500.6, 486.8, 427.5, 492.3, 486.8, 481.9, 445.4, 481.9, 449.5, 481.9, 480.6, 468.8, 445.4, 455.1 and 491.6 MPa. The corresponding tension-compression fatigue test results, as given by [37], are shown in Table 4.8.

Table 4.8. Tension-compression fatigue scan data from ref. [37]

Sample ID	σ_{max} (MPa)	σ_{min} (MPa)	cycles to failure, *N*
578-20A	427.5	-68.9	810
604-23A	427.5	-68.9	1,127
606-15B	427.5	-68.9	10
580-26A	399.9	-68.9	4,840
594-1A	399.9	-68.9	4,980
603-10A	399.9	-68.9	1,675
596-23B	372.3	-68.9	10,500
582-2B	372.3	-68.9	11,055
601-18B	372.3	-68.9	6,997
601-20B	344.7	-68.9	10,651
580-16B	344.7	-68.9	16,030
596-26A	344.7	-68.9	10,000
582-3A	317.2	-68.9	25,520
603-18B	317.2	-68.9	36,500
604-5A	317.2	-68.9	78,710
578-21A	289.6	-68.9	130,720
583-13A	289.6	-68.9	78,290
606-19B	289.6	-68.9	188,887
594-22B	262	-68.9	111,600
583-7B	262	-68.9	414,560
601-21A	262	-68.9	485,190
582-25B	234.4	-68.9	1,047,000
578-16B	234.4	-68.9	1,322,440
596-3A	234.4	-68.9	2,104,510
580-26B	399.9	-110.3	1,402
594-7A	399.9	-110.3	3,251
601-17A	399.9	-110.3	1,010
578-22A	344.7	-110.3	10,906
582-5B	344.7	-110.3	11,445
604-24B	344.7	-110.3	3,981
580-22A	262	-110.3	213,539
603-16A	262	-110.3	55,380
606-12A	262	-110.3	43,485
604-16B	234.4	-110.3	123,672
580-15A	234.4	-110.3	749,444
606-3A	234.4	-110.3	638,880

Based on the principles suggested by Yang and Liu [36-37], they determined the b, c, and K values to be 12.267, 12 and $5.56\text{x}10^{-27}$. However, if the criteria of minimizing the total absolute error for the three central moments were followed, as suggested in Chapter 2, b, c, and K values would have been 10, 9, and $9\text{x}10^{-23}$, respectively. The two sets of b, c, and K values are obviously different, but they both can provide a reasonable estimate of the fatigue life at a given stress level, and the residual strength at a given number of pre-cycles.

Additional residual tensile strengths and tension-compression fatigue life were reported in ref. [37], which were used to compare with the prediction given by the two sets of b, c and K values. In ref. [37], twenty specimens were subjected to 2,150 pre-cycles and the corresponding residual tensile strengths were 402, 415.8, 439.9, 440.6, 444.7, 445.4, 458.5, 461.3, 465.4, 468.2, 470.2, 481.3, 484.7, 485.4, 488.8, 488.8, 493, 495.7, 497.8 and 505.4MPa, after subjected to cyclic stresses with maximum of 344.7MPa and minimum of -110.3MPa. The estimated residual strength for (b=12.267, c=12, K=$5.56\text{x}10^{-27}$) and (b=10, c=9, K=$9\text{x}10^{-23}$) are 461.8MPa and 453.4MPa, respectively, both of which are within the range of the scatter measured for the residual tensile strength values.

Considering the other tension-compression fatigue result at σ_{max}=399.9MPa, and σ_{min}=-110.3MPa, the number of cycles to fatigue failure for 20 specimens tested were 5, 57, 71, 316, 330, 1010, 1167, 1385, 1402, 1473, 1510, 1740, 1930, 2186, 2356, 2685, 3251, 3406, 3430, 3453. If the fatigue life was evaluated using the two sets of model parameters (b=12.267, c=12, K=$5.56\text{x}10^{-27}$) and (b=10, c=9, K=$9\text{x}10^{-23}$), they are

1,437cycles and 1,480cycles respectively. These values are also within the range of the scatter measured for the fatigue life.

From the above illustration, it is recognized that the b, c, and K determined using a set of monotonic test data and a set of fatigue scan data does provide satisfactory estimate of the fatigue life and residual strength under tension-compression cyclic loading, with the consideration of potential scattering of the measured data. Irrespective of the two sets of different model parameters, both resulted in a reasonable estimate of $\sigma_n(n)$ and N.

The same procedure was applied to assess the tension-tension fatigue data published in [70]. The result of 15 measured ultimate strengths (MPa) is 558, 559.9, 569.1, 577, 584.6, 584.7, 596.5, 596.7, 600.2, 603.2, 604.4, 624.5, 624.6, 640.9, and 661.8. The tension-tension fatigue scan data provided in ref. [70] are tabulated in Table 4.9. Stress ratio used for all tests was 1/36.

Table 4.9. Tension-tension fatigue scan data provided by ref. [70]

σ_{max} (MPa)	N cycles	σ_{max} (MPa)	N cycles	σ_{max} (MPa)	n cycles	σ_n (MPa)
493.7	1,000	406.2	27,690	406.2	20,000	542.6
493.7	1,330	406.2	30,320	406.2	20,000	486.9
493.7	2,430	406.2	126,590	435.2	7,000	552.9
464.2	6,090	406.2	60,150	435.2	7,000	517.5
464.2	5,230	406.2	103,580	389.7	56,000	444
464.2	22,380	406.2	125,790	389.7	56,000	442.5
464.2	25,300	394.7	137,420	389.7	56,000	471.6
435.1	24,530	394.7	56,130	389.7	56,000	343.2
435.1	42,880	377.1	589,190	389.7	56,000	476.5
435.1	8,520	377.1	133,390	389.7	56,000	478.4
435.1	20,490	377.1	155,270	389.7	56,000	484.6
435.1	21,420	377.1	154,600	389.7	56,000	490.5
		348.2	454,110	377.2	100,000	492.4
				377.2	100,000	438.6

For specimens loaded cyclically until fracture, it is assumed that fracture occurs when the residual strength is equal to the maximum applied cyclic stress, and n is equal to N when calculating the equivalent ultimate strength σ_{eq}. The values of b, c, and K were found to be 12.2, 14.98 and 7.49E-32 by Yang et. al using 15 measured ultimate strength and the fatigue scan data in Table 4.9. Following the implementation procedure and utilizing the idea of minimizing the total absolute error in, b, c, and K, I determined the values to be 11.2, 14 and $4\text{x}10^{-25}$, respectively.

Additional test results were available in ref. [70] to verify the prediction capability of the model. At a maximum applied stress of 389.8MPa and 56,000 pre-cycles, the residual strengths of the 16 specimens were recorded in MPa as [70]: 452.5, 473, 475.5, 481.3, 487.5, 495.7, 507, 510.8, 523.4, 546.4, 559.2, 560.3, 561, 585.9, 587.6, and 618.9. The estimated residual strength for (b=12.2, c=14.98, K=$7.49\text{x}10^{-32}$) and (b=11.2, c=14, K=$4\text{x}10^{-25}$) are 551.6MPa and 494.2MPa, respectively. Both values are within the range of the scatter among the measured data.

Now the attention is shifted to the fatigue lives of specimens subjected to a maximum cyclic stress of 417.6MPa and a stress ratio of 1/36. The number of life cycles to fatigue fracture obtained from experiments [70] are 15080, 17960, 22000, 23390, 23980, 25000, 25900, 27340, 32870, 37860, 39540, 40680, 43510, 46080, 49440, 51700, 52510, 70450, 72630 and 135500. At the same time, the approximation given by the YL model with (b=12.2, c=14.98, K=$7.49\text{x}10^{-32}$) and (b=11.2, c=14, K=$4\text{x}10^{-25}$) are 30,989 cycles and 27,546 cycles. These numbers are within the range of the collected data. Therefore, it is believed that both sets of model parameters are capable of predicting the residual strength, as well as the fatigue life for specimens under tension-tension-fatigue loading.

It can be concluded that the three parameters determined from one set of monotonic test data and fatigue scan data based on the idea of mean square difference and total absolute error can both be used to predict the fatigue life and residual strength, provided that the data came from the same material. From the above two cases, it is obvious that those values determined in ref. [37, 70] are not unique. In fact, both sets of parameters offer a fairly accurate estimate within the range of the experimental results.

In the case of glass-filled polycarbonate subjected to flexural fatigue loading, the *b*, *c*, and *K* were determined to be 9.5, 39 and 3E-26 by minimizing the total absolute error between the corresponding central moments obtained from monotonic and fatigue scan data. It was shown in Figure 4.11 that this set of values cannot give a sensible approximation of the measured residual strength at R=0.5 and σ_{max}=60% of the flexural ultimate strength. Therefore, it is suspected that the model parameters are not unique, and some *b*, *c* and *K* values do not predict the residual strength well. It is also worth noting that the YL model was never demonstrated under flexural loading. Thus, modification to the parameter-determining procedure was needed, to give a different selection approach for *b*, *c*, and *K* values for estimating the fatigue life and residual strength.

The new approach used an additional criterion to minimize the total absolute error associated with residual strength. This was through a set of residual strength data after cyclic loading at a given stress ratio and maximum stress, to narrow down the possible values of *b*, *c*, and *K*. The fractional error associated with residual strength can be formulated as shown in equation (4-3),

$$\text{Fractional error associated with residual strength} = \left| \frac{\sigma^c_{theoretical}(n) - \sigma^c_{measured}(n)}{\sigma^c_{measured}(n)} \right| \tag{4-3}$$

where $\sigma^c_{theoretical}(n)$ and $\sigma^c_{measured}(n)$ are the theoretical and measured residual strengths to the power *c*, respectively. The sum of fractional error between the theoretical predictions and 9 experimental values was quantified. For each value of *c* from 8 to 43, the *b* and *K* values were chosen to give the minimum sum of fractional error associated with the residual strength. Thirty six of such possibilities are shown in Table 4.10. Out of all those choices of *b*, *c*, and *K*, one set of values that has the minimum total absolute error of 0.461 was selected, which has *b*, *c* and *K* of 9.4, 26 and 5E-20, respectively. A plot of residual strength against the number of fatigue cycles predicted using this set of *b*, *c* and *K* values is shown in Figure 4.12, which yields a much better agreement with the experimental values.

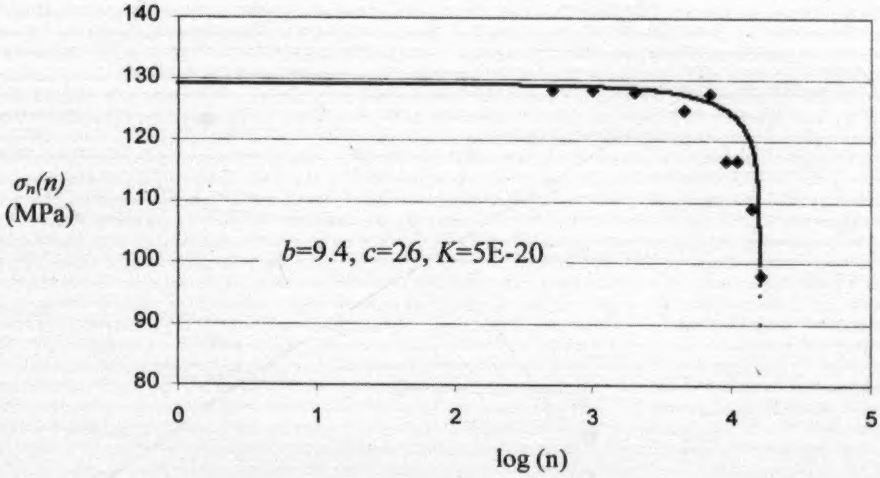

Figure 4.12. Residual strength estimation by the YL model and the measured data of glass-filled polycarbonate at R=0.5 and $\sigma_{max}=0.6\sigma_n(0)$

Table 4.10. The 36 possible *b*, *c* and *K* values that yield the minimum sum of fractional difference associated with the theoretical and measured residual strength

c	***b***	***K***	**Fractional Error Associated with Residual Strength**	**Total Absolute Error equation (2-79)**
8	10.3	2E-21	0.83	108.22
9	10.3	2E-21	0.91	69.08
10	18.8	6E-35	0.76	3100.63
11	9.9	9E-21	0.98	26.15
12	13.2	5E-26	1.33	109.31
13	16.4	4E-31	1.77	304.79
14	16.4	4E-31	2.40	217.64
15	17.5	7E-33	2.92	238.51
16	12	4E-24	3.55	20.92
17	16.8	9E-32	4.36	107.75
18	10.3	2E-21	5.41	5.49
19	18.9	4E-35	6.40	131.45
20	20	7E-37	7.36	145.07
21	19.9	1E-36	8.65	113.84
22	10.1	4E-21	11.05	1.87
23	14.9	9E-29	12.26	17.27
24	11.1	1E-22	15.79	2.65
25	19.4	6E-36	16.73	47.96
26	***9.4***	***5E-20***	***18.97***	***0.46***
27	17.4	9E-33	24.32	20.58
28	10.6	6E-22	26.45	0.64
29	9.3	7E-20	36.51	0.81
30	15.1	4E-29	34.25	6.79
31	16.2	7E-31	43.11	8.58
32	16.1	1E-30	47.93	7.36
33	11.8	7E-24	89.79	0.82
34	20.3	2E-37	67.99	18.06
35	18.7	7E-35	88.13	10.94
36	18	9E-34	97.05	8.17
37	11.5	2E-23	128.14	0.68
38	9.9	7E-21	128.82	1.21
39	9.5	3E-20	135.84	1.39
40	20.5	9E-38	223.91	10.20
41	13.7	6E-27	232.62	1.06
42	12.4	7E-25	457.06	0.75
43	18.2	4E-34	252.10	4.24

4.3 Prediction Accuracy of the DC Model

D'Amore and Caprino [34] developed a 2-parameter residual strength degradation model, based on an assumption that the rate of decrease of the residual strength is a power-law function of the number of pre-cycles. Two constants α and β that appear in the governing equation (2-29) as shown below, depend on both material and loading mode.

$$\left(\frac{\sigma_n(0)}{\sigma_{\max}}-1\right)\cdot\left(\frac{1}{1-R}\right)=\alpha\cdot(N^{\beta}-1) \tag{2-29}$$

The model was used to predict fatigue life and residual ultimate strength of glass-filled polycarbonate.

4.3.1 Fatigue Life Estimation

Fatigue life is the number of cycles that the material can sustain before reaching the complete failure. It is an important piece of information when designing parts or structural components that are constantly subjected to cyclic loading, so that preventative measures can be taken to avoid catastrophic failure. In order to predict the fatigue life of glass-filled polycarbonate at various loading conditions, the model constants must be evaluated from the monotonic and fatigue data in Tables 4.1 and 4.2. It was determined that α and β are 0.103 and 0.265, respectively for the purpose of illustration. The ultimate strength of the virgin material $\sigma_n(0)$ was taken to be the scale parameter of the Weibull distribution, that is, the ultimate strength that allows 37% of the sample to survive, and is equal to 130.5MPa. The fatigue life can be represented as a function of R and σ_{max}, as indicated in equation (2-28), and shown in the following:

$$N = [1 + \frac{1}{\alpha \cdot (1 - R)} \cdot (\frac{\sigma_0}{\sigma_{max}} - 1)]^{\frac{1}{\beta}} \qquad (2\text{-}28)$$

Prediction of N at various stress levels and stress ratios of 0.1 - 0.5, based on equation (2-28) is presented in Figure 4.13, together with the experimental data.

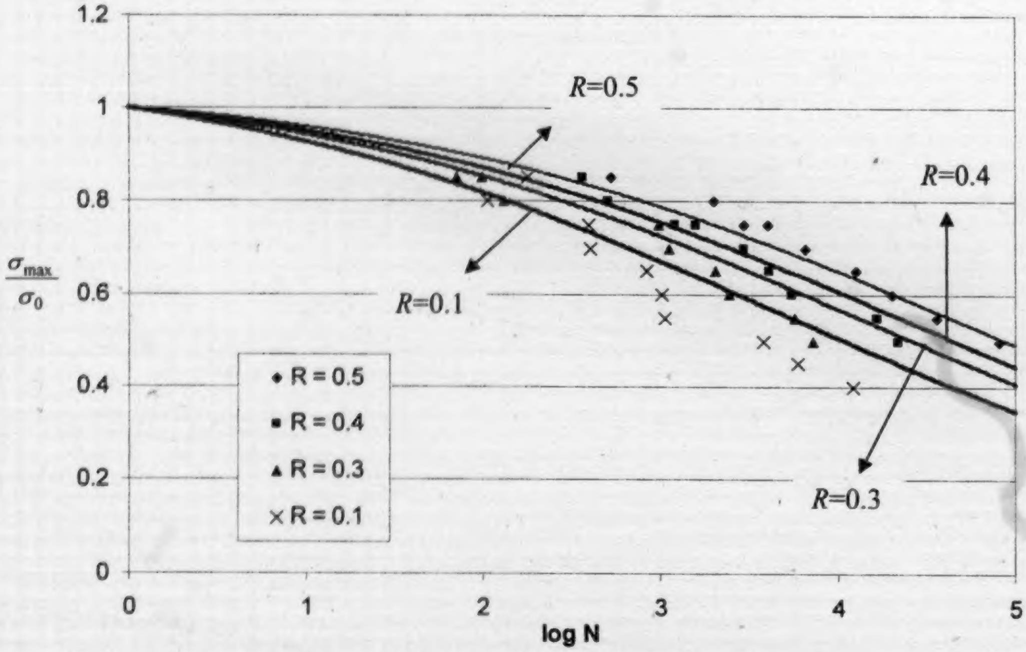

Figure 4.13. Non-dimensional maximum applied cyclic stress versus log N for the theoretical and measured flexural fatigue data of glass-filled polycarbonate at R=0.5, 0.4, 0.3 and 0.1

Figure 4.13 suggests that the theoretical prediction of fatigue life at stress ratios of 0.5, 0.4, 0.3 and 0.1 are generally consistent with the experimental data. Similar results were also observed for other α and β values determined with other stress ratio(s) in Table 4.6. At a given σ_{max}, the life always increases with the increase of R value. However, slight discrepancies do exist between the theoretical prediction and the experimental results. Nevertheless, the results support that the DC model can effectively describe the effect of stress ratio on the fatigue life. This is also evident from the observation that all fatigue data listed in Table 4.2 collapsed to a single master curve irrespective of the stress ratio when Q is plotted against log N, as shown in Figure 4.14.

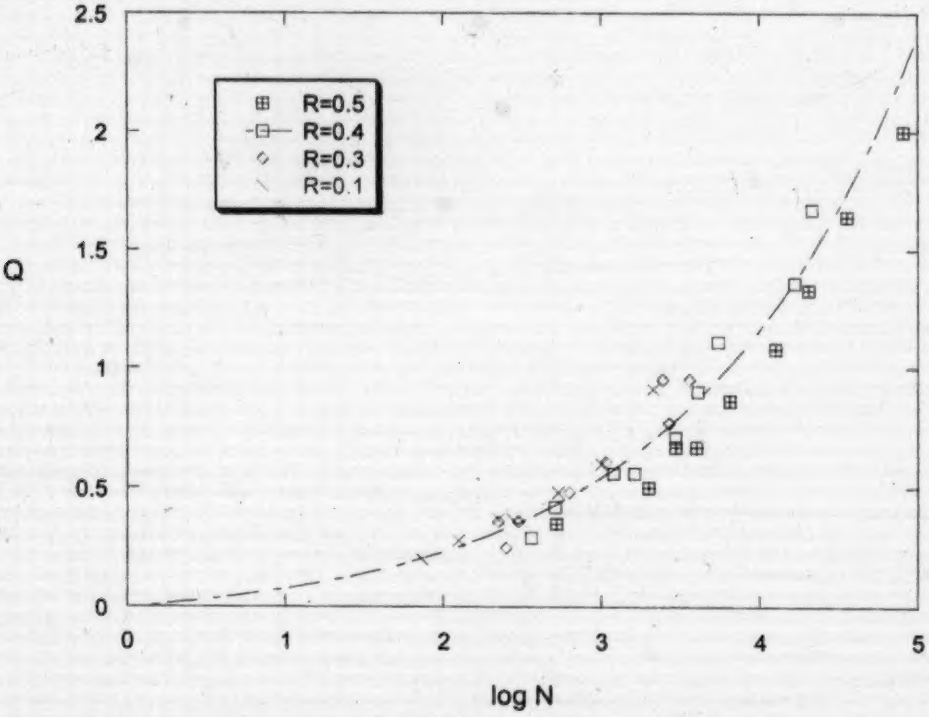

Figure 4.14. A plot of Q with respect to log N for all the flexural fatigue data of glass-filled polycarbonate irrespective of stress ratios

4.3.2 Residual Strength Approximation

The DC model [34] was developed based on the hypothesis that the residual strength of the material decreases monotonically with the increase of the number of cycles. Therefore, it should also be able to estimate the residual strength of the specimens after being subjected to any given number of cycles. In order to verify this capability, flexural monotonic tests were carried out on pre-cycled specimens, at a stress ratio R of 0.5 and maximum cyclic stress equal to 60% of the flexural ultimate strength. The measured residual strength values as a function of n in Table 4.3 are compared with the theoretical prediction based on the DC model (α=0.103, β=0.265) in Figure 4.15, which shows that the model predicts a gradual drop in residual strength with the increase of the number of cycles. However, the measured data maintained the ratio of $\sigma_n(n)$ to $\sigma_n(0)$ at the same level to nearly 10^4 cycles, and dropped much sharply afterwards. Therefore, the theory has underestimated the ultimate strength of the material after the cyclic loading, and the assumption of the rate of residual strength degradation was not supported by the measured data. Similar results were also observed for other α and β values determined with other stress ratio(s) in Table 4.6. Because of this problem, our attention was shifted to the YL model for estimation of both fatigue life and residual strength of the glass-filled polycarbonate. Since the YL model has 3-parameters (b, c and K), offering one more degree of freedom than the 2-parameter (α and β) DC model, it may give a better prediction of fatigue life and residual strength.

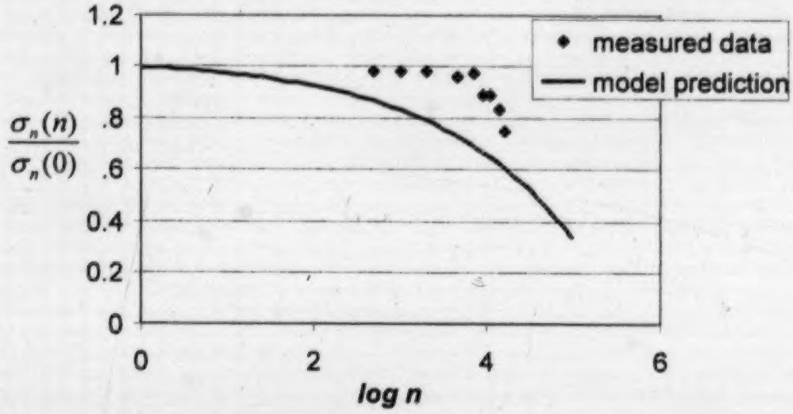

Figure 4.15 Comparison of the DC model prediction and the measured data of glass-filled polycarbonate on residual strength

4.4 Prediction Accuracy of the YL Model

The YL model [36-37] was proposed in 1976 and based on the assumption that the rate of degradation of residual strength is inversely proportional to the residual strength in a non-linear fashion. There are three constants, b, c, and K, associated with this model, which can be determined using the monotonic and fatigue data. In this study, prediction accuracy on fatigue life and residual strength of glass-filled polycarbonate, as well as the ability of the YL model to account for the effect of stress ratio, was investigated in detail.

4.4.1 Fatigue Life Estimation

Since properties of glass-filled polycarbonate panels are batch-dependent, all specimens had to come from the same panel. This has limited the number of specimens available for the study. That is, only the fatigue scan data in Table 4.2 are available for the analysis. Although the attention was on the correct representation of fatigue life of the scan data, the model should be capable of estimating the life at other loading condition. This was shown to be the case for other existing experimental results for tension-compression [37] and tension-tension [70] fatigue, as in section 4.2.3.

Utilizing the flexural monotonic and fatigue scan data, and a set of residual strength data at R=0.5, the model parameters were determined to be b=9.4, c=26, K=5x10^{-20}. The fatigue life with respect to various levels of maximum cyclic stress and stress ratio of 0.5, 0.4, 0.3 and 0.1 can be estimated according to equation (2-57),

$$N = \frac{\sigma_n^c(0) - \sigma_{\max}^c}{\lambda^c K S^b} \qquad (2\text{-}57)$$

Stress ratio was proven to have a significant effect on fatigue life [34], that is, the smaller the stress ratio, the shorter is the fatigue life at the same maximum cyclic stress. Since the stress ratio does not explicitly appear in equation (2-57), its effect is believed to be incorporated in stress ranges (σ_{max} - σ_{mix}). If the stress range is rewritten in terms of σ_{max} and R, then equation (2-57) becomes:

$$N = \frac{\sigma_n^c(0) - \sigma_{\max}^c}{\lambda^c K(\sigma_{\max} - \sigma_{\max} \cdot R)^b} \tag{4-4}$$

One possibility is that the YL model can predict the fatigue life for different stress ratios at a given maximum cyclic stress by varying R in equation (4-4), as this was the case for the DC model [34-35, 49]. In Figure 4.16, the measured fatigue life as in Table 4.2 associated with stress ratio of 0.5, 0.4, 0.3, 0.1 and the corresponding theoretical representations from the YL model are compared.

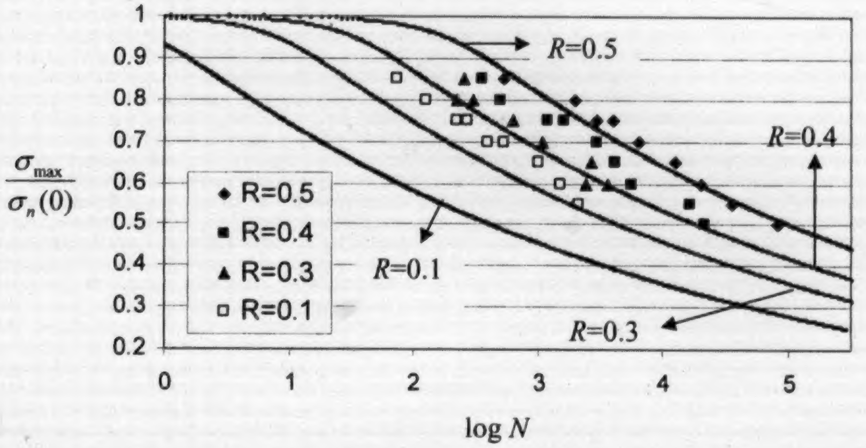

Figure 4.16. Theoretical and experimental non-dimensional maximum applied stress against fatigue life of glass-filled polycarbonate for various stress ratio, with b=9.4, c=26, K=5E-20

The YL model shows the fact that for the same maximum applied cyclic stresses, the higher the stress ratio, the longer is the fatigue life. Due to the inherent nature of fatigue data, scatter in the measurements cannot be avoided. In my opinion, a closer approximation of the fatigue life such as that shown for the stress ratio of 0.5 can be achieved for other stress ratios. The discrepancy in Figure 4.16 was probably due to the use of one set of residual strength data at R=0.5 for the determination of b, c, and K values. Nevertheless, the goal of providing a more accurate representation of fatigue life motivated us to examine the relationship between the stress ratio and the model parameters.

4.4.2 Correlation of Stress Ratio and Model Parameters

It was suggested by Ryder and Walker [61] that the YL model parameters b and K may depend on either the stress ratio or the minimum cyclic stress. Since the ability of accounting for the effect of stress ratio is one of main concerns for the YL model, the relationship between R and K, and that between R and b were investigated separately to identify a useful correlation between the stress ratio and the model parameters.

By varying K while holding c and b fixed, different K values were determined to fit the measured fatigue life data at each stress ratio, as shown in Figure 4.17.

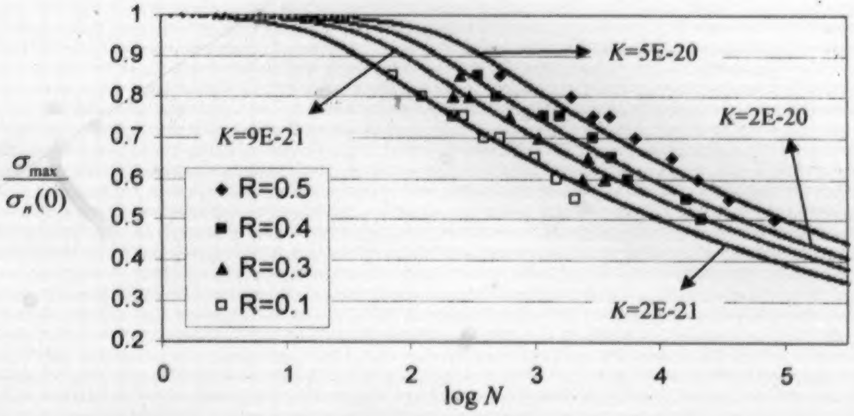

Figure 4.17. Non-dimensional maximum applied cyclic stress versus log N for the YL model prediction and the fatigue life data of glass-filled polycarbonate, with fixed constant c=26 and b=9.4

By adjusting the value of K for each of the stress ratios, the model seems to give a satisfactory estimate for N. Through try and error, the same procedure was applied to obtain the S-N curve approximation with respect to R, but this time the parameter c and K were kept constant.

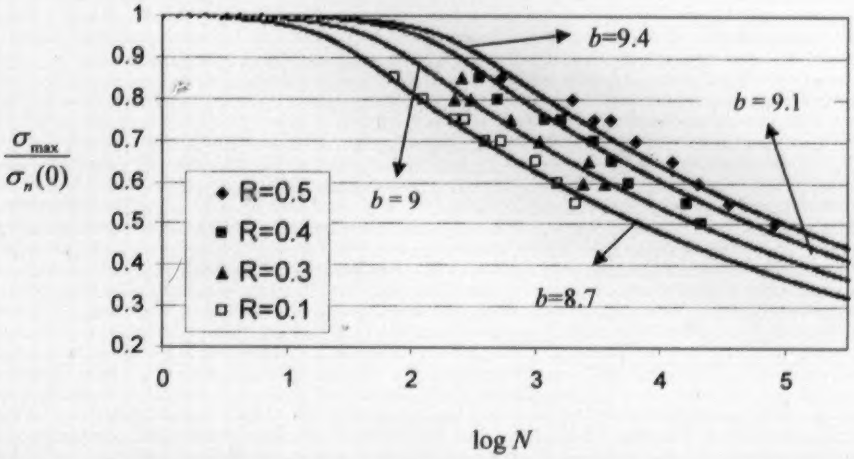

Figure 4.18. Non-dimensional maximum applied cyclic stress versus log N for the YL model prediction and the fatigue life data of glass-filled polycarbonate, with fixed constant c=26 and K=5E-20

It is shown in Figures 4.17 and 4.18 that as the stress ratio reduces from 0.5 to 0.1, the values of *b* and *K* also decrease accordingly. Therefore, it is suspected that parameters *b* and *K* may be functions of stress ratio. In order to assess their relationships further and find out the type of functions that relates them to stress ratio, plots of *b* against *R* by fixing *c* and *K* at 26 and 5E-20, respectively, and that of *K* against *R* by fixing *c* and *b* at 26 and 9.4, respectively, are summarized in Figures 4.19 and 4.20.

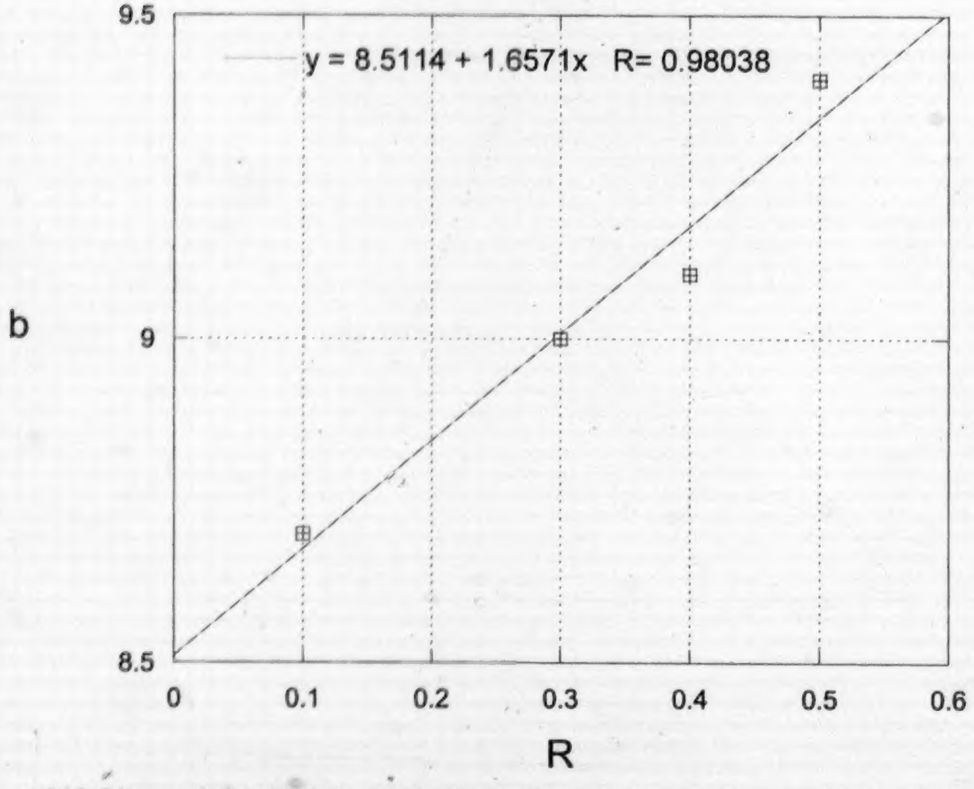

Figure 4.19. Linear relationship between the YL model parameter *b* and stress ratio *R*, with *c* and *K* fixed at 26 and 5E-20 respectively

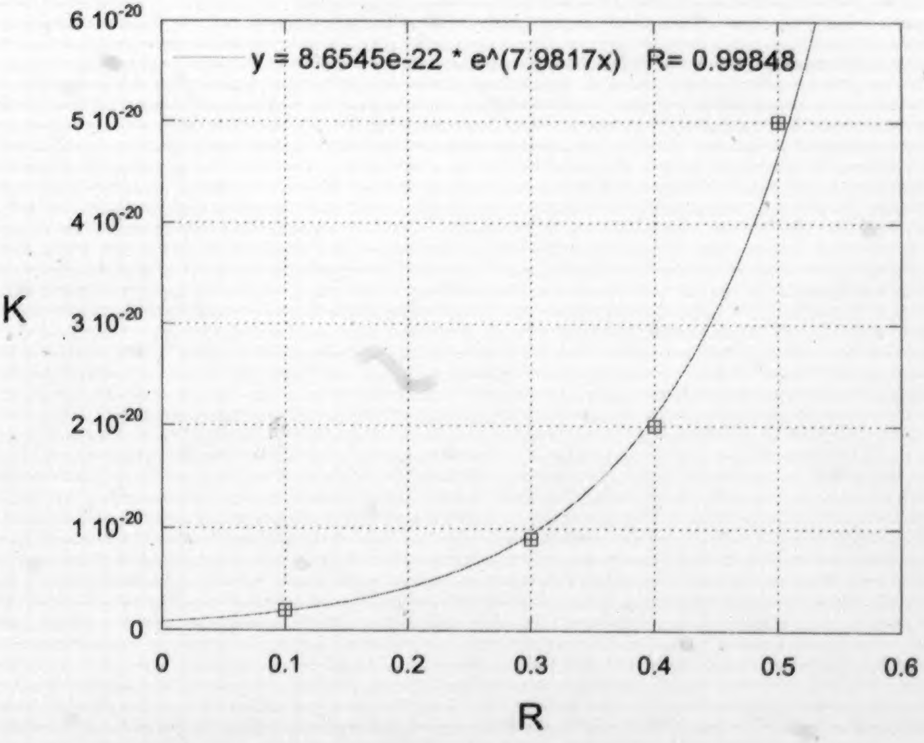

Figure 4.20. Exponential relationship between the YL model parameter *K* and stress ratio *R*, with *c* and *b* fixed at 26 and 9.4 respectively

Although there are only 4 data points in each figure, an apparent correlation can be demonstrated between *b* and *R*, as well as between *K* and *R*. In Figure 4.19, a linear relationship is exhibited between parameter *b* and *R*, suggesting that *b* can be expressed as a linear function of *R*. The linear function was found to be $b=1.7R+8.5$. While *K* varies with *R* exponentially, the corresponding equation was determined to be $K=8.7\text{x}10^{-22}e^{8R}$. Alternatively, if the relationship between *K* and *R* is presented in a semi-log plot, a linear relationship can also be obtained, as shown in Figure 4.21. The function for Figure 4.21 is $(\ln K)=8R-48.5$.

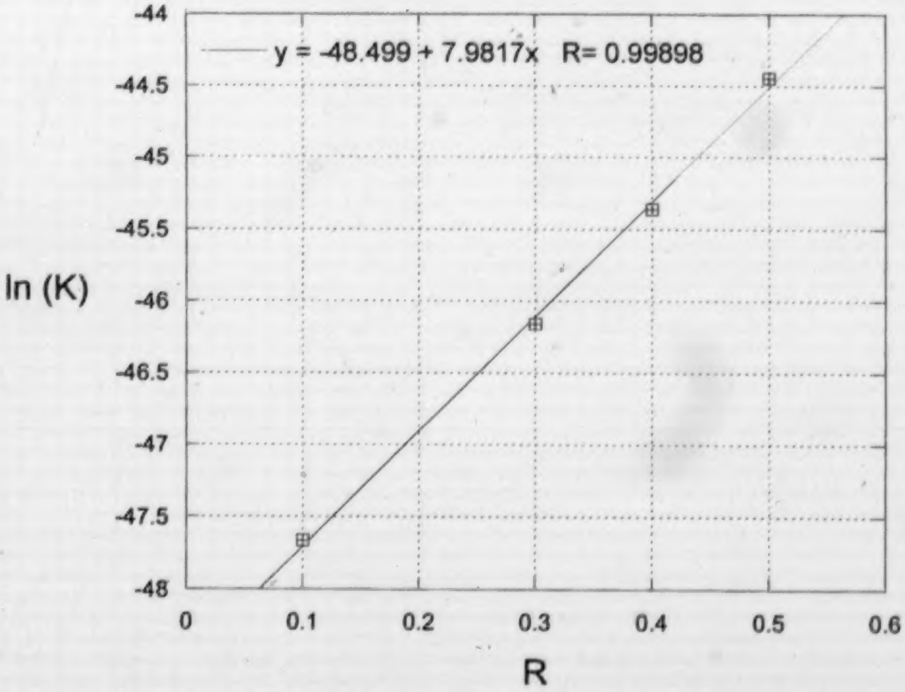

Figure 4.21. A semi-ln plot of *K* against *R*, with *c* and *b* fixed at 26 and 9.4 respectively

The above findings are significant in regards to the S-N curve approximation for various stress ratios, as the linear function between *b* and *R*, and between *log K* and *R* are relatively simple to determine, and should be incorporated in the YL model. However, the underlining assumption for the above analysis is that the remaining parameters should be invariants regardless of stress ratio and maximum cyclic stress. This assumption will be examined in the following section.

4.4.3 Examination of the Invariability of the Parameters in the YL Model

Based on the formulation of the governing equation, it is speculated that one of the parameters depends on stress ratio, the second one depends on maximum cyclic stress and the last one is a material constant and possibly a function of the loading mode. For the first case, if b varies with the stress ratio R the other two parameters c and K should be constant irrespective of stress ratio and maximum cyclic stress. Several approaches were considered to check the validity of this assumption.

Based on Figure 4.19, b is a linear function of R. Let us assume that K is a material constant. By rearranging equation (4-4), we have:

$$K = \frac{\sigma_n^c(0) - \sigma_{\max}^c}{\lambda^c N \sigma_{\max}^b (1-R)^b} \tag{4-5}$$

At two different loading conditions, for examples, R_1 and σ_{max}, R_2 and σ_{max}, values of K_1 and K_2 can be determined from equation (4-5), and should be the same as it is a material constant. By equating K_1 and K_2, the value of c at this σ_{max} level can be determined. The same procedure can be followed for different σ_{max} values. However, it turned out that all terms containing c were cancelled out since the $\sigma_n(0)$, σ_{max} and λ are the same for a given σ_{max}. Thus, the equality cannot be established. Then loading conditions of different stress ratios and maximum cyclic stress, R_1 and σ_{max1}, R_2 and σ_{max2}, were assessed using equation (4-5). The c value turns out to be very close to zero, which does not make sense as this would lead to zero for K as well.

Therefore, another approach was taken by only assuming that the parameter b is a function of R. By rearranging the governing equation, equation (2-57), we have:

$$b = \left(\frac{1}{\log S}\right) \cdot \log\left(\frac{\sigma_n^c(0) - \sigma_{\max}^c}{\lambda^c K N}\right) \tag{4-6}$$

Using four different loading conditions, R_1 and σ_{max1_1}, R_1 and σ_{max1_2}, R_2 and σ_{max2_1}, R_2 and σ_{max2_2}, we have two equations from equating the b value, as shown in equations (4-7) and (4-8):

$$\left(\frac{1}{\log[\sigma_{\max1\_1}(1-R_1)]}\right)\cdot\log\left(\frac{\sigma_n^c(0)-\sigma_{\max1\_1}^c}{\lambda^c K_1 N_{1\_1}}\right)=\left(\frac{1}{\log[\sigma_{\max1\_2}(1-R_1)]}\right)\cdot\log\left(\frac{\sigma_n^c(0)-\sigma_{\max1\_2}^c}{\lambda^c K_1 N_{1\_2}}\right) \tag{4-7}$$

$$\left(\frac{1}{\log[\sigma_{\max2\_1}(1-R_2)]}\right)\cdot\log\left(\frac{\sigma_n^c(0)-\sigma_{\max2\_1}^c}{\lambda^c K_2 N_{2\_1}}\right)=\left(\frac{1}{\log[\sigma_{\max2\_2}(1-R_2)]}\right)\cdot\log\left(\frac{\sigma_n^c(0)-\sigma_{\max2\_2}^c}{\lambda^c K_2 N_{2\_2}}\right) \tag{4-8}$$

These two non-linear equations contain two unknowns *c* and *K*, that can be solved using numerical method. However, as non-linear equations, *c* and *K* may not be unique and are difficult to determine. Also, some knowledge about the range of *c* and *K* values must be known. As a result, it seems that the assumption of *b* being a function of stress ratio does not provide a reasonable justification for *c* and *K* being constants.

Thus, attention was shifted to Figure 4.21 where parameters *b* and *c* are assumed to be invariants regardless of stress ratio or maximum cyclic stress, while *K* varies with loading conditions. Let's assume *K* to be a function of *R*. Two equations are needed to solve for *b* and *c*. Consider four different loading conditions as R_1 and σ_{max1_1}, R_1 and σ_{max1_2}, R_2 and σ_{max2_1}, R_2 and σ_{max2_2}. The two equations for different *K* values are given in the following, according to equation (4-5):

$$\frac{\sigma_n^c(0)-\sigma_{\max1\_1}^c}{\lambda^c N_{1\_1}\sigma_{\max1\_1}^b(1-R_1)^b}=\frac{\sigma_n^c(0)-\sigma_{\max1\_2}^c}{\lambda^c N_{1\_2}\sigma_{\max1\_2}^b(1-R_1)^b} \tag{4-9}$$

$$\frac{\sigma_n^c(0)-\sigma_{\max2\_1}^c}{\lambda^c N_{2\_1}\sigma_{\max2\_1}^b(1-R_2)^b}=\frac{\sigma_n^c(0)-\sigma_{\max2\_2}^c}{\lambda^c N_{2\_2}\sigma_{\max2\_2}^b(1-R_2)^b} \tag{4-10}$$

Since the above equations are non-linear, solving for *b* and *c* can also be complicated, as previously discussed. Consequently, a different approach was investigated by assuming *c* to be a constant and *b* a material constant, while *K* changed with stress ratio *R*.

For example, the fatigue lifetimes at two loading conditions with the same σ_{max}, but different stress ratios of R_1 and R_2, were measured. The above hypotheses led to formulation of the expression for b in equation (4-6) as:

$$\left(\frac{1}{\log[\sigma_{\max}(1-R_1)]}\right)\cdot\log\left(\frac{\sigma_n^c(0)-\sigma_{\max}^c}{\chi^c K_1 N_1}\right)=\left(\frac{1}{\log[\sigma_{\max}(1-R_2)]}\right)\cdot\log\left(\frac{\sigma_n^c(0)-\sigma_{\max}^c}{\chi^c K_2 N_2}\right) \qquad (4\text{-}11)$$

Values for K_1 and K_2 were determined from Figure 4.21 based on R_1 and R_2 values. The only unknown in equation (4-11) is the parameter c, which was determined with respect to different loading conditions, as given in Table 4.11, where (R_1, N_1, b_1) and (R_2, N_2, b_2) are the stress ratio, measured fatigue life and calculated b value according to equation (4-6) with respect to the 1st and 2nd loading condition. Since equation (4-11) in terms of c is non-linear, c was evaluated numerically by minimizing the difference between the left and right-hand side of equation (4-11).

Table 4.11. The calculated *c* values with the corresponding loading conditions on glass-filled polycarbonate

R_1	R_2	σ_{max}	N_1	N_2	c	b_1	b_2
0.5	0.4	65.23	81,186	21,624	6.04	9.49	9.62
0.5	0.4	71.75	35,635	16,503	6	9.46	9.45
0.5	0.1	71.75	35,635	2,138	6.79	9.46	9.57
0.4	0.1	71.75	16,503	2,138	6.77	9.45	9.57
0.5	0.4	78.28	20,257	5,534	7.64	9.39	9.52
0.5	0.3	78.28	20,257	3,636	7.64	9.39	9.45
0.5	0.1	78.28	20,257	1,531	7.64	9.39	9.45
0.4	**0.3**	**78.28**	**5,534**	**3,636**	**0.0038**	**7.92**	**7.92**
0.4	**0.1**	**78.28**	**5,534**	**1,531**	**0.14**	**8.84**	**8.84**
0.3	**0.1**	**78.28**	**3,636**	**1,531**	**19.2**	**9.43**	**9.43**
0.5	0.4	84.8	12,544	4,120	8.68	9.31	9.39
0.5	0.3	84.8	12,544	2,670	8.69	9.31	9.34
0.5	0.1	84.8	12,544	1,004	8.69	9.31	9.37
0.4	**0.3**	**84.8**	**4,120**	**2,670**	**0.008**	**7.97**	**7.98**
0.4	**0.1**	**84.8**	**4,120**	**1,004**	**1.04**	**9.16**	**9.16**
0.3	0.1	84.8	2,670	1,004	8.69	9.34	9.37
0.5	0.4	91.32	6,476	2,935	10	9.3	9.3
0.5	0.3	91.32	6,476	1,069	10.01	9.3	9.39
0.5	0.1	91.32	6,476	537	10	9.3	9.35
0.4	0.3	91.32	2,935	1,069	10	9.3	9.39
0.4	0.1	91.32	2,935	537	10	9.3	9.35
0.3	**0.1**	**91.32**	**1,069**	**537**	**0.16**	**8.72**	**8.72**
0.5	0.4	97.84	3,993	1,605	11.73	9.25	9.28
0.5	0.3	97.84	3,993	625	11.44	9.25	9.36
0.5	0.1	97.84	3,993	275	11.44	9.25	9.35
0.4	0.3	97.84	1,605	625	11.86	9.28	9.36
0.4	0.1	97.84	1,605	275	11.48	9.28	9.35
0.3	**0.1**	**97.84**	**625**	**275**	**3.03**	**9.26**	**9.25**
0.5	0.4	104.37	1,998	507	14.08	9.26	9.41
0.5	0.3	104.37	1,998	300	14.11	9.26	9.38
0.5	0.1	104.37	1,998	125	14.11	9.26	9.38
0.4	**0.3**	**104.37**	**507**	**300**	**0.13**	**8.59**	**8.59**
0.4	**0.1**	**104.37**	**507**	**125**	**1.51**	**9.14**	**9.14**
0.3	0.1	104.37	300	125	14.11	9.38	9.38
0.5	**0.4**	**110.89**	**530**	**363**	**0.0004**	**7.09**	**7.09**
0.5	**0.3**	**110.89**	**530**	**253**	**0.00089**	**7.29**	**7.29**
0.5	**0.1**	**110.89**	**530**	**74**	**0.45**	**8.83**	**8.83**
0.4	**0.3**	**110.89**	**363**	**253**	**0.0027**	**9.34**	**9.27**
0.4	0.1	110.89	363	74	17.63	9.34	9.36
0.3	0.1	110.89	253	74	17.65	9.27	9.36

Table 4.11 suggests that the *b* values are fairly consistent, implying that *b* may indeed be a material constant. The general trend of *c* value increasing with the maximum cyclic stress was also noted and plotted in Figure 4.22, though, some *c* values did not follow such a trend and were quite far off. If those irregular *c* values from Table 4.11 were replaced by those following the trend, the corresponding *b* values are consistent with the rest, as tabulated in Table 4.12.

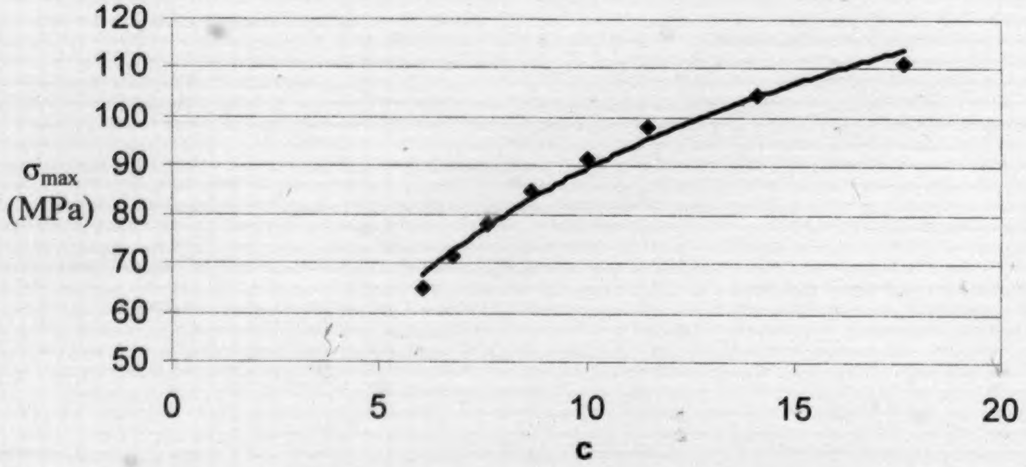

Figure 4.22. The general increasing trend of maximum cyclic stress with respect to the value of parameter *c* based on tests conducted on glass-filled polycarbonate

Table 4.12. The *b* value evaluated when those irregular *c* are replaced with the value observed in the trend in Figure 4.22

R_1	R_2	σ_{max}	N_1	N_2	c	b_1	b_2
0.5	0.4	65.23	81,186	21,624	6.04	9.49	9.62
0.5	0.4	71.75	35,635	16,503	6	9.46	9.45
0.5	0.1	71.75	35,635	2,138	6.79	9.46	9.57
0.4	0.1	71.75	16,503	2,138	6.77	9.45	9.57
0.5	0.4	78.28	20,257	5,534	7.64	9.39	9.52
0.5	0.3	78.28	20,257	3,636	7.64	9.39	9.45
0.5	0.1	78.28	20,257	1,531	7.64	9.39	9.45
0.4	**0.3**	**78.28**	**5,534**	**3,636**	**7.64**	**9.52**	**9.45**
0.4	**0.1**	**78.28**	**5,534**	**1,531**	**7.64**	**9.52**	**9.45**
0.3	**0.1**	**78.28**	**3,636**	**1,531**	**7.64**	**9.45**	**9.45**
0.5	0.4	84.8	12,544	4,120	8.68	9.31	9.39
0.5	0.3	84.8	12,544	2,670	8.69	9.31	9.34
0.5	0.1	84.8	12,544	1,004	8.69	9.31	9.37
0.4	**0.3**	**84.8**	**4,120**	**2,670**	**8.69**	**9.39**	**9.34**
0.4	**0.1**	**84.8**	**4,120**	**1,004**	**8.69**	**9.39**	**9.37**
0.3	0.1	84.8	2,670	1,004	8.69	9.34	9.37
0.5	0.4	91.32	6,476	2,935	10	9.3	9.3
0.5	0.3	91.32	6,476	1,069	10.01	9.3	9.39
0.5	0.1	91.32	6,476	537	10	9.3	9.35
0.4	0.3	91.32	2,935	1,069	10	9.3	9.39
0.4	0.1	91.32	2,935	537	10	9.3	9.35
0.3	**0.1**	**91.32**	**1,069**	**537**	**10**	**9.39**	**9.35**
0.5	0.4	97.84	3,993	1,605	11.73	9.25	9.28
0.5	0.3	97.84	3,993	625	11.44	9.25	9.36
0.5	0.1	97.84	3,993	275	11.44	9.25	9.35
0.4	0.3	97.84	1,605	625	11.86	9.28	9.36
0.4	0.1	97.84	1,605	275	11.48	9.28	9.35
0.3	**0.1**	**97.84**	**625**	**275**	**11.48**	**9.36**	**9.35**
0.5	0.4	104.37	1,998	507	14.08	9.26	9.41
0.5	0.3	104.37	1,998	300	14.11	9.26	9.38
0.5	0.1	104.37	1,998	125	14.11	9.26	9.38
0.4	**0.3**	**104.37**	**507**	**300**	**14.11**	**9.41**	**9.38**
0.4	**0.1**	**104.37**	**507**	**125**	**14.11**	**9.41**	**9.38**
0.3	0.1	104.37	300	125	14.11	9.38	9.38
0.5	**0.4**	**110.89**	**530**	**363**	**17.63**	**9.44**	**9.34**
0.5	**0.3**	**110.89**	**530**	**253**	**17.63**	**9.44**	**9.27**
0.5	**0.1**	**110.89**	**530**	**74**	**17.63**	**9.44**	**9.36**
0.4	**0.3**	**110.89**	**363**	**253**	**17.63**	**9.34**	**9.27**
0.4	0.1	110.89	363	74	17.63	9.34	9.36
0.3	0.1	110.89	253	74	17.65	9.27	9.36

It should be noted that regardless of the choice of *c* values, the corresponding *b* values are close to 9. Therefore, it seems that the resulting *b* values are insensitive to the change in *c*. For example, using a completely reversed trend of Figure 4.22, i.e. *c* decreases with respect to increasing maximum cyclic stress, the *b* values determined from each of the loading conditions are still around 9, as given in Table 4.13.

Table 4.13. The *b* values evaluated when the *c* follow a completely reverse trend

R	σ_{max}	N	c	b
0.5	65.23	81,186	50	9.35
0.5	71.75	35,635	45	9.34
0.5	78.28	20,257	43	9.28
0.5	84.80	12,544	38	9.23
0.5	91.32	6,476	32	9.24
0.5	97.84	3,993	25	9.22
0.5	104.37	1,998	15	9.26
0.5	110.89	530	3	9.25
0.4	65.23	21,624	50	9.49
0.4	71.75	16,503	45	9.34
0.4	78.28	5,534	43	9.42
0.4	84.80	4,120	38	9.32
0.4	91.32	2,935	32	9.25
0.4	97.84	1,605	25	9.26
0.4	104.37	507	15	9.41
0.4	110.89	363	3	9.15
0.3	78.28	3,636	43	9.36
0.3	84.80	2,670	38	9.27
0.3	91.32	1,069	32	9.34
0.3	97.84	625	25	9.33
0.3	104.37	300	15	9.38
0.3	110.89	253	3	9.10
0.1	71.75	2,138	45	9.47
0.1	78.28	1,531	43	9.36
0.1	84.80	1,004	38	9.30
0.1	91.32	537	32	9.30
0.1	97.84	275	25	9.33
0.1	104.37	125	15	9.38
0.1	110.89	74	3	9.19

The above table shows that the *b* values remains similar even if the corresponding *c* values are in the extreme. The results seem to suggest that the terms that contain parameter *c* in equation (4-6) have to cancel out. If this is the case, then the expression for *b* becomes the following:

$$b^* = \left(\frac{1}{\log S}\right)\cdot\log\left(\frac{1}{KN}\right) \tag{4-12}$$

where $$\left(\frac{\sigma_n^c(0)-\sigma_{\max}^c}{\lambda^c}\right)=1 \tag{4-13}$$

Rearranging and take the inverse logarithm of equation (4-12) gives the following expression:

$$KS^{b^*}N = 1 \tag{4-14}$$

Equation (4-14) is similar to the representation of the $S - \overline{N}$ curve in equation (2-52).

$$KS^{b}\overline{N} = 1 \tag{2-52}$$

For which the constant amplitude fatigue data can be approximated by associating the characteristic life with the stress range through constants b and K. However, $\overline{N}$ is a function of S only, while the N in equation (4-14) is a function of both K and S. Table 4.14 shows the values of b^* and c determined according to equations (4-12) and (4-13) for each of the loading conditions used in this study.

Table 4.14. The values of b^* and c according to equations (4-12) and (4-13) with respect to different loading conditions

R	σ_{max}	N	b^*	c	R	σ_{max}	N	b^*	c
0.5	65.23	81,186	9.51	5.83	0.3	78.28	3,636	9.48	7.65
0.5	71.75	35,635	9.49	6.77	0.3	84.80	2,670	9.37	8.68
0.5	78.28	20,257	9.42	7.65	0.3	91.32	1,069	9.42	9.85
0.5	84.80	12,544	9.34	8.68	0.3	97.84	625	9.40	11.68
0.5	91.32	6,476	9.33	9.92	0.3	104.37	300	9.43	14.55
0.5	97.84	3,993	9.29	11.17	0.3	110.89	253	9.33	17.69
0.5	104.37	1,998	9.32	14.55	0.1	71.75	2,138	9.60	6.77
0.5	110.89	530	9.51	17.59	0.1	78.28	1,531	9.48	7.65
0.4	65.23	21,624	9.65	5.83	0.1	84.80	1,004	9.40	8.68
0.4	71.75	16,503	9.47	6.77	0.1	91.32	537	9.38	10.01
0.4	78.28	5,534	9.54	8.55	0.1	97.84	275	9.39	11.84
0.4	84.80	4,120	9.42	8.69	0.1	104.37	125	9.43	14.55
0.4	91.32	2,935	9.34	10.55	0.1	110.89	74	9.42	18.15
0.4	97.84	1,605	9.33	11.68					
0.4	104.37	507	9.46	14.01					
0.4	110.89	363	9.40	17.68					

All the b^* values are around 9, while c increase with increase in maximum cyclic stress, similar to the trend described in Figure 4.22. Based on the above analysis, it is evident that *K* can be assigned as a function of stress ratio *R*, while *b* is a material constant and *c* depends on maximum cyclic stress. Note that although *c* is a function of σ_{max}, its overall effect in determining the fatigue life seems to be extremely small.

As a summary, if assuming *b* and *K* are linear functions of stress ratio and material constant, respectively, a equality based on *K* cannot be established with two loading conditions of same maximum cyclic stress and different stress ratio. Also, the *c* and *K* values evaluated from two loading conditions of different maximum cyclic stress and stress ratio are very close to zero, which does not make sense. Two non-linear equations in terms of *c* and *K* are generated if the parameter *b* was treated as the material constant. However, the *c* and *K* values calculated using numerical methods may not be unique and are difficult to determine.

Therefore, another approach was taken by assuming *K* is a function of stress ratio, while *b* is a material constant instead. Two non-linear equations was again resulted in the formulation of *K* using 4 different loading conditions. Finally, the *c* can be determined through a single equation according to the formulation of *K* using two loading conditions with same σ_{max}, but different stress ratios. The *c* values seem to follow an increasing trend with the increasing of the maximum cyclic stress, while the values of *b* are all close to 9. A completely different trend of *c* was used to assess the variability of the *b* values, which showed that values of *b* stay close to 9. With the influence of the *c* values being cancelled out in the determination of *b*, the calculated *c* values seems to resemble the increasing trend. Therefore, it was concluded that the *K* is a function of stress ratio and *b* is a material constant. While *c* is a function of maximum cyclic stress, it has an insignificant effect on the predicted fatigue life.

4.4.4 Residual Strength Approximation

Due to the limited number of specimens, the measurement of residual strength on pre-cycled specimens was only taken on R=0.5 and $\sigma_{max}=0.6\sigma_n(0)$. However, I believe that the model is capable of predicting the residual strength after any n at a given loading condition.

The theoretical prediction of residual strength by the YL model at loading conditions, for example R=0.3, $\sigma_{max}=0.6\sigma_n(0)$ and R=0.4, $\sigma_{max}=0.6\sigma_n(0)$ are presented in Figure 4.23 together with the measured residual strengths at R=0.5, and $\sigma_{max}=0.6\sigma_n(0)$.

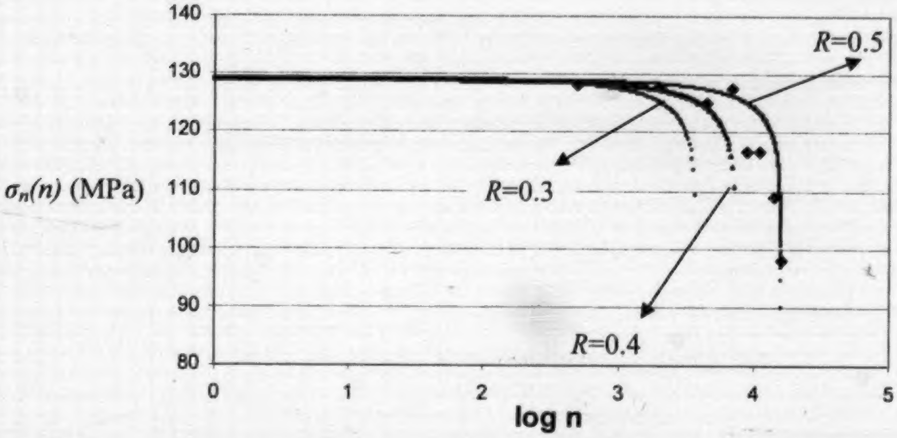

Figure 4.23. Residual strength estimation by the YL model at R=0.5, 0.4, 0.3 and $\sigma_{max}=0.6\sigma_n(0)$, with measured data (◆) of glass-filled polycarbonate at R=0.5 and $\sigma_{max}=0.6\sigma_n(0)$

Each of the points in Figure 4.23 represents the measured ultimate strength of a specimen after subjecting to a certain number of fatigue cycles as indicated on the abscissa. The YL model captured the trend of the measured residual strength very closely at a stress ratio of 0.5 and maximum cyclic stress at 60% of the ultimate strength of the virgin material. It was observed that the smaller the stress ratio, the sooner the drop appeared in the theoretical prediction with respect to fatigue cycle. The stress amplitude increases as the stress ratio decreases, creating more damage in the specimen during the cyclic loading, thus the material lost its strength faster. This is evident by observing the drop of predicted residual strength for R=0.3 and R=0.4 at $10^{3.2}$ and $10^{3.7}$ cycles respectively, which happened earlier than those for R=0.5 at 10^4 cycles.

Through the above preliminary assessment of the prediction capability of residual strength at the same stress level, but different stress ratios, it is speculated that the model is able to provide a reasonable estimate of the ultimate strength after pre-cycled at other loading conditions. Nevertheless, more experimental data should be established to validate the YL model which utilizes the modified parameter-determining procedure, regarding its potential in residual strength approximation.

4.5 Residual Mechanical Properties of Glass-Filled Polycarbonate and ABS

In this study, two materials were used to investigate the residual mechanical properties for failure in either brittle or ductile manner, based on the trend of residual strength and residual energy, respectively. According to the study by Jar et al. [76], the residual energy of cyclically loaded high-thermal-resistant ABS (relatively ductile material) degraded rapidly during early cycles, and then decreased gradually afterwards. The trend is similar to that described by the residual strength degradation assumption in the DC model. Therefore, in the case of ductile failure, the residual strength degradation assumption could be modified to be a residual energy degradation model for materials failing in a ductile manner.

Let's evaluate the difference between residual strength and residual energy with respect to the number of fatigue cycles for brittle and ductile fractured materials. The plots of residual strength and residual energy of glass-filled polycarbonate with respect to *n* at the loading condition of R=0.5 and $\sigma_{max}=0.6\sigma_n(0)$, as given in Figure 4.24 and 4.25, show that the trends of degradation are similar for this relative brittle material.

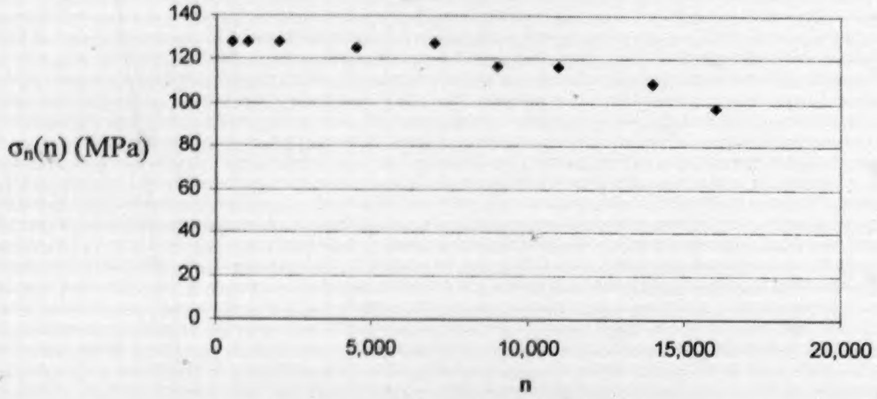

Figure 4.24. Plot of residual strength against the number of pre-cycle at a loading condition of R=0.5 and $\sigma_{max}=0.6\sigma_n(0)$ for glass-filled polycarbonate

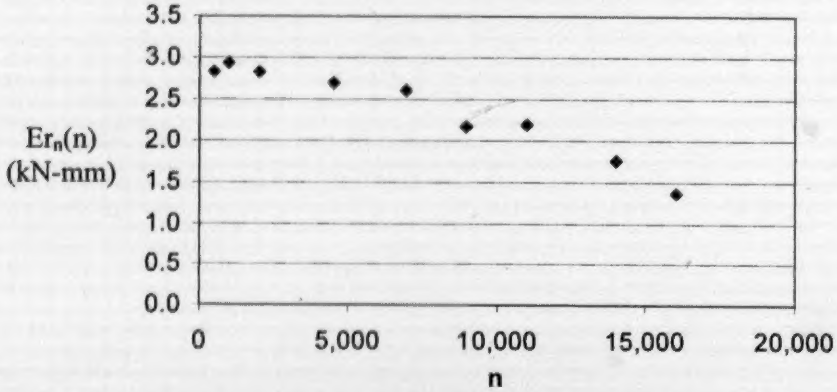

Figure 4.25. Plot of residual energy against the number of pre-cycle at a loading condition of R=0.5 and $\sigma_{max}=0.6\sigma_n(0)$ for glass-filled polycarbonate

Figures 4.24 and 4.25 both exhibited a clear degradation trend with respect to *n*. This is different from that of high-thermal resistant ABS, described in ref. [76]. ABS is a relatively ductile material, for which the fracture behavior can be quite different than that expected for the glass-filled polycarbonate.

The plots of residual strength against *n* for cyclically loaded high impact grade ABS at 4 different loading conditions [R=0.5, σ_{max}=0.8$\sigma_n(n)$; R=0.3, σ_{max}=0.8$\sigma_n(n)$; R=0.1, σ_{max}=0.8 $\sigma_n(n)$; R=0.3, σ_{max}=0.6 $\sigma_n(n)$] based on the data in Table 4.4 are shown in Figures 4.26 - 4.29 respectively.

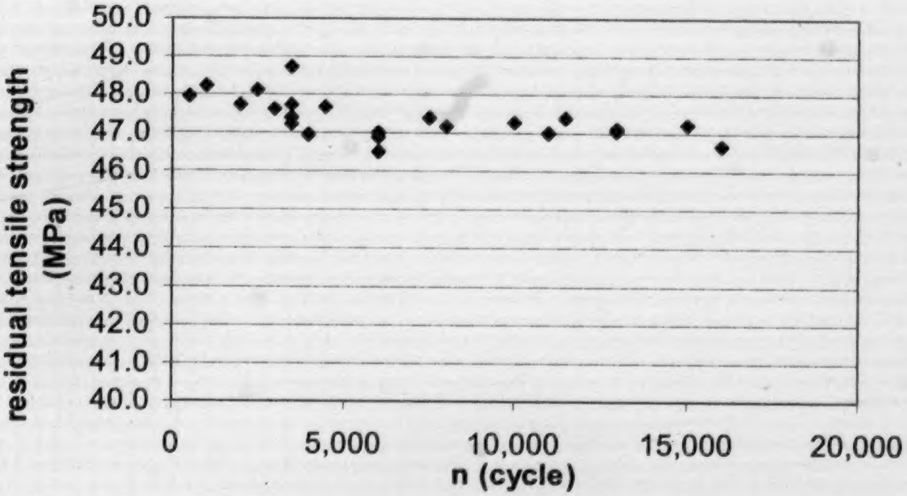

Figure 4.26. A plot of residual tensile strength of ABS against *n* at $R=0.5$, and $\sigma_{max}=0.8\sigma_n(0)$

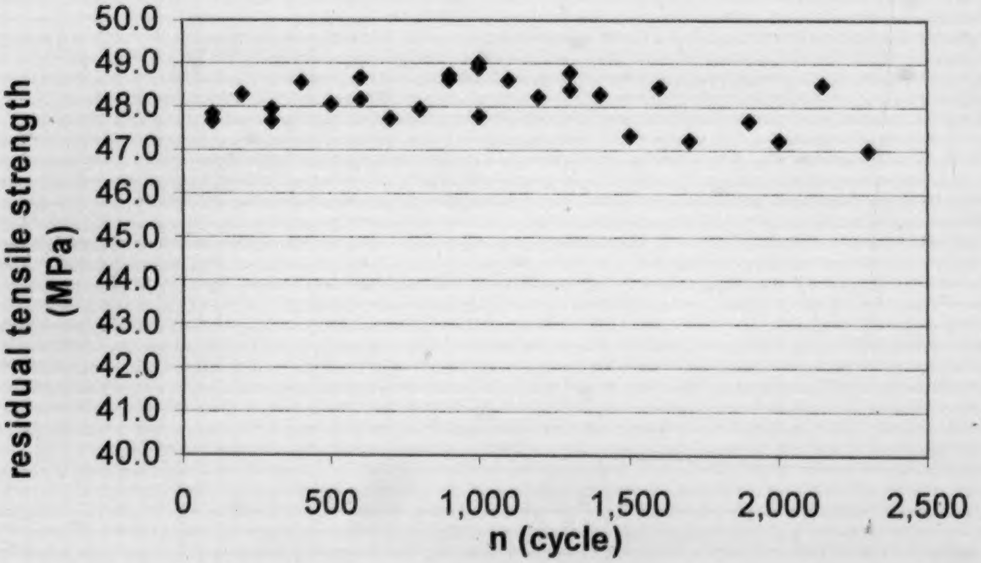

Figure 4.27. A plot of residual tensile strength of ABS against *n* at $R=0.3$, and $\sigma_{max}=0.8\sigma_n(0)$

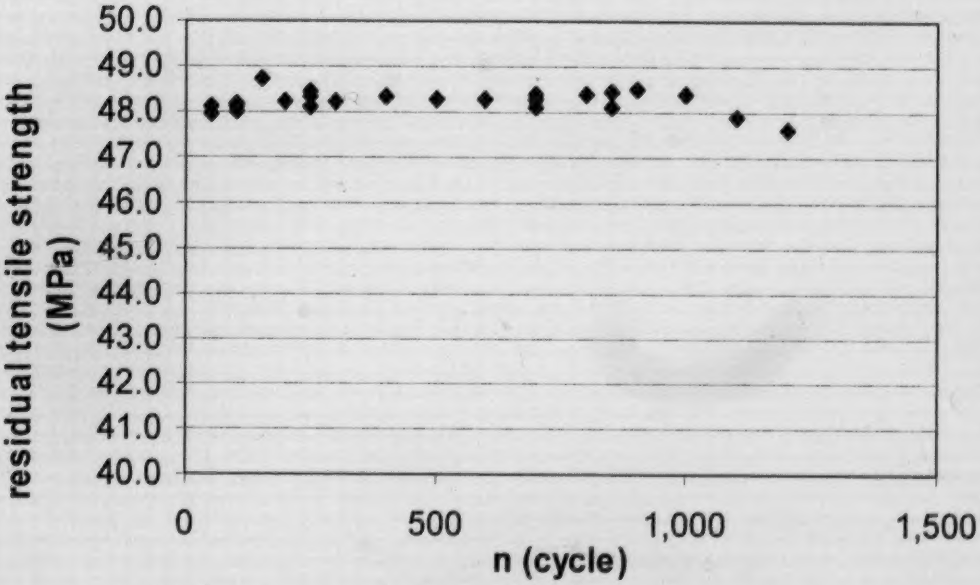

Figure 4.28. A plot of residual tensile strength of ABS against *n* at $R=0.1$, and $\sigma_{max}=0.8\sigma_n(0)$

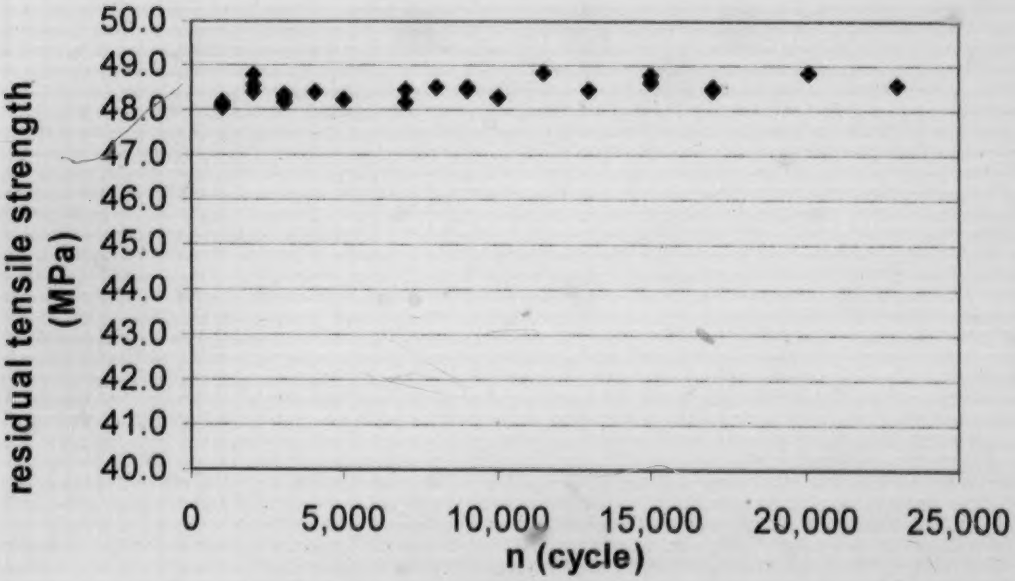

Figure 4.29. A plot of residual tensile strength of ABS against *n* at $R=0.3$, and $\sigma_{max}=0.6\sigma_n(0)$

They all show similar behavior as the residual strength does not change dramatically with the increasing number of fatigue cycles. However, the residual energy and maximum elongation at failure exhibited a rapid drop at the beginning of fatigue loading, and then decreased gradually as the number of cyclic loading progresses, which are represented in Figures 4.30 - 4.33 according to the data in Table 4-5.

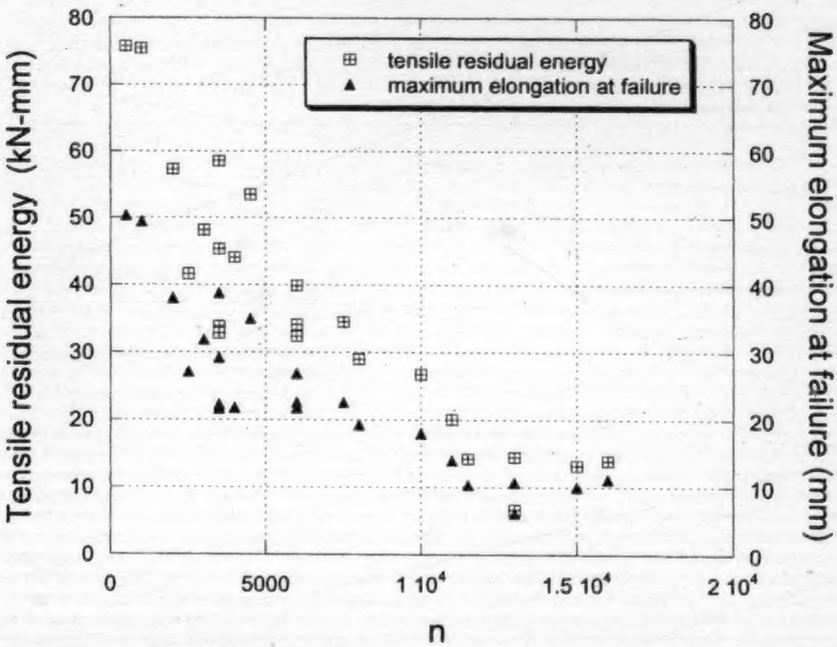

Figure 4.30. A plot of tensile residual energy and maximum elongation at failure of ABS against *n* at $R=0.5$, and $\sigma_{max}=0.8\sigma_n(0)$

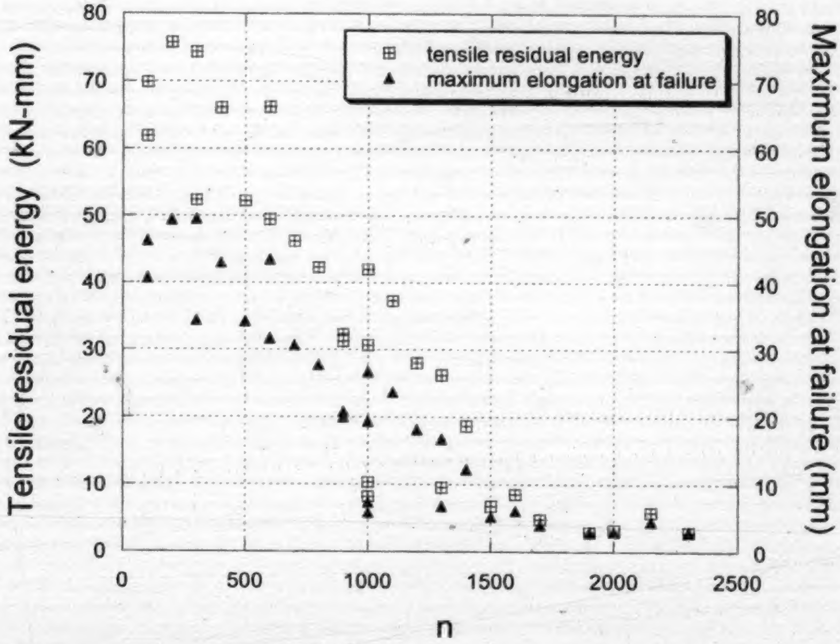

Figure 4.31. A plot of tensile residual energy and maximum elongation at failure of ABS against *n* at $R=0.3$, and $\sigma_{max}=0.8\sigma_n(0)$

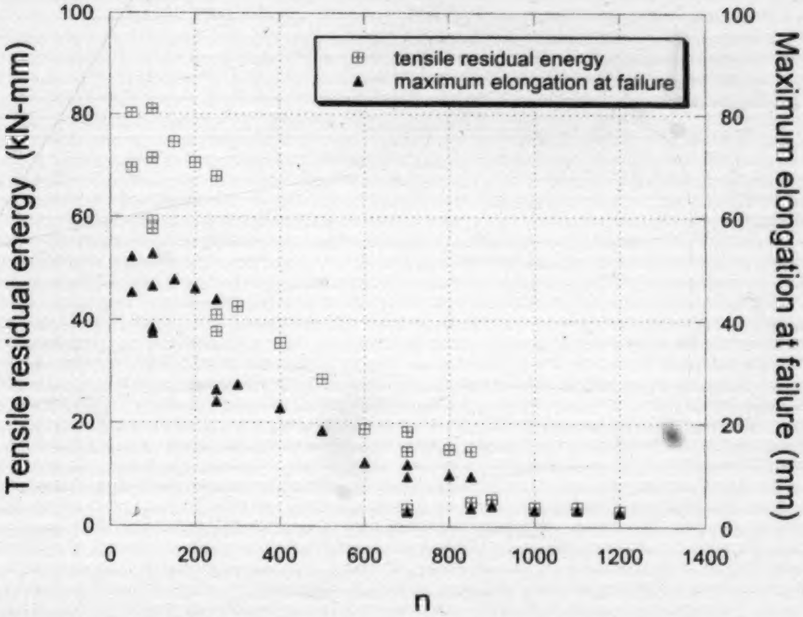

Figure 4.32. A plot of tensile residual energy and maximum elongation at failure of ABS against n at $R=0.1$, and $\sigma_{max}=0.8\sigma_n(0)$

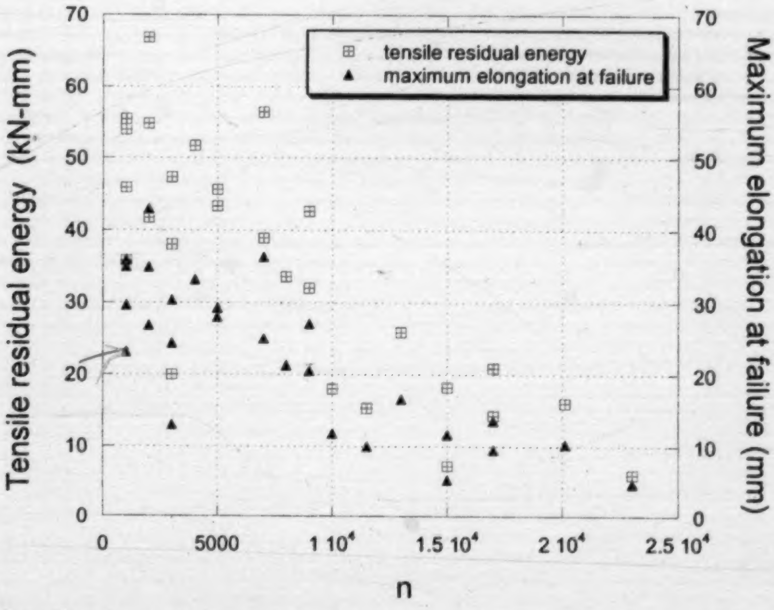

Figure 4.33. A plot of tensile residual energy and maximum elongation at failure of ABS against n at $R=0.3$, and $\sigma_{max}=0.6\sigma_n(0)$

The residual energy possessed by the specimen is defined as the area under the load-displacement curve. It can be observed from Figures 4.30-4.33 that the residual energy and maximum elongation at failure decrease if the specimen is subjected to the same number of fatigue cycle with a decreasing stress ratio from 0.5 to 0.1. This is because a larger stress amplitude imposes more damage to the specimen under cyclic loading, therefore, reducing its energy absorption ability. The effect of maximum cyclic stress on the residual energy and maximum elongation at failure can be examined from Figures 4.31 and 4.33. At the same number of n, the higher the σ_{max}, the lower the residual energy and maximum elongation at failure for the specimen. A higher maximum stress level or stress range would inflict a greater degree of damage to the specimen, causing the residual energy and elongation of the specimen to decrease.

The difference between the residual strength degradation and residual energy degradation in ABS is because of its ductile fracture. It is known that the material would not break immediately after reaching the yield point, instead its load-carrying capability dropped gradually and then leveled off. This means the material has a greater ability in absorbing energy arising from the loading without fracture. Thus, the residual strength and residual energy degradation behavior with respect to the number of fatigue cycles is entirely different.

The DC model and the YL model may not be applicable on materials that fail in a ductile manner, due to the fact that no strength degradation was observed. However, the residual energy does show degradation in an exponential manner, which is similar to the degradation assumption in the DC model. Besides, the characteristic of rapid drop in energy during early fatigue cycles is important for the determination of YL model parameters. Therefore, it is speculated that a fatigue model based on the assumption of residual energy degradation can be developed especially for materials failing in a ductile manner.

Although an equation representing the trend of residual energy with respect to the number of fatigue cycles was not obtained due to the wide scattering of data in Table 4.5, it is believed that a fatigue model based on residual energy degradation could be used to predict fatigue behavior of ductile materials. For this study, however, due to the residual stress generated by injection-molding, the data were not consistent enough to determine values of the parameters in the model.

5. CONCLUSIONS AND SUGGESTIONS FOR FUTURE STUDIES

This study examined the residual mechanical properties of polymers under cyclic loading. The difference in fatigue resistance of cyclically loaded brittle (glass-filled polycarbonate) and ductile (high-impact grade ABS) materials was compared, while the prediction accuracy of two existing residual strength degradation models (the DC and YL models) was evaluated. It was found that residual strength degradation was only observed in glass-filled polycarbonate, whereas a decreasing trend was detected in residual energy of ABS.

For the study of a relatively brittle material, flexural monotonic and fatigue tests were conducted on glass-filled polycarbonate, from which data were used to verify the DC and YL models for their capability in predicting fatigue life and residual strength. The DC model assumes that the residual strength decreases monotonically, following a degradation power-law relationship with increasing number of cycles. Experimental results suggested that the estimation of life with respect to various stress ratios and stress levels was satisfactory; however the measured residual strength did not validate the monotonic degradation assumption.

In an effort to provide a more accurate residual strength prediction, the YL model which has one additional degree of freedom was considered. This model was developed based on the assumption that the rate of degradation of residual strength is inversely proportional to the residual strength in a non-linear fashion. Instead of following that recommended in the literature, an alternative approach was proposed for determining the three model parameters (b, c and K), which takes into account the fractional error associated with three central moments obtained from the monotonic and fatigue test data, as well as the theoretical and measured residual strength. The results showed that, the model gave consistent residual strength after cyclic loading, but the fatigue life was generally under-estimated with respect to the stress ratio.

The relationship between the YL model parameters (*b* and *K*) and stress ratio, and also the nature of the parameters *b*, *c* and *K* were investigated. A linear correlation was observed between *b* and *R* and (log *K*) and *R*. For the former case, the investigation did not support the assumption of the invariability of parameters *c* and *K* irrespective of stress ratio and maximum cyclic stress. Through extensive analysis of the other relationship, between (log *K*) and *R*, it was found that the effect of *c* in the life prediction is extremely small. It was also evident that *c* and *K* are a function of maximum cyclic stress and stress ratio, respectively, while *b* is a material constant. This finding enables the incorporation of the stress ratio into the YL model to broaden its applicability and versatility.

The residual strength and residual energy degradation trends for glass-filled polycarbonate were similar, since the material failed immediately after attaining the highest load, and it lacked the ability of absorbing energy. The characteristic of energy absorption in ductile fracture of ABS provided an entirely different degradation trend in residual strength and residual energy. However, the lack of degradation in material strength with respect to the number of fatigue cycles prevented the application of the DC and YL models. While the decreasing trend of residual energy provided me with an insight into the development of a fatigue model based on residual energy degradation, the wide scattering of residual energy data prevented me from conducting an effective analysis of an energy-based degradation model.

Based on the results obtained from the current work, the following recommendations are suggested for the future studies:

1. Developing an energy-based fatigue model by measuring the residual energy degradation trend of a relatively ductile material with insignificant amount of residual stress, so that a more reliable result can be obtained. The equation for degradation rate can then be formulated accordingly, and the governing equation can be determined if the boundary conditions are properly identified. The proposed residual energy degradation model should be verified experimentally with different types of ductile fracture materials.
2. It would be interesting to extend the current study to examine the damage growth during cyclic loading with various stress ratios and loading frequencies. For example, SEM images of the material surface can be compared after the specimen has been subjected to different numbers of fatigue cycles, to elucidate the causes of the orientation and orderly arrangement of fibre in the crack initiation region. The study will also reveal the progressive damage process during the cyclic loading.
3. The prediction capability on residual strength with respect to stress ratio of the modified YL model is yet to be verified experimentally. The verification should include different materials to check its versatility.
4. It may be possible that the lack of degradation trend in residual strength of ABS is due to the testing method - tensile versus flexural tests. For the tensile tests, since the entire cross section within the gauge section is subjected to uniform loading, the reduction of material strength by local damage at a corner of the cross section

might not be as significant. On the other hand, the flexural 4-point bending test subjects the top and bottom surfaces of the rectangular specimen to maximum compressive and tensile stresses, respectively. As soon as a crack is generated on the tensile side of the cross section, fracture of the specimen is imminent. Therefore, it is worth conducting the flexural 4-point bending test on the ABS specimens to examine the trend of residual strength reduction with respect to the fatigue life, and compare the results with those from the tensile tests.

6. BIBLIOGRAPHY

[1] Committee E-9 on Fatigue., *"Manual on Fatigue Testing"*, American Society for Testing Materials, Philadelphia, (1950).

[2] Juvinall, R. C. and Marshek, K. M., *"Fundamentals of Machine Component Design"*, John Wiley, New York, (2000).

[3] McEvily, A.J., *"Metal Failures: Mechanisms, Analysis, Prevention"*, Wiley, New York, (2002).

[4] Schütz, W., *"A History of Fatigue"*, Engineering Fracture Mechanics, Vol. 54 (2), p. 263-300, (1996).

[5] Fuchs, H.O., *"Metal Fatigue in Engineering"*, Wiley, New York, (1980).

[6] Irwin, G. R., *"Analysis of Stresses and Strains Near the End of a Crack Traversing a Plate"*, Journal of Applied Mechanics, Vol. 24, p. 361, (1957).

[7] Eric A. Grulke, *"Polymer Process Engineering"*, PTR Prentice Hall, Englewood Cliffs, NJ, (1994).

[8] Peter C. Powell, *"Engineering with Polymers"*, Chapman and Hall, London; New York, (1983).

[9] Kulkarni, N., Mahfuz, H., Jeelani, S., *"Fatigue Failure Mechanism and Crack Growth in Foam Core Sandwich Composites under Flexural Loading"*, SAGE Publications Ltd, Vol. 23, p. 83-94, (2004).

[10] Mallick, P. K., Little, R. E., and Thomas, J., *"Fatigue Damage in Notched Pultruded Composite Rods."*, Composite Materials: Fatigue and Fracture. ASTM, Philadelphia, PA, USA, p. 197-209, (1986).

[11] Chen, A. S., and Matthews, F. L., *"Static and cyclic biaxial bending of CFRP panels"*, Elsevier Science Ltd, Oxford, Engl, Vol. 52, p. 267-273, (1994).

[12] Imanaka, M., Hidaka, K., Turui, T., *"In-situ observation in adhesive layer of adhesively bonded butt joints with a thin adherend under cyclic loading"*, Society of Materials Science Japan, Kyoto, Japan, Vol. 49, p. 561-566, (2000).

[13] Hayashi, M., *"High-Cycle Thermal Fatigue Crack Initiation and Growth Behavior in a Semi-Infinite Plate Model"*, Journal of Pressure Vessel Technology (Transactions of the ASME), Vol. 123 (3), p. 305-309, (2001).

[14] Gao, C. H., Huang, J. M., Lin, X. Z., *"Stress analysis of thermal fatigue fracture of brake disks based on thermomechanical coupling"*, American Society of Mechanical Engineers, New York, NY 10016-5990, United States, Vol. 129, p. 536-543, (2007).

[15] Petersen, C., and Rodrian, D., *"Thermo-Mechanical Fatigue Behavior of Reduced Activation Ferrite /martensite Stainless Steels"*, Journal of Nuclear Materials, Netherlands, Vol. 307-311, Part 1p. 500-504. Dec, (2002).

[16] Lafarie-Frenot, M. C., *"Damage Mechanisms Induced by Cyclic Ply-Stresses in Carbon–Epoxy Laminates: Environmental Effects"*, International Journal of Fatigue, Vol. 28 (10), p. 1202-1216, (2006).

[17] Kang, H.T., Lee, Y. L., Chen, J., Fan, D., *"A Thermo-Mechanical Fatigue Damage Model for Variable Temperature and Loading Amplitude Conditions "*, International Journal of Fatigue, Vol. 29 (9-11), p. 1797-1802, (2007).

[18] B. Fournier, M. Sauzay, C. Caës, M. Noblecourt, M. Mottot, A. Bougault, V. Rabeau and A. Pineau, *"Creep-Fatigue-Oxidation Interactions in a 9Cr–1Mo Martensitic Steel. Part II: Effect of Compressive Holding Period on Fatigue Life"*, International Journal of Fatigue, (2007).

[19] Legrand, N., Remy, L., Molliex, L., Dambrine, B., *"Damage Mechanisms and Life Prediction in High Temperature Fatigue of a Unidirectional SiC–Ti Composite"*, International Journal of Fatigue, Vol. 24 (2-4), p. 369-379, (2002).

[20] Rohatgi, P. K., Alaraj, S., Thakkar, R. B., *"Variation in fatigue properties of cast A359-SiC"*, Elsevier Ltd, Oxford, OX5 1GB, United Kingdom, Vol. 38, p. 1829-1841, (2007).

[21] Matsubara, G., Matsuda, H., and Tanaka, K., *"Damage tolerant evaluation of interlaminar delamination in a high strength GFRP helicopter rotor component"*, Japan Society of Mechanical Engineers, Tokyo, 160-0016, Japan, Vol. 73, p. 244-251, (2007).

[22] Cerny, I., Mayer, R. M., and Furbacher, I., *"An effect of microstructure defects on fatigue resistance of glass fibre reinforced polymer composites used for springs of freight vehicles"*, University of Zilina, Zilina, SK 010 26, Slovakia, Vol. 8, p. 21-24, (2006).

[23] Kim, J. K., and Lee, D. G., *"Effects of applied pressure and temperature during curing operation on the strength of tubular single-lap adhesive joints",* VSP BV, Vol. 18, p. 87-107, (2004).

[24] Mahdi, S., Kim, H. -., Gama, B. A., *"A comparison of oven-cured and induction-cured adhesively bonded composite joints",* SAGE Publications Ltd, Vol. 37, p. 519-542, (2003).

[25] Degrieck, J., and Van Paepegem, W., *"Fatigue Damage Modeling of Fibre-Reinforced Composite Materials: Review",* Applied Mechanics Review (USA), Vol. 54 (4), p. 279-300, (2001).

[26] Chou, P. C., and Croman, R., *"Residual Strength in Fatigue Based on the Strength-Life Equal Rank Assumption.",* Vol. 12, p. 177-194, (1978).

[27] Hahn, H. T., and Kim, R. Y., *"Proof Testing of Composite Materials.",* Vol. 9, p. 297-311, (1975).

[28] Chou, P. C., and Croman, R., *"Degradation and Sudden-Death Models of Fatigue of Graphite/epoxy Composites.",* Conf on Compos Mater, Test and Des, 5th, ASTM, Philadelphia, Pa, p. 431-454, (1979).

[29] Fawaz, Z., and Ellyin, F., *"Fatigue failure model for fibre-reinforced materials under general loading conditions",* Technomic Publ Co Inc, Lancaster, PA, USA, Vol. 28, p. 1432-1451, (1994).

[30] Yang, J. N., Jones, D. L., *"Load sequence effects on the fatigue of unnotched composite materials",* Fatigue of fibrous composite materials; Proceedings of the Symposium, San Francisco, Calif ; United States; 22-23 May 1979; Fatigue of fibrous composite materials, Philadelphia, Pa , American Society for Testing and Materials, p. 213-232, (1981).

[31] Daniel, I. M., and Charewicz, A., *"Fatigue Damage Mechanisms and Residual Properties of Graphite/epoxy Laminates.",* Mech of Damage and Fatigue, Vol. 25, p. 793-808, (1985).

[32] Schaff, J. R., and Davidson, B. D., *"Life prediction methodology for composite structures. Part I-constant amplitude and two-stress level fatigue",* Vol. 31, p. 128-157, (1997).

[33] Schaff, J. R., and Davidson, B. D., *"Life prediction methodology for composite structures. Part II-spectrum fatigue"*, Vol. 31, p. 158-181, (1997).

[34] D'Amore, A., Caprino, G., Stupak, P., *"Effects of Stress Ratio on the Flexural Fatigue Behavior of Continuous Strand Mat Reinforced Plastics"*, Science and Engineering of Composite Materials (UK), Vol. 5 (1), p. 1-8, (1996).

[35] Caprino, G., and D'Amore, A., *"Flexural fatigue behaviour of random continuous-fibre-reinforced thermoplastic composites"*, Elsevier Sci Ltd, Exeter, Engl, Vol. 58, p. 957-965, (1998).

[36] Yang, J. N., *"Residual Strength Degradation Model and Theory of Periodic Proof Tests for Graphite/epoxy Laminates."*, Vol. 11, p. 176-203, (1977).

[37] Yang, J. N., *"Fatigue and Residual Strength Degradation for Graphite/Epoxy Composites Under Tension-Compression Cyclic Loadings"*, Journal of Composite Materials, Vol. 12 (1), p. 19-39, (1978).

[38] Hwang, S., and Su, Y., *"Effects of stress frequency and stress ratio on the fatigue of glass/epoxy composite materials"*, Trans Tech Publications Ltd, Stafa-Zuerich, CH-8712, Switzerland, Vol. 326-328 II, p. 1031-1034, (2006).

[39] Tokaji, K., *"Effect of stress ratio on fatigue behaviour in SiC particulate-reinforced aluminium alloy composite"*, Blackwell Publishing Ltd, Oxford, OX4 2XG, United Kingdom, Vol. 28, p. 539-545, (2005).

[40] Singh, N., Khelawan, R., and Mathur, G. N., *"Effect of stress ratio and frequency on fatigue crack growth rate of 2618 aluminium alloy silicon carbide metal matrix composite"*, Indian Academy of Sciences, Vol. 24, p. 169-171, (2001).

[41] Mahfuz, H., Maniruzzaman, M., Krishnagopalan, J., *"Effects of stress ratio on fatigue life of carbon-carbon composites"*, Elsevier Science B.V., Amsterdam, Netherlands, Vol. 24, p. 21-31, (1995).

[42] Miyano, Y., Nakada, M., and McMurray, M. K., *"Influence of stress ratio on fatigue behavior in the transverse direction of unidirectional CFRPS"*, Technomic Publ Co Inc, Lancaster, PA, USA, Vol. 29, p. 1808-1822, (1995).

[43] Kadi, H. E., and Ellyin, F., *"Effect of stress ratio on the fatigue of unidirectional glass fibre/epoxy composite laminae"*, Butterworth-Heinemann Ltd, Oxford, Engl, Vol. 25, p. 917-924, (1994).

[44] Scrivner, G. C., and Chan, W. S., *"Effects of stress ratio on edge delamination characteristics in laminated composites"*, Fatigue and Fracture; 4th Symposium on Composite Materials, Publ by ASTM, Philadelphia, PA, USA, p. 538-551, (1993).

[45] Shigley, J. E. and Mischke, C. R., *"Mechanical Engineering Design"*, McGraw-Hill, New York, (1989).

[46] Abernethy, R.B., *"The New Weibull Handbook"*, North Palm Beach, Fla, (1998).

[47] *"Location Parameter of the Weibull Distribution"*, *http://www.weibull.com/hotwire/issue15/relbasics15.htm*, ReliaSoft Corporation, August 14, 2007.

[48] Wang, S. S., Suemasu, H., and Chim, E. S. M., *"Analysis of Fatigue Damage Evolution and Associated Anisotropic Elastic Property Degradation in Random Short-Fiber Composite"*, Journal of Composite Materials, Vol. 21 (12), p. 1084-1105, (1987).

[49] Caprino, G., D'Amore, A., and Facciolo, F., *"Fatigue sensitivity of random glass fibre reinforced plastics"*, Technomic Publ Co Inc, Lancaster, PA, USA, Vol. 32, p. 1203-1220, (1998).

[50] Epaarachchi, J. A., and Clausen, P. D., *"An empirical model for fatigue behavior prediction of glass fibre-reinforced plastic composites for various stress ratios and test frequencies"*, Elsevier Science Ltd, Vol. 34, p. 313-326, (2003).

[51] Sendeckyj, G. P., *"Life Prediction for Resin Matrix Composite Materials"*, (1990).

[52] Hertzberg, R.W. and Mason, J.A., *"Fatigue of Engineering Plastics"*, Academic Press, New York, (1980).

[53] Bach, P. W., *"ECN Investigation of Polyester Composite Materials"*, German Aerospace Establishment, European Commission-EUR 16684, (1996).

[54] Sys, W., *"RUG Investigation of Polyester Composite Materials"*, German Aerospace Establishment, European Commission-EUR 16684, (1996).

[55] Kensche, C., *"DLR Investigation of Polyester Composite Materials"*, German Aerospace Establishment, European Commission-EUR 16684, (1996).

[56] *DOE-MSU Wind Turbine Blade Composite Material Fatigue Database*, Department of Chemical Engineering, Montana State University at Bozman, Montan 59717, USA, (1998-1999).

[57] Mandell, J. F., and Meier, U., *"Effects of Stress Ratio, Frequency, and Loading Time on the Tensile Fatigue of Glass-Reinforced Epoxy."*, Long-Term Behavior of Composites, Symposium. ASTM, Philadelphia, Pa, USA, p. 55-77, (1983).

[58] D'Amore, A., Caprino, G., and Facciolo, F., *"Correlation between flexural and tensile fatigue response of short glass fibre reinforced plastics"*, Adcotec Ltd., Vol. 5, p. 53-58, (1996).

[59] Caprino, G., *"Predicting fatigue life of composite laminates subjected to tension-tension fatigue"*, SAGE Publications Ltd, Lancaster, PA, USA, Vol. 34, p. 1334-1355, (2000).

[60] Halpin, J. C., Jerina, K. L., and Johnson, T. A., *"Characterization of Composites for the Purpose of Reliability Evaluation."*, ASTM Spec Tech Publ 521 1973, p. 5-64, (1972).

[61] Ryder, J. T., and Walker, E. K., *"Ascertainment of the Effect of Compressive Loading on the Fatigue Life of Graphite Epoxy Laminates for Structural Applications"*, p. 274p, (Dec 1976).

[62] Halpin, J. C., Jerina, K. L., and Johnson, T. A., *"Characterization of Composites for the Purpose of Reliability Evaluation"*, p. 101p, (Dec 1972).

[63] Manning, S. D., Lemon, G. H., and Waddoups, M. E., *"Composite Wing for Transonic Improvement, Volume III. Structural Reliability Studies"*, p. 240p, (Nov 1972).

[64] Wolff, R. V., and Lemon, G. H., *"Reliability Prediction for Adhesive Bonds"*, p. 75p, (Oct 1972).

[65] Wolff, R. V., and Lemon, G. H., *"Reliability Prediction for Composite Joints - Bonded and Bolted"*, p. 110p, (Mar 1976).

[66] Halpin, J. C. 1., Johnson, T. A. 1., and Waddoups, M. E., *"Kinetic fracture models and structural reliability"*, Vol. 8, p. 465-468, (Dec. 1972).

[67] Jen, M. R., Hsu, J. M., and Hwang, D. G., *"Fatigue Degradation in Centrally Notched Quasi-Isotropic Laminates"*, Journal of Composite Materials, Vol. 24 (8), p. 823-837, (1990).

[68] Tanimoto, T., Ishikawa, H., Amijima, S., *"Residual Strength Degradation Model for Glass/polyester Laminates Under Repeated Tension and Compression Loadings."*, Mechanical Behaviour of Materials - 4, Proceedings of the 4th International Conference. Pergamon Press, Oxford, Engl, p. 539-547, (1984).

[69] Yang, J. N., Jones, D. L., *"Statistical Fatigue of graphite/epoxy Angle-Ply Laminates in Shear"*, Journal of Composite Materials, Vol. 12, p. 371-389, (1978).

[70] Yang, J. N., Miller, R. K., and SUN, C. T., *"Effect of High Load on Statistical Fatigue of Unnotched Graphite /epoxy Laminates"*, Journal of Composite Materials, Vol. 14, p. 82-94. (1980).

[71] Yang, J. N., and Sun, C. T., *"Proof Test and Fatigue of Unnotched Composite Laminates"*, Journal of Composite Materials, Vol. 14 (2), p. 168-176, (1980).

[72] Radhakrishnan, K., *"Fatigue and Reliability Evaluation of Unnotched Carbon Epoxy Laminates"*, Journal of Composite Materials, Vol. 18 (1), p. 21-31, (1984).

[73] edited by the staff of Modern plastics magazine, *"Plastics Handbook"*, McGraw-Hill, New York, (1994).

[74] Mark, H. F., Bikales, N. M., Overberger, C. G., Menges, G., *"Encyclopedia of Polymer Science and Engineering"*, John Wiley & Sons, (1985).

[75] Dally, J. W., and Broutman, L. J., *"Frequency Effects on the Fatigue of Glass Reinforced Plastics"*, Journal of Composite Materials, Vol. 1 (4), p. 424-442, (1967).

[76] Jar, P.-Y. B., Konishi, K., and Shinmura, T., *"Characterization of Toughness Variation due to Intrinsic Defects in High-Thermal-Resistant Poly(Acrylonitrile-Butadiene-Styrene) (ABS)"*, Journal of Materials Science (USA), Vol. 37 (21), p. 4521-4528, (2002).